1996 CEDAR Workshop
Boulder, Colorado
June 16-22, 1996

Tutorial Lecture

by Iain Reid
University of Adelaide

Intercomparison of Wind Measuring Techniques in the Upper Middle Atmosphere with Particular Reference to MF Radar

Intercomparison of Wind Measuring Techniques in the Upper Middle Atmosphere with Particular Reference to MF Radar

Iain Reid

Department Physics & Math Physics

University of Adelaide

Adelaide 5005

Australia

Recently, the spotlight has been on Medium Frequency (MF) radar techniques because of:

- The AIDA 89 campaign
- The Development of Radar Interferometric Techniques and their application at MF
- Lidar user comments on Wavelength-Period relations for gravity waves
- HRDI / WINDI / MF wind comparisons
- The development of new Meteor wind measuring techniques and consequent Meteor / MF wind comparisons

The saturated-cascade model for atmospheric gravity wave spectra, and the wavelength-period (W-P) relations

E.M. Dewan
Phillips Lab., GPOS, 29 Randolph Road, Hanscom AFB, MA

Abstract. The case will be presented for the hypothesis that over a certain wave number range all the atmospheric gravity wave spectra (and the Wavelength-Period Relations as well) are a direct consequence of a "saturated-cascade" of the waves.

Introduction

The purpose of this paper is to present a model explaining all the atmospheric gravity wave spectra and, in addition, a wavelength-period constraint observed by many researchers and which will henceforth be designated the W-P Relations. [These include Vincent and Reid (1983), Reid (1986), Manson (1990), for mainly radar observations and Gardner and Voelz (1987), Beatty et al (1992) and Gardner (1993) for lidar observations. Here the reader must keep in mind that a major result of the AIDA-89 Campaign (JATP, March 1993) was that MF radar measurements of winds above 80 km with averaging periods less than two hours are unreliable.] The power spectral densities (PSD's) in terms of horizontal, k_x, and vertical, k_z, wave numbers, and frequency, ω, will be obtainable from this model for horizontal and vertical velocity components, temperature, and density fluctuations, etc. as a function primarily of buoyancy frequency, N, and turbulent dissipation rate ε. The W-P Relations will also be functions of these parameters; and, as a result, numerous experimental predictions will be available for the purpose of testing the model. Comparisons with available data will be shown to be in agreement with the model.

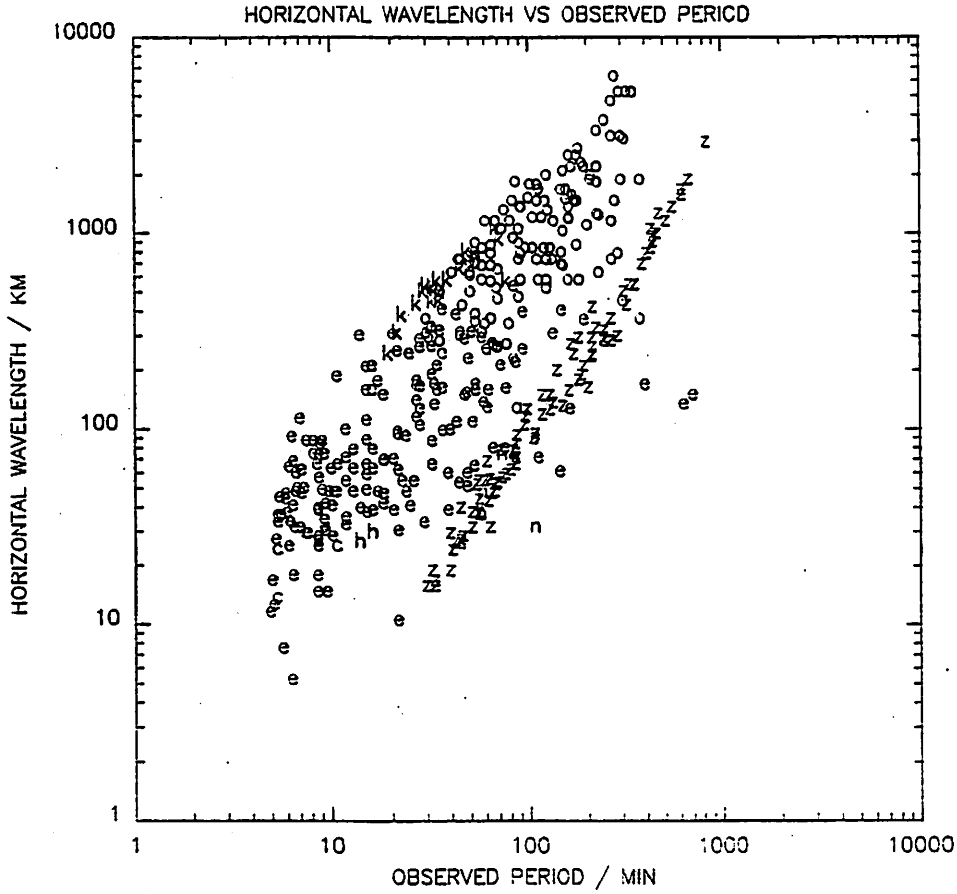

HORIZONTAL WAVELENGTH VS OBSERVED PERIOD
HORIZONTAL WAVELENGTH / KM
OBSERVED PERIOD / MIN

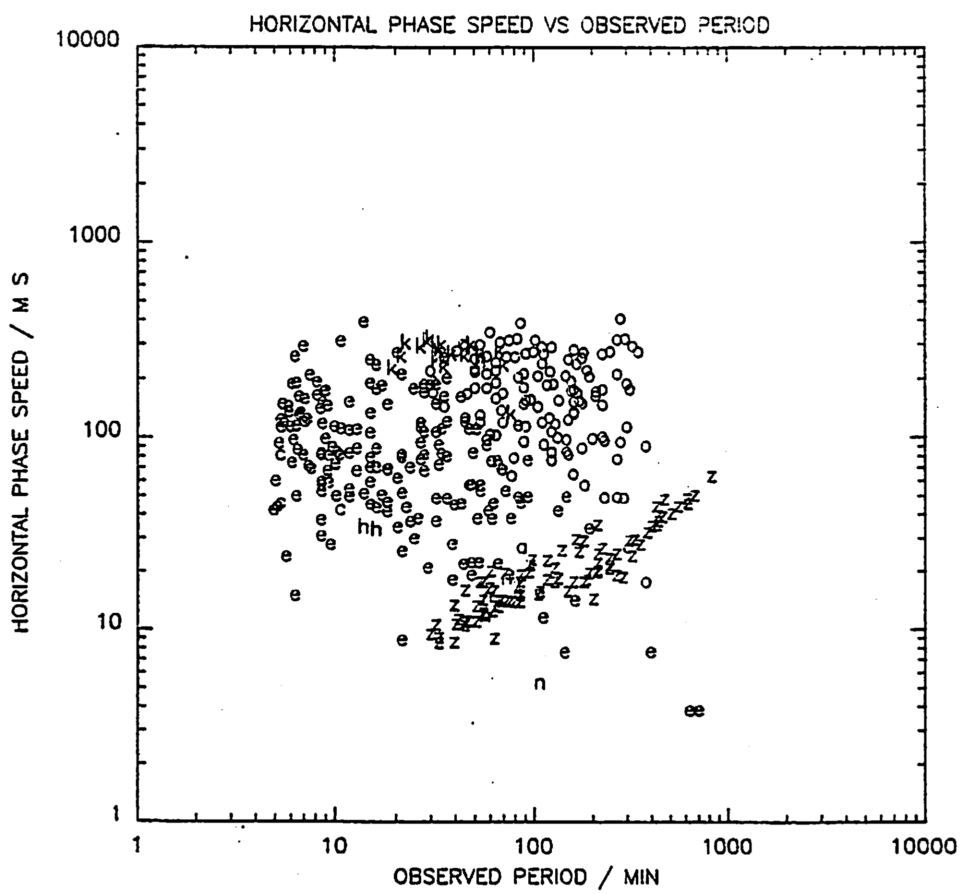

HORIZONTAL PHASE SPEED VS OBSERVED PERIOD
HORIZONTAL PHASE SPEED / M S
OBSERVED PERIOD / MIN

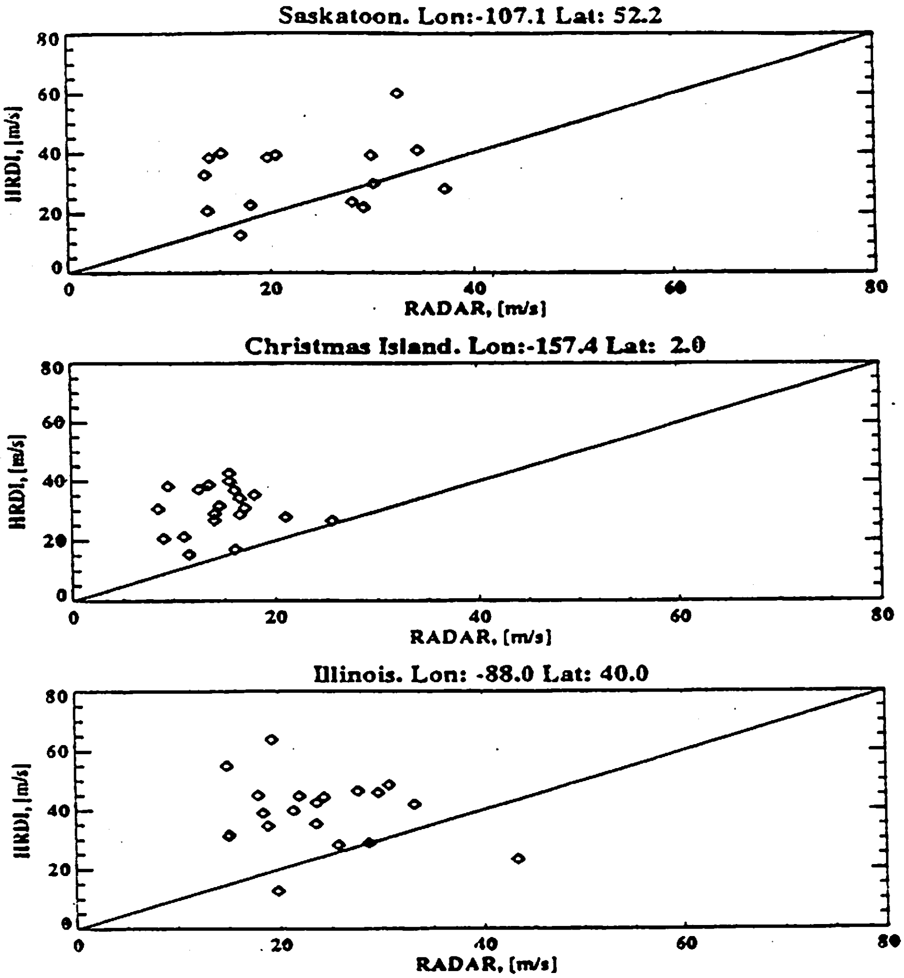

Figure 5. Approximate monthly mean tidal amplitudes from HRDI and radars. Tidal amplitudes are computed as half of the difference between maximum and minimum of the hourly averaged monthly mean winds at 96 km. Both zonal and meridional components are plotted.

(Khattatov et al., 1996)

"HRDI measures larger winds than MF radars, but the size of the discrepancy varies significantly between different stations" Burrage et al., JGR, 101, 10,365, 1996.

"HRDI wind magnitudes are somewhat more consistent with measurements obtained by rocket launched falling sphere measurements..."

May 1994

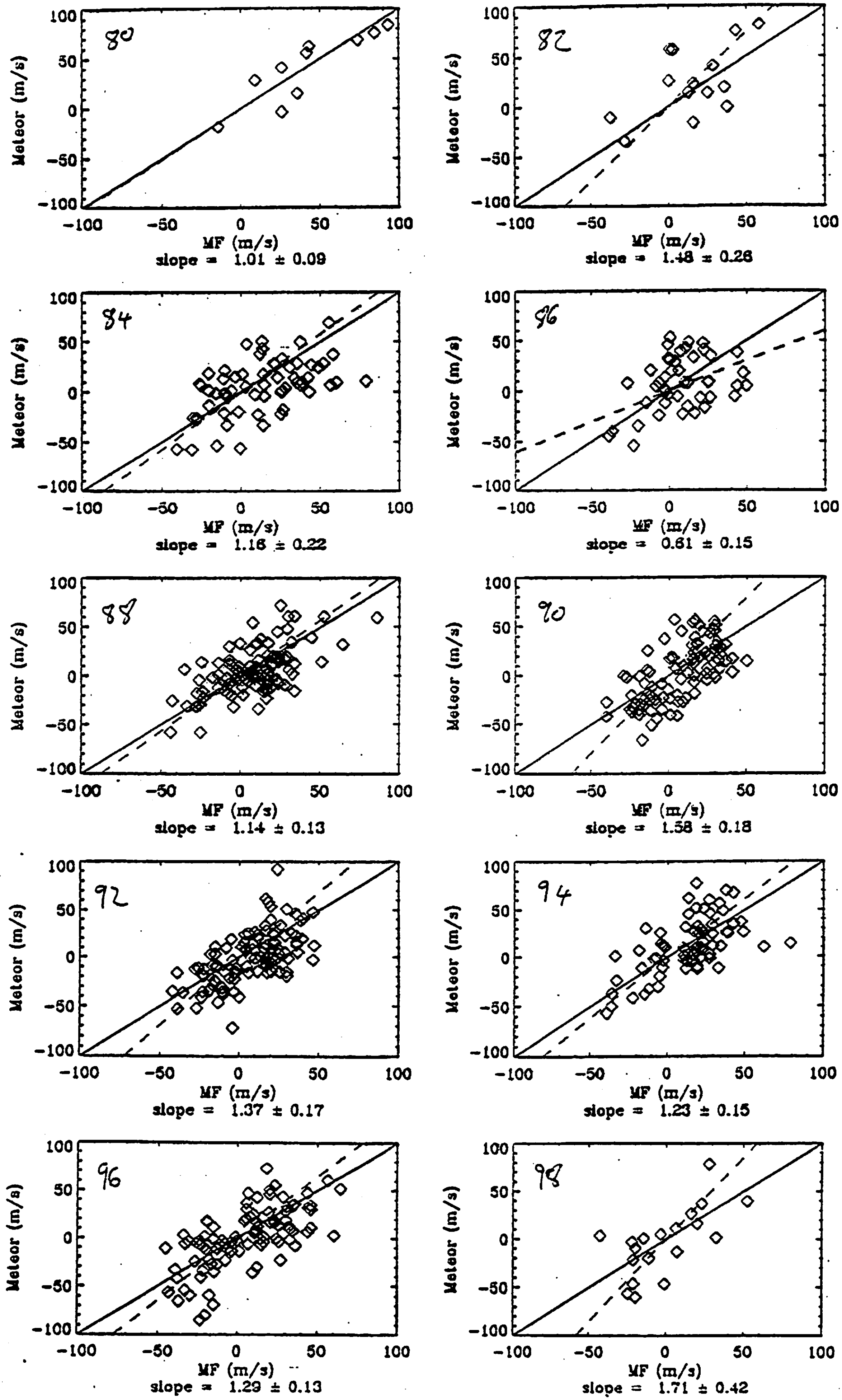

→ Importance of outliers

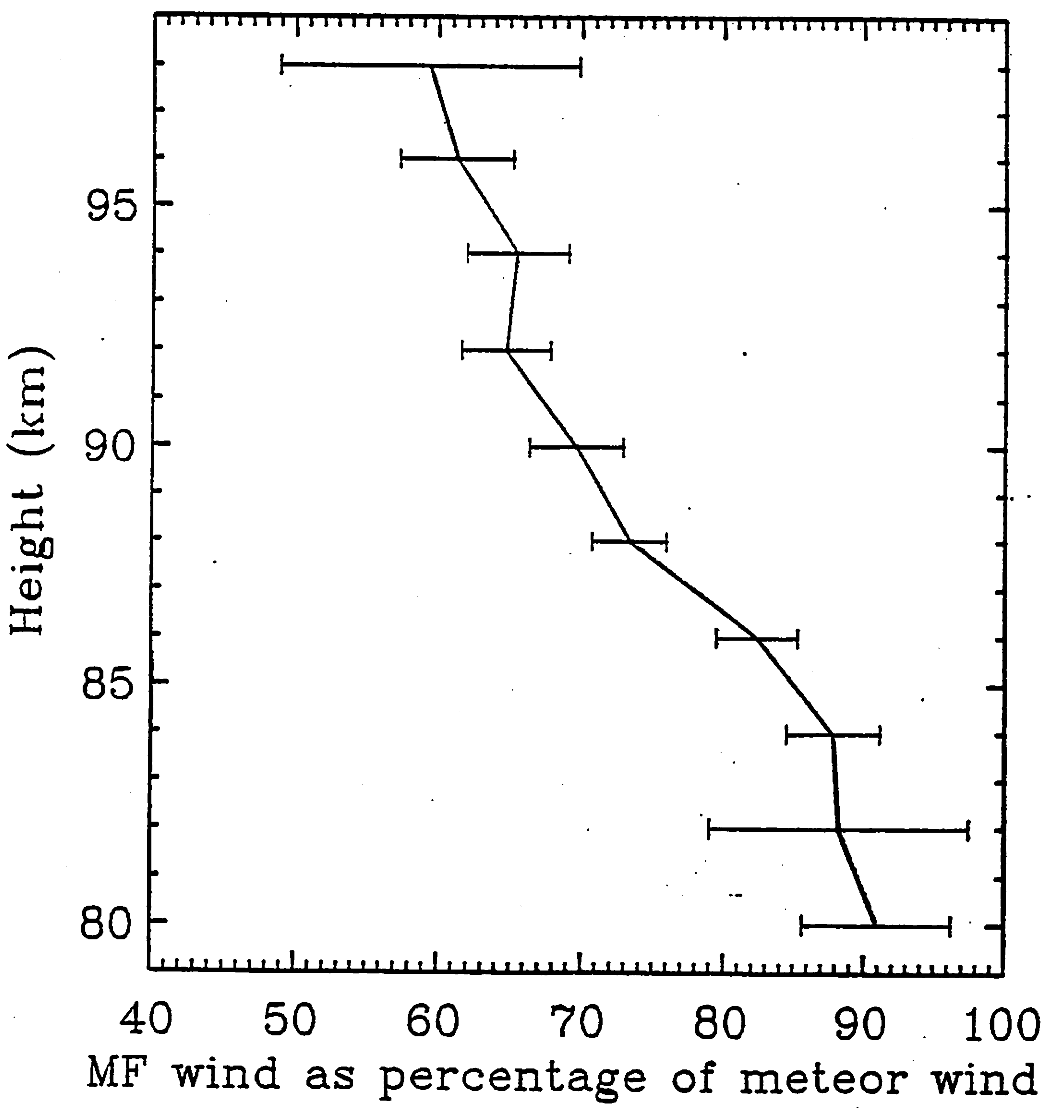

Height (km)
95
90
85
80
40
50
60
70
80
90
100
MF wind as percentage of meteor wind

This has been very healthy from a Scientific point of view. Naturally, in any scientific intercomparison we ensure that:

- We are comparing like with like. This would include ensuring
  - similar spatial averaging
  - similar temporal averaging
  - similar sampling

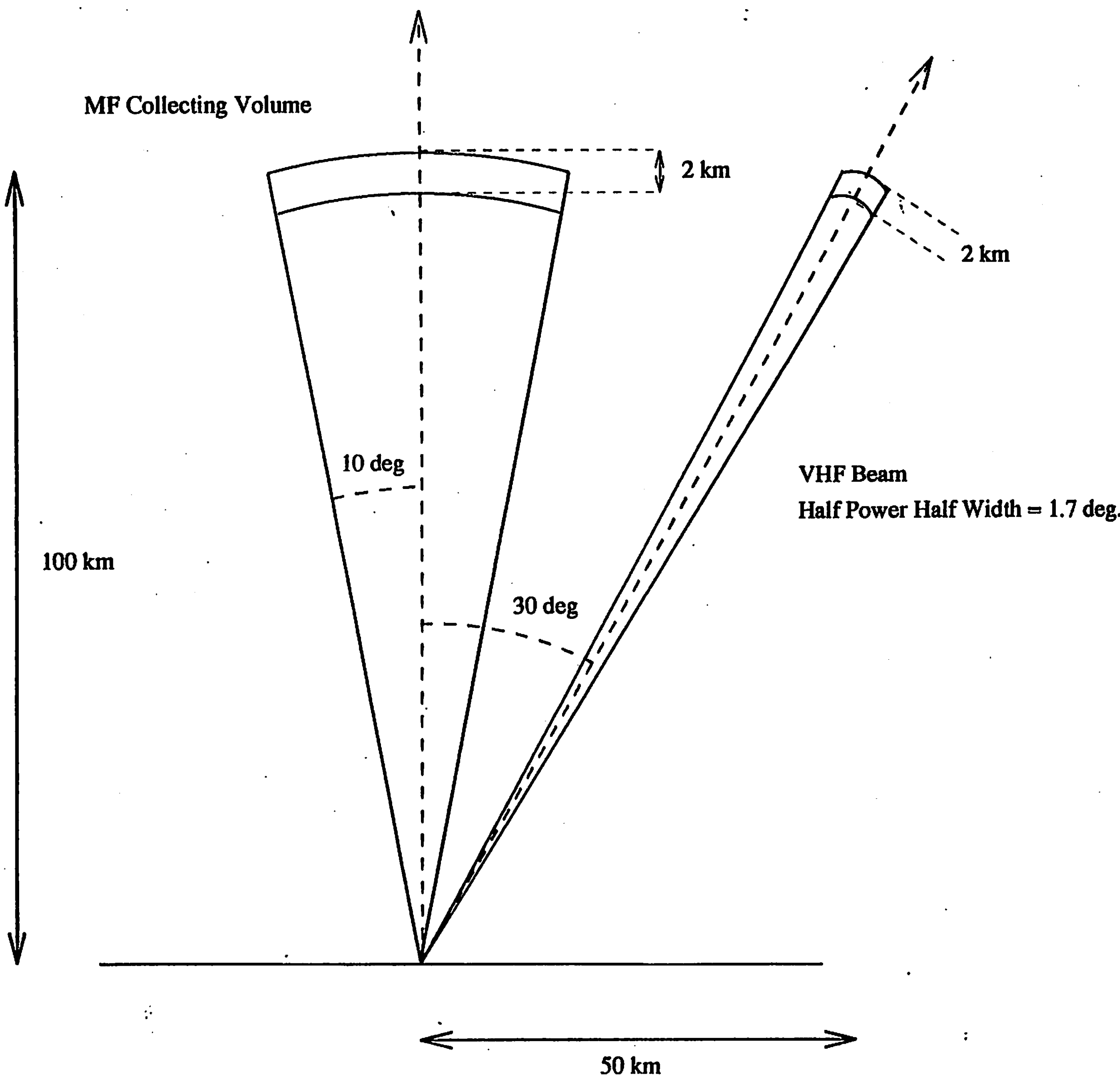

MF Collecting Volume
2 km
2 km
10 deg
30 deg
100 km
VHF Beam
Half Power Half Width = 1.7 deg.
50 km

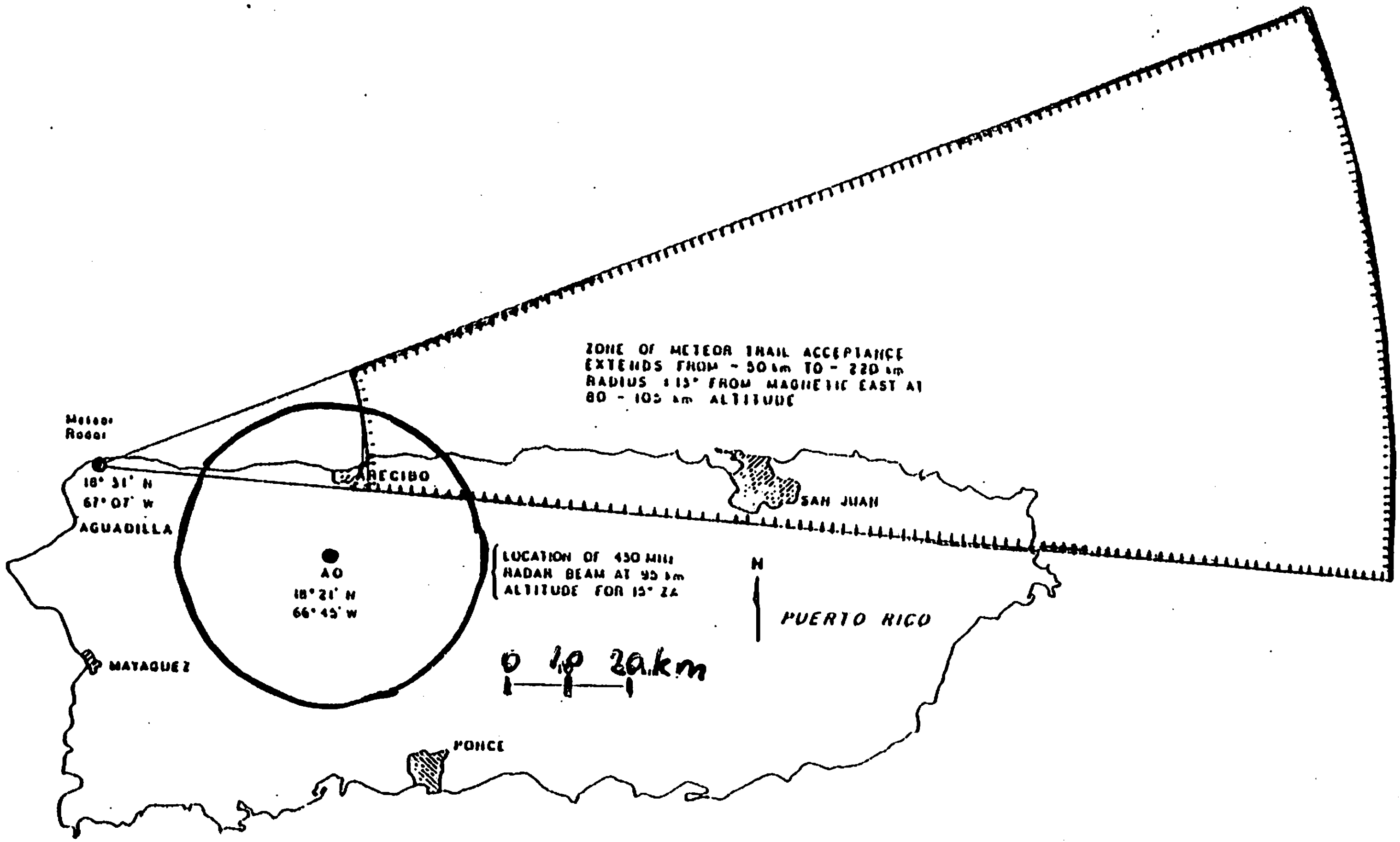

FIG. 1. A MAP OF PUERTO RICO SHOWING THE LOCATIONS OF BOTH THE AGUADILLA METEOR RADAR AND THE ARECIBO THOMSON SCATTER RADAR.

Also shown are projections to ground level of the effective radar beam patterns. Note that the meteor radar collects data from an extensive region while the Thomson scatter pattern lies unresolved on the 15° zenith angle (ZA) circle shown. Thomson scatter radar wind data were collected "looking" both geographically north and east.

Scientific intercomparison (cont.). We also ensure:

- The assumptions underlying a technique are valid for a particular application
- The limitations of a technique are understood
- We agree on what "good" or "bad" agreement is before the comparison*

*because statistical analysis is often not possible

*because it is not always possible to match spatial & temporal averaging, or sampling

State the Obvious

- All techniques have advantages and disadvantages
- All techniques have limitations
- There is no generic "reference" technique

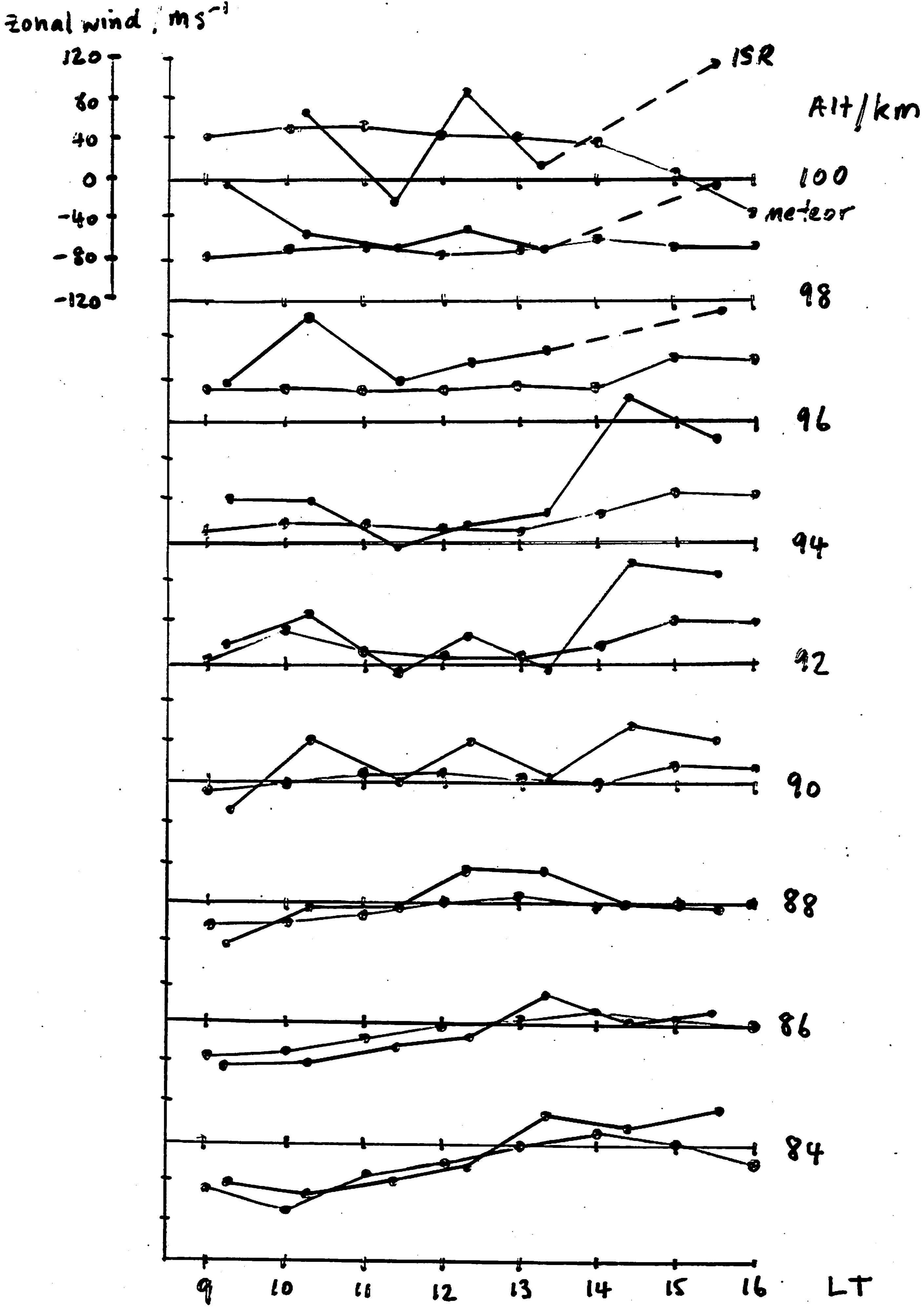

MATHEWS et al., 1981; PSS, 29, 341-348.

INCOHERENT SCATTER RADAR VS METEOR WINDS

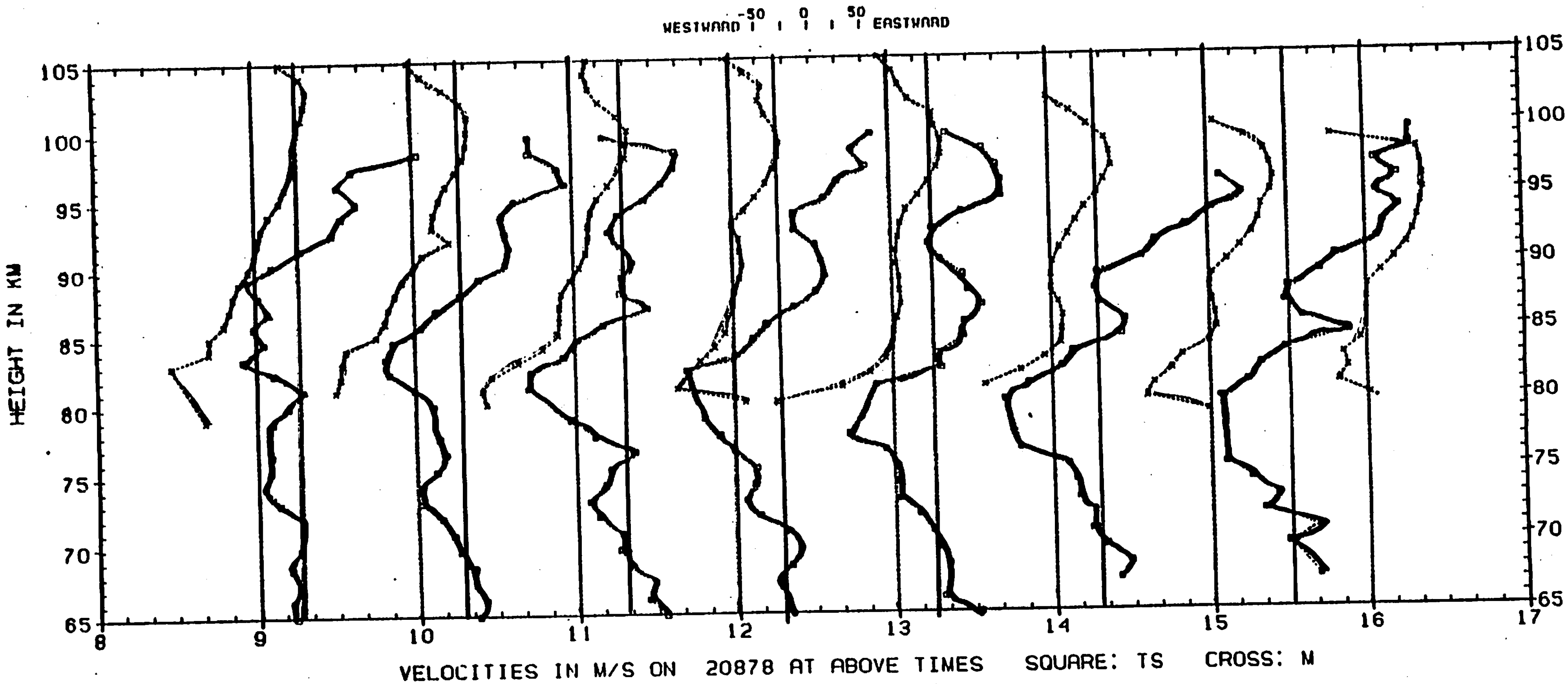

FIG. 3. SIMILAR TO FIG. 2 BUT FOR 2 AUGUST 1978.

Note the very large wind speeds near 80 km altitude and 11:00 h time. Wind speeds in excess of 100 m s^{-1} with shears of 10 m s^{-1} km^{-1} are often observed in this altitude region.

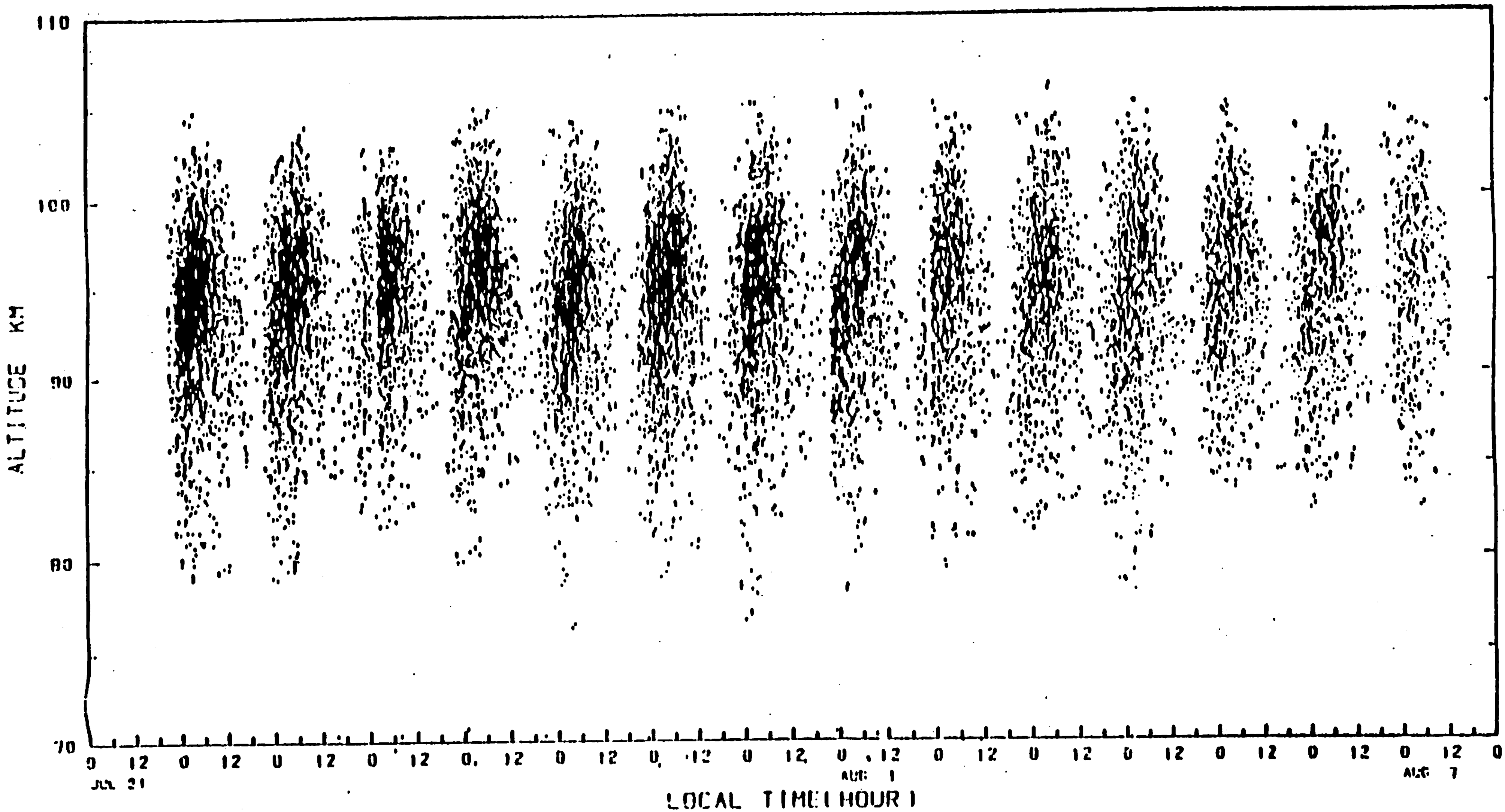

Fig. 4.4 Height-time distribution of underdense echoes during July 24 to August 7, 1978.

Valentic et al (1996)

Intercomparison of Processing Techniques

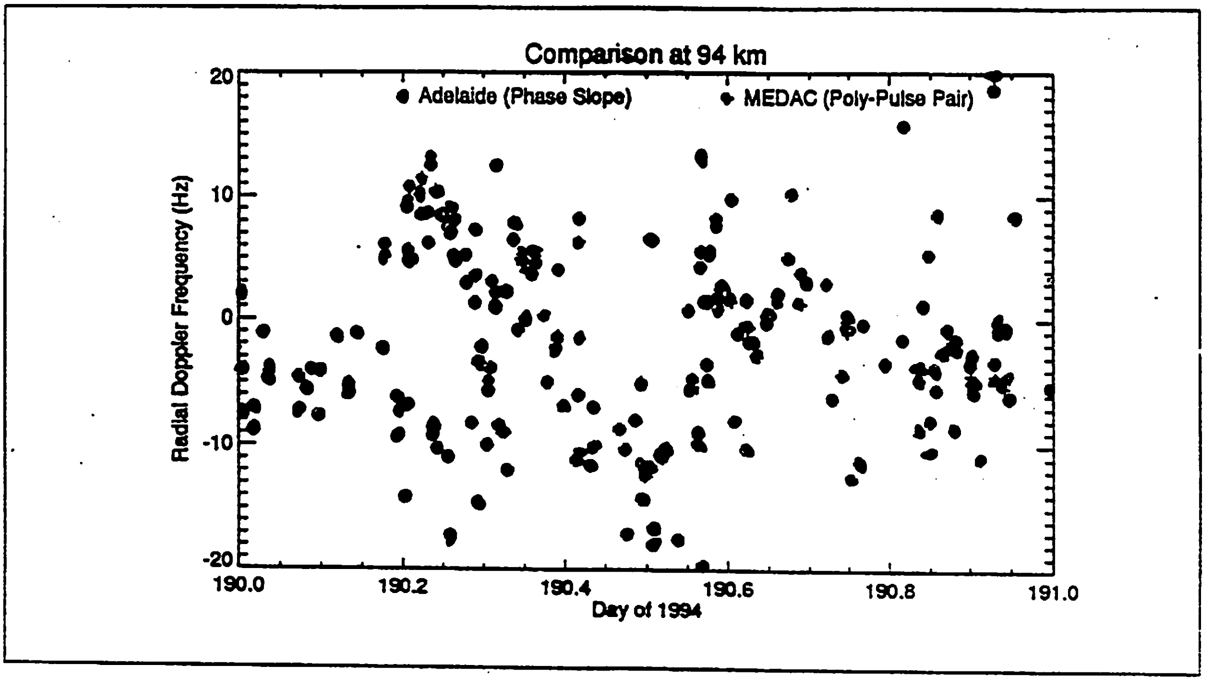

It is important to note that there is not just *one* MF radar technique. Rather, there are many. These include:

- The Doppler Beam Swinging (DBS) technique (rare at MF)
- The Spaced Antenna (SA) Technique with
  - Full Correlation Analysis
  - Full Spectral Analysis
  - Spatial Correlation Analysis
  - Interferometric Analyses (Many varieties)
- Hybrid Techniques

extra

AFTER VANDEPEER, 1994 ~~Ha tbook for STEP on Taiwan MST~~ nference
Ph D Thesis University Adelaide

Taxonomy of spaced-sensor techniques

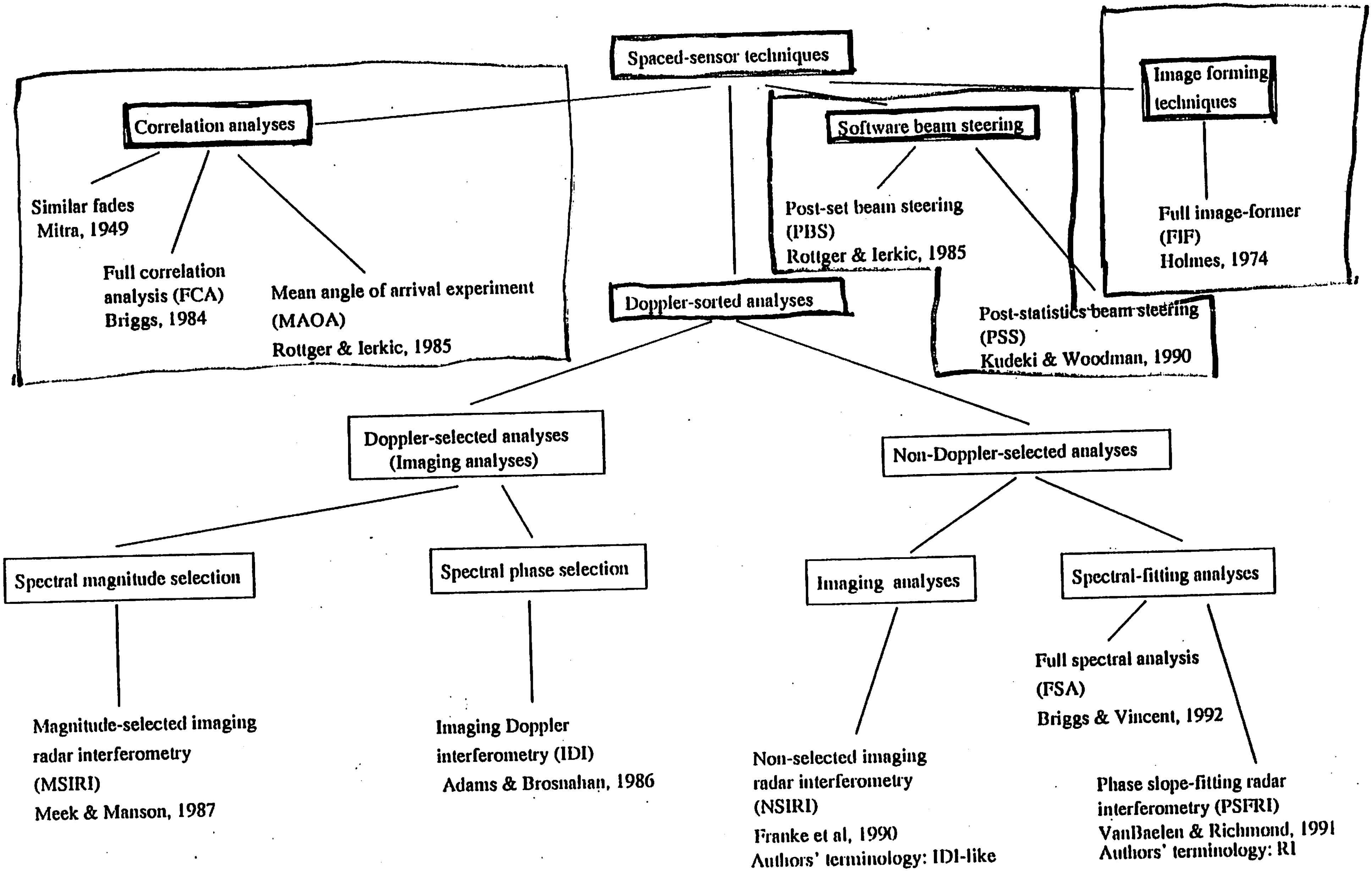

Doppler Technique

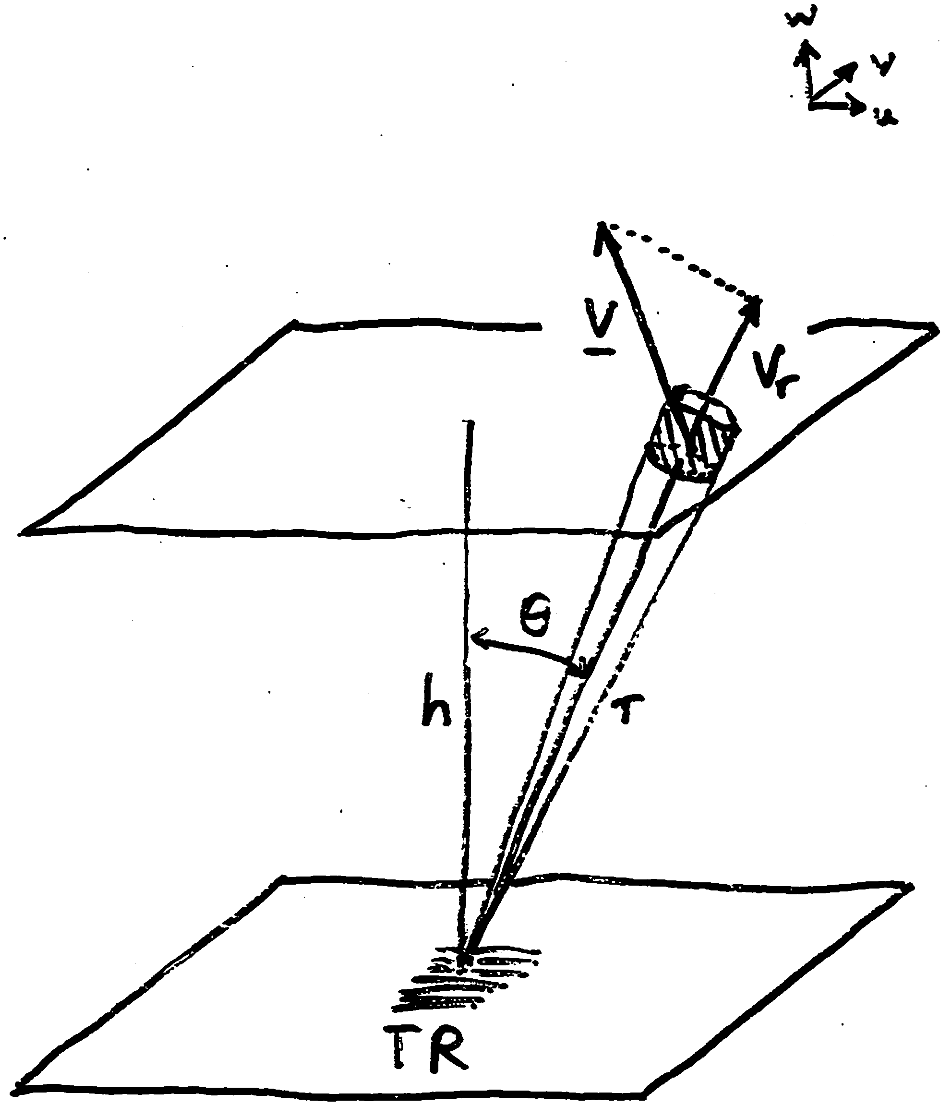

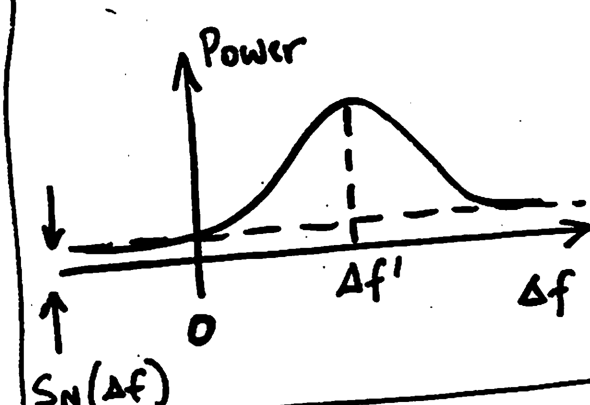

Spectrum of Returned Signal

$$v_r = -\frac{\Delta f' \lambda}{2}$$

extra

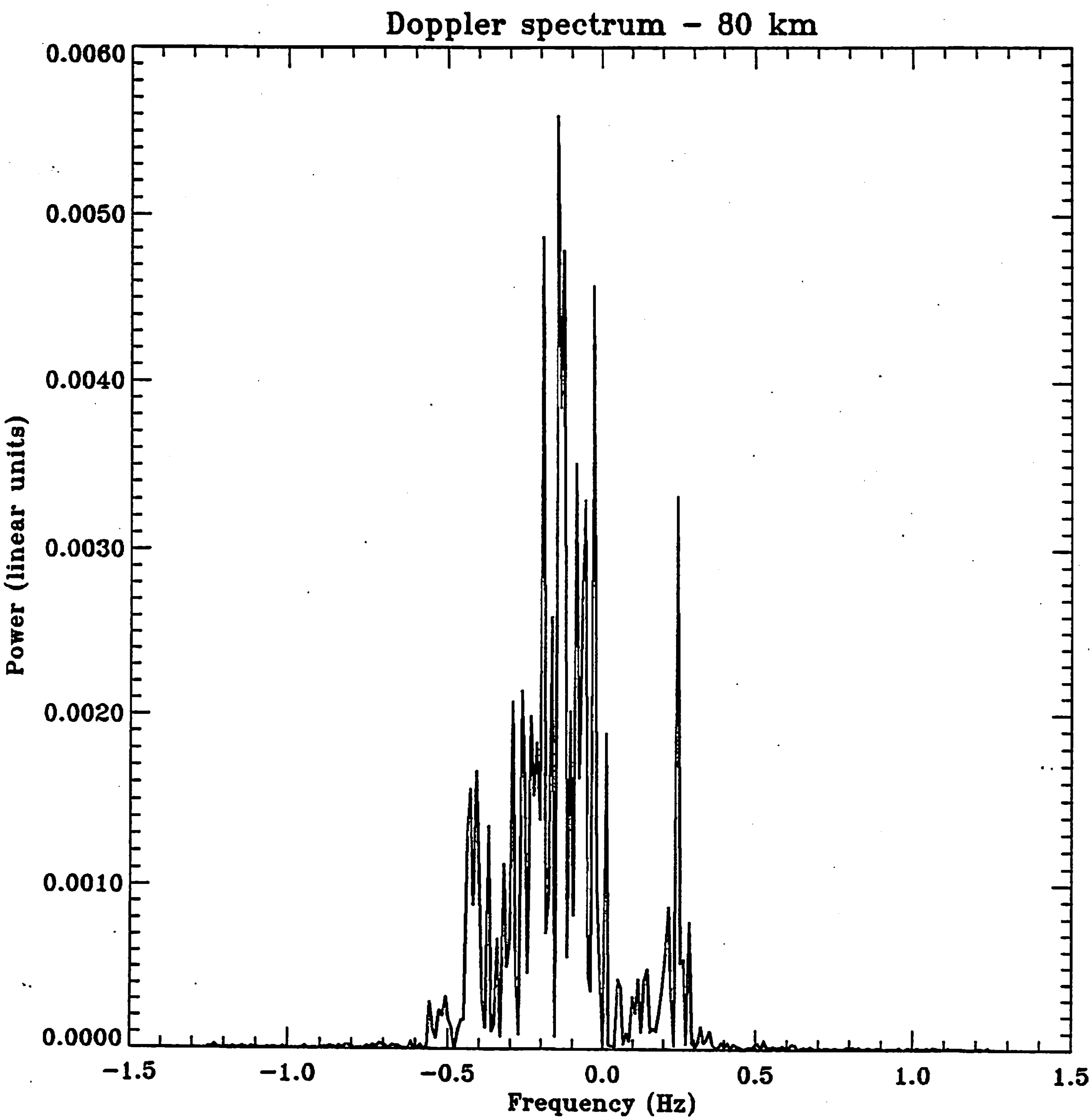
Doppler spectrum - 80 km
Power (linear units)
0.0060
0.0050
0.0040
0.0030
0.0020
0.0010
0.0000
−1.5
−1.0
−0.5
0.0
0.5
1.0
1.5
Frequency (Hz)

extra

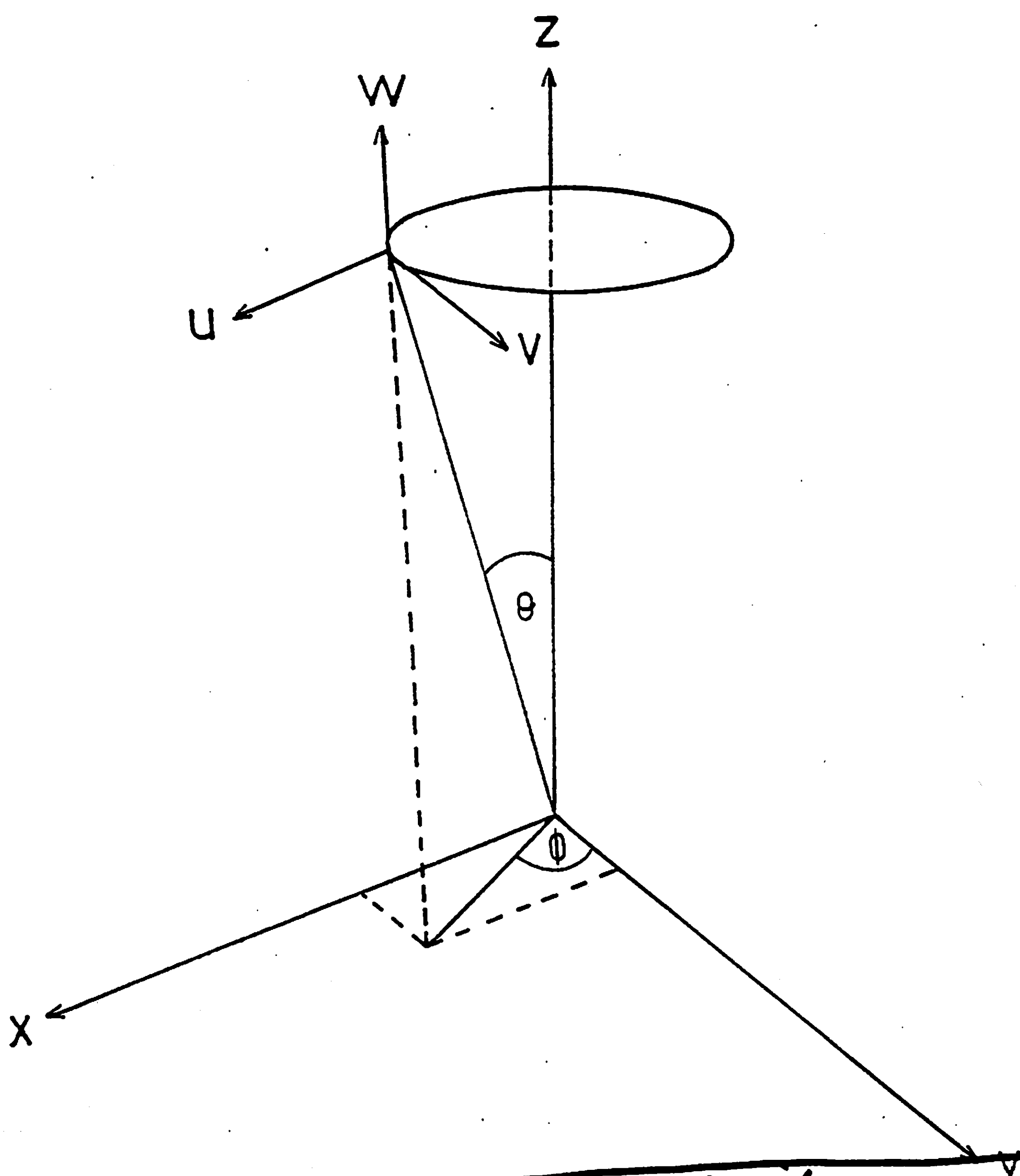

Instantaneous Radial Velocity

$$V_R(R,\theta,\phi) = u\sin\theta\sin\phi + v\sin\theta\cos\phi + w\cos\theta$$

extra

Atmospheric Radars

Doppler Radar

Instantaneous Radial given above

Mean Square Radial

$$
\left.
\begin{aligned}
\overline{V_R'^2}(\phi) = {} & \left(\overline{u'^2}\sin^2\phi + \overline{v'^2}\cos^2\phi\right)\sin^2\theta \\
& + \overline{w'^2}\cos^2\theta
\end{aligned}
\right\} \text{variance terms}
$$

$$
\left.
\begin{aligned}
& + \overline{v'w'}\sin 2\theta\cos\phi \\
& + \overline{u'v'}\sin^2\theta\sin 2\phi \\
& + \overline{u'w'}\sin 2\theta\sin\phi
\end{aligned}
\right\} \text{covariance terms}
$$

Must have a number of Doppler Beam Directions to separate these terms.

extra

Large Scale Motions

mean terms

$$\overline{V_R}(\phi) = \bar{u}_0 \sin\theta \sin\phi + \bar{v}_0 \sin\theta \cos\phi + \bar{w}\cos\theta$$

$$+ \left(\frac{\partial \bar{u}}{\partial x} + \frac{\partial \bar{v}}{\partial y}\right) \frac{R \sin^2\theta}{2}$$

horizontal divergence

$$+ \left(\frac{\partial \bar{v}}{\partial y} - \frac{\partial \bar{u}}{\partial x}\right) \cos 2\phi \frac{R \sin^2\theta}{2}$$

stretching deformation

$$+ \left(\frac{\partial \bar{u}}{\partial y} + \frac{\partial \bar{v}}{\partial x}\right) \sin 2\phi \frac{R \sin^2\theta}{2}$$

shearing deformation

$$\boxed{\text{Must have a number of Doppler Beam Directions to separate these terms}}$$

extra

Spaced Antenna Technique

FCA assumes volume scatter

(however modelling by Holdsworth & Reid [1995a,b] shows that it performs well with as few as five scatterers – which the interferometric techniques do not).

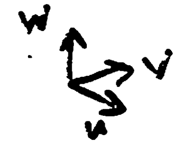

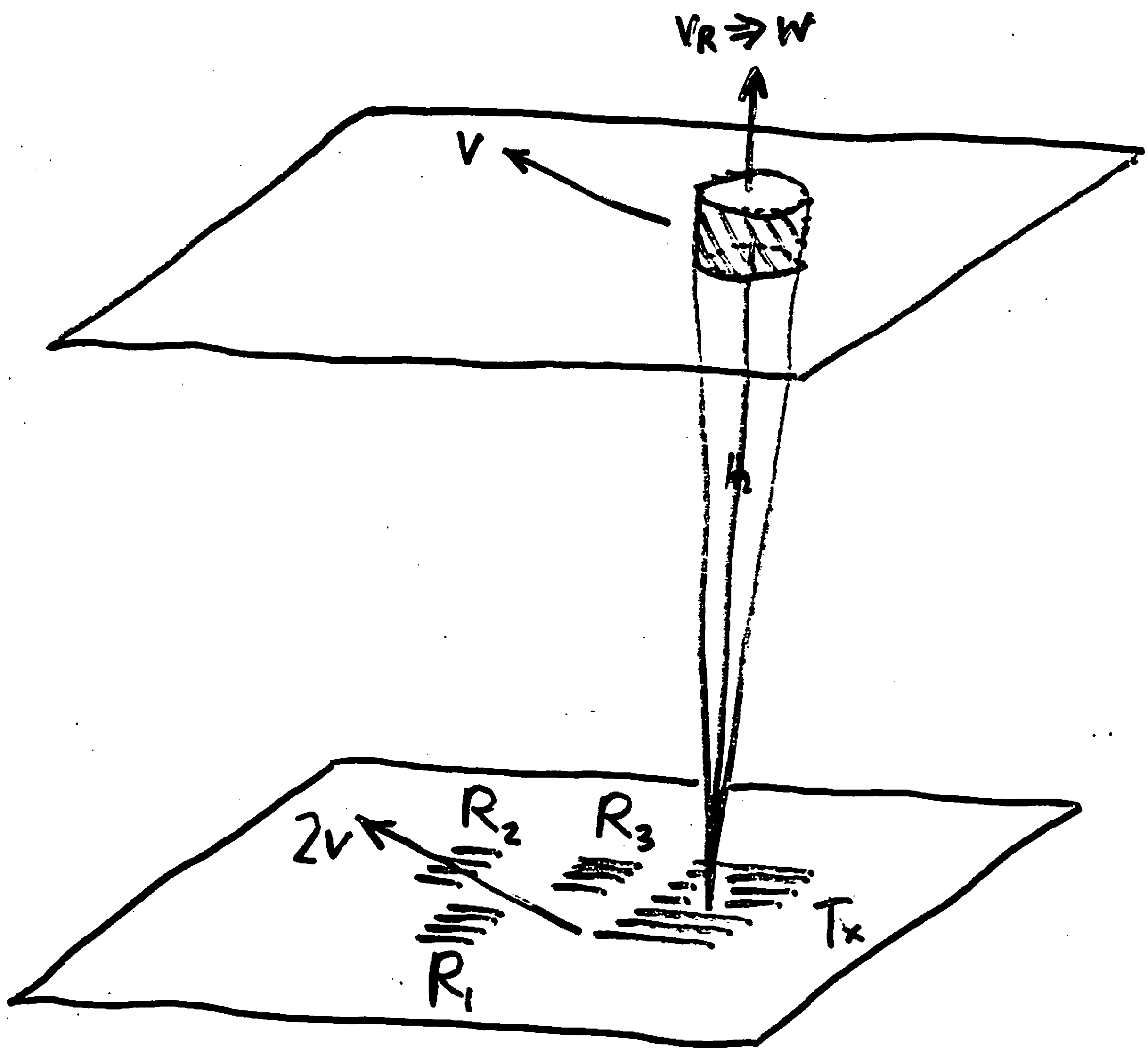

"True" velocity →	correction made for random changes in pattern as it moves across the ground and also for any anisotropy of the pattern
"Apparent" velocity →	no correction.

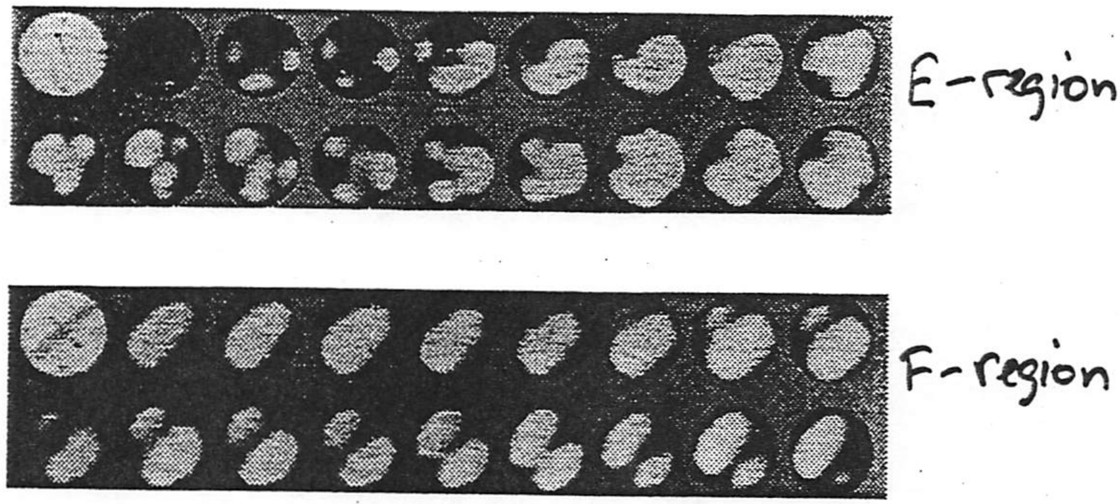

Figure 3.10: Two examples of the evolution of the ground diffraction pattern image obtained by *Felgate and Golley* [1971]. The top figure illustrates a random pattern from a night-time sporadic E-layer obtained at 0.5 s intervals. The bottom plot illustrates a periodic fringe pattern from a night-time F-region layer obtained at 0.75 s intervals.

spacings considerably shorter than the mean pattern scale. The Buckland Park MF array has been successfully employed for this purpose (e.g. *Felgate and Golley*, [1971]). The production of these images allows the application of the spatial correlation analysis (e.g. *Briggs*, [1968]. The production of such images are also especially important for the determination of the mechanisms responsible for the radiowave backscatter, and the verification of the assumptions made by the FCA and about the behavior of the ground diffraction pattern and the spatio-temporal correlation function.

The images of the ground diffraction pattern produced by *Felgate and Golley* [1971] were obtained using the 89 East-West aligned dipoles of the BP MF array. Each dipole was connected to a single receiver. The amplitude of the signal output of each receiver was used to vary the intensity of a small filament lamp. The lamps were arranged in the same configuration as the individual dipoles, and mounted behind a sheet of ground glass in order to smoothen the resulting image. Two examples of the evolution of the resulting ground diffraction pattern image are illustrated in Figure 3.10. The top figure illustrates a random pattern obtained from a night-time sporadic E-layer, while the bottom plot illustrates a periodic fringe pattern obtained from a night-time F-region layer.

The radar backscatter model has been employed to produce similar images of the ground diffraction pattern. The model-generated data-set MOD-MF-GDP-V50 has been produced using the MF simulation parameters without turbulent or gravity wave motions, with a model input velocity of 50 ms^{-1} eastwards. The resulting pattern has been sampled using a 60 by

extra

<u>Formation of moving diffraction pattern</u>
(Briggs, 1980)

Consider the following situation for 2-d radar with scattering from complementary angles, ±θ,

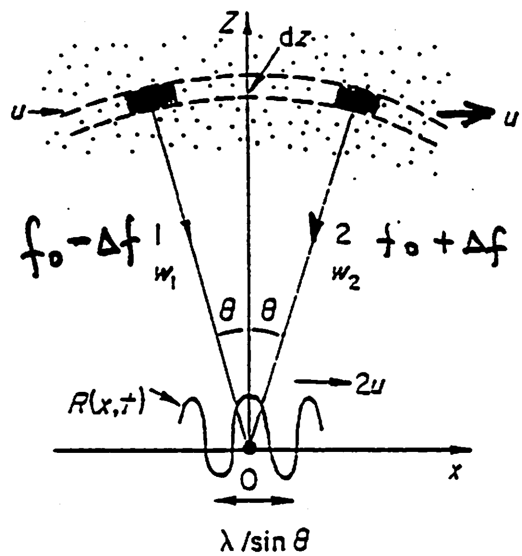

Scatterers move with constant velocity *u* in positive *x*-direction.

Differential Doppler shifts cause Fourier component to move with a velocity of 2*u*.

Random pattern, formed by superposition of components from all θ, moves with velocity 2*u*.

<u>Both Doppler and SA methods rely on scatter from several off-vertical directions to obtain the horizontal velocity</u>

extra

Analysis Techniques

Radar Interferometry

• Interferometric techniques based on estimating the atmospheric wind velocity using located positions for atmospheric radio-wave scatter occurs together with associated radial velocity information.

• At each Doppler frequency ω_i scattering positions located using spectral phase information. For two receivers j and k, the scatterers zenith angle along the line of the receivers θ_{ijk} can be obtained by

$$\theta_{ijk} = arcsin\left(\frac{\phi_{ijk}\lambda}{2\pi D}\right) \tag{7}$$

where ϕ_{ijk} is the phase difference between the receivers for each ω_i, λ is the radar wavelength, and D is the receiver spacing. Scattering positions $\vec{r_i}$ then obtained from zenith angles.

• Scattering positions and radial velocity information for each ω_i used to determine the wind velocity, using a least squares solution to the set of equations

$$\frac{\omega_i}{2k} = -(V_x\hat{x} + V_y\hat{y} + V_z\hat{z}) \cdot \frac{\vec{r_i}}{|\vec{r_i}|}, \tag{8}$$

where $\vec{V} = (V_x, V_y, V_z)$ is the wind velocity, and k is the radar wavenumber.

extra

Interferometry

may assume discrete targets

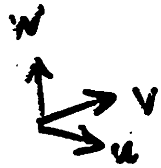

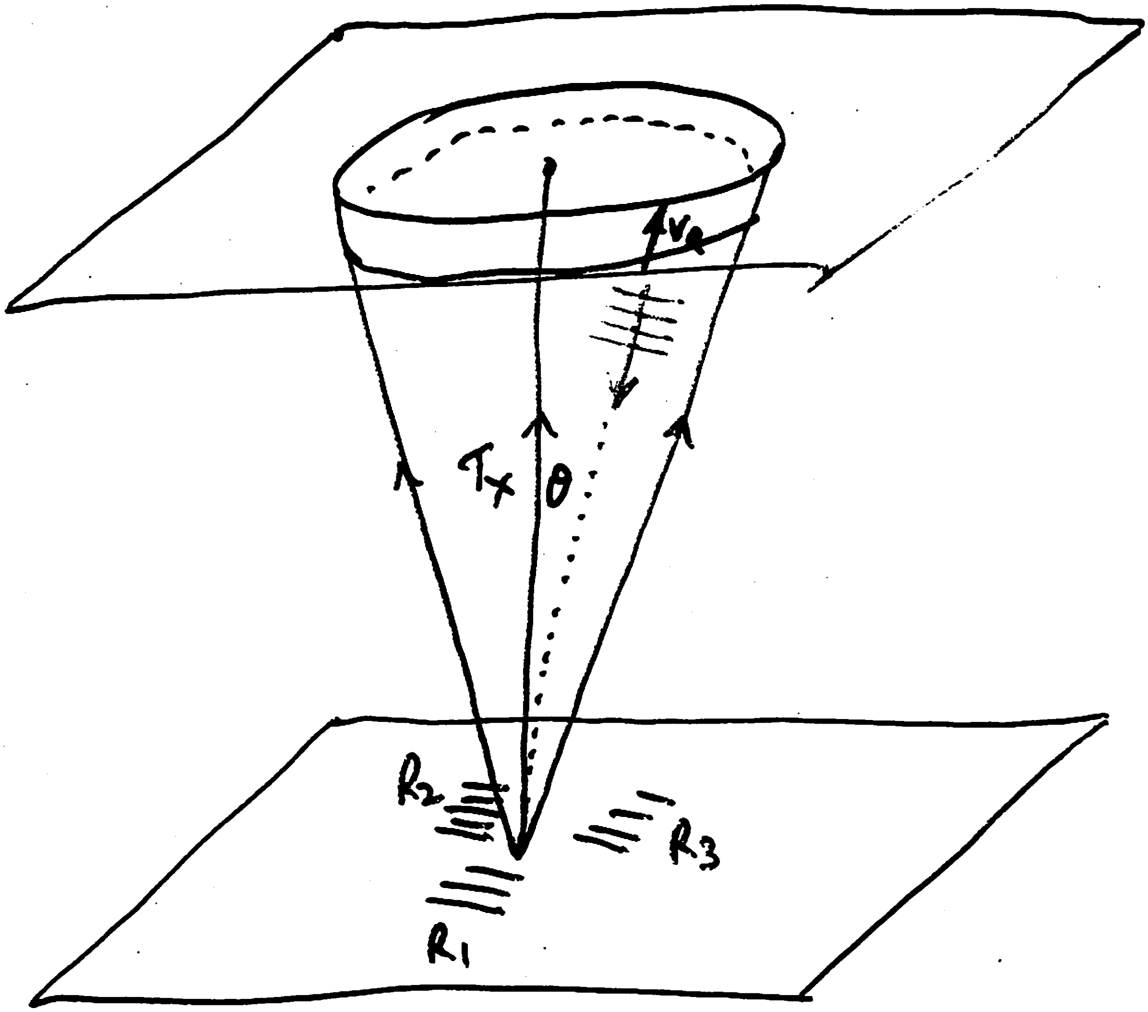

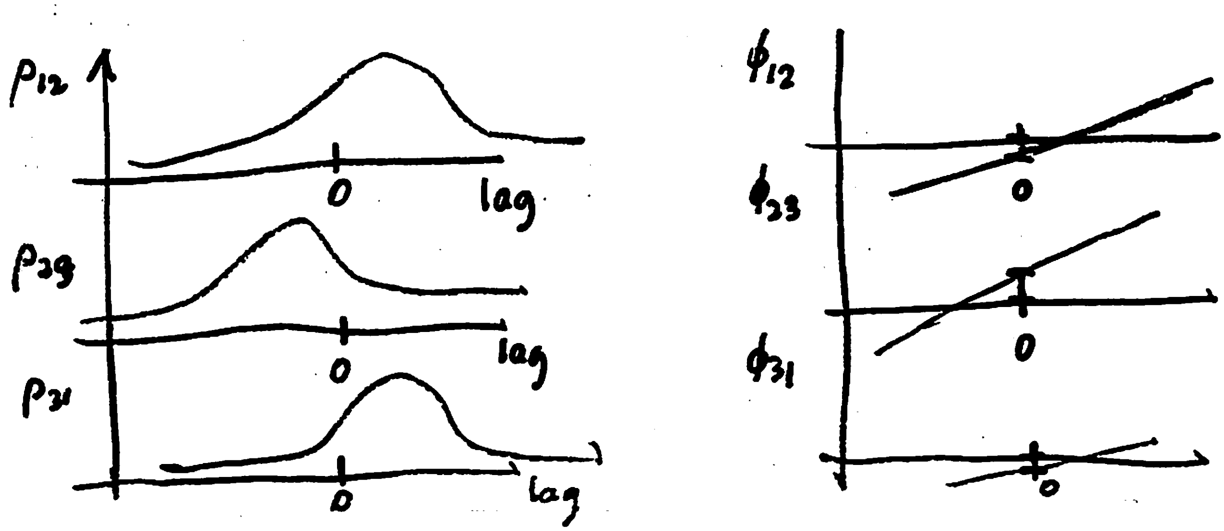

Historical Perspective

- FCA of Spaced Antenna data was applied to *total reflections* from the E-region at MF until the early 1970's. This technique is quite distinct from the analysis of *partial reflection* data and is (unfortunately) called the Spaced Antenna Drift (SAD) technique. It is limited by (and thereby fell into disuse because of):
  - A time-varying reflection height (over which there is no experimental control at a fixed frequency)
  - It is basically a single height determination
  - The possibility of gravity wave contamination in the wind velocities derived

extra

E- REGION "DRIFTS" VS METEOR WINDS

(note: these observations use total reflection)

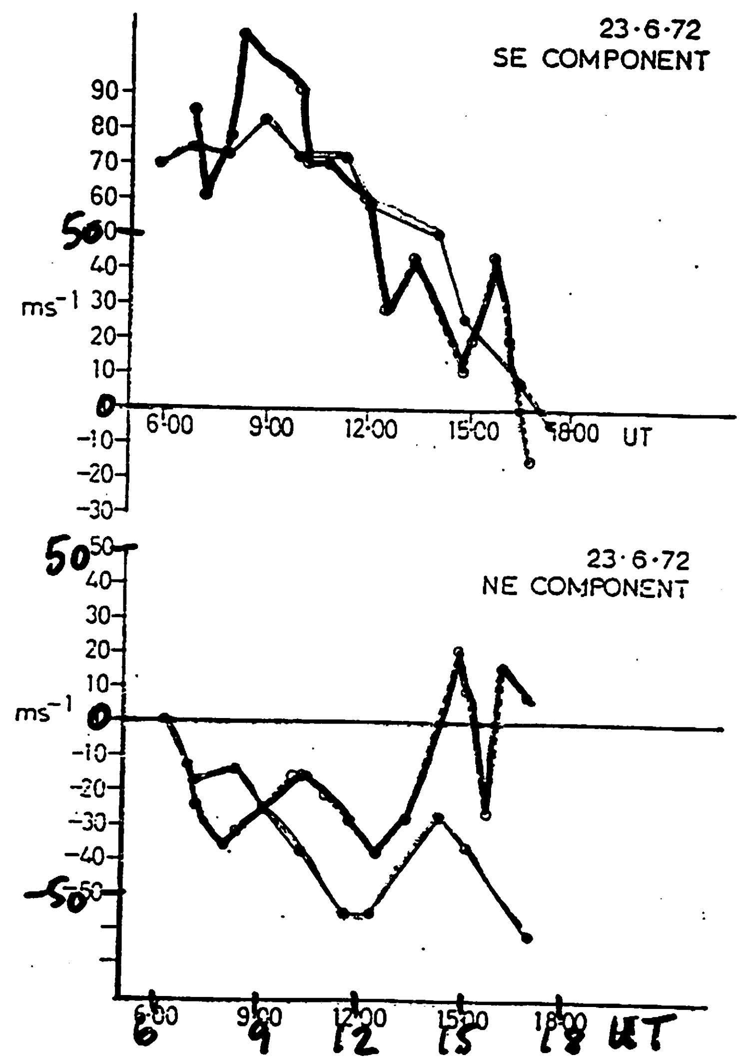

. Ionospheric drifts ●——● measured at Lancaster together with Sheffield meteor winds ⊕——⊙ for 23 June 1972.

Felgate et al., 1975, PSS, 23, 389-400.

extra

D-REGION "DRIFTS" VS METEOR WINDS

(note: these results use partial reflection)

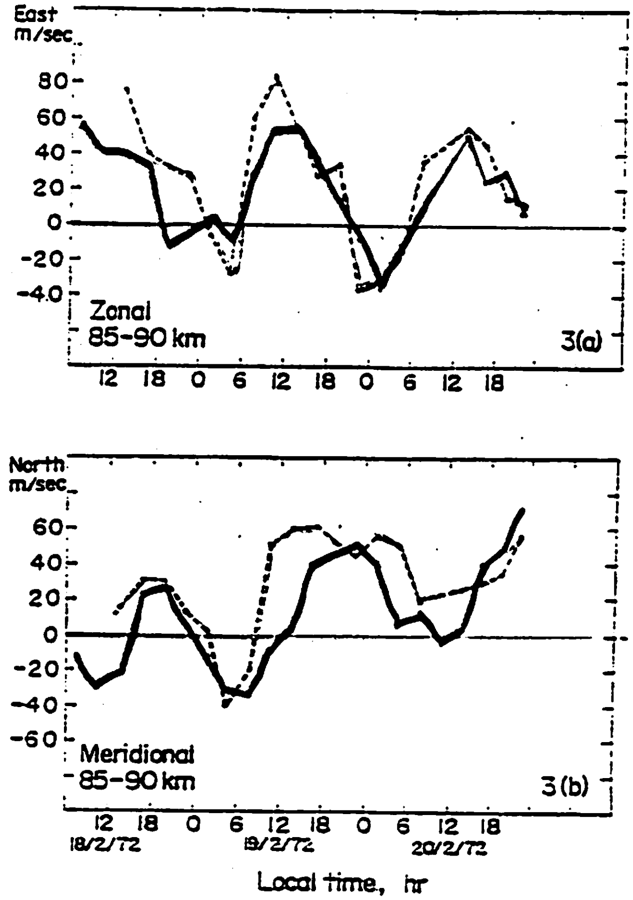

Fig. 3. A 3-day comparison of ionospheric drifts (full lines) and meteor radar estimates (broken lines) for February 1972.

Stubbs(1973)

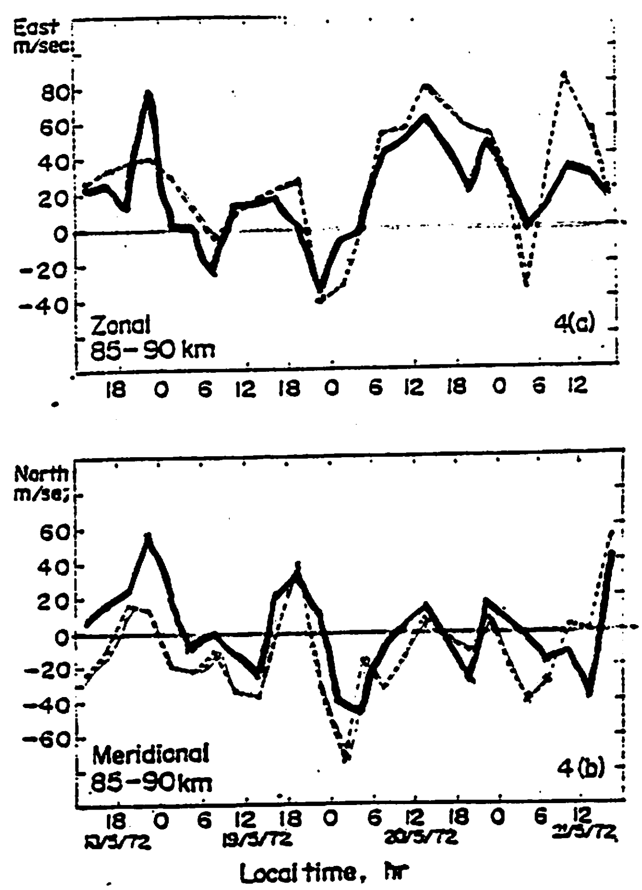

Fig. 4. A 3-day comparison of ionospheric drifts and meteor radar wind estimates for May 1972.

extra

D-REGION "DRIFTS" VS METEOR WINDS

(again partial reflection)

extra

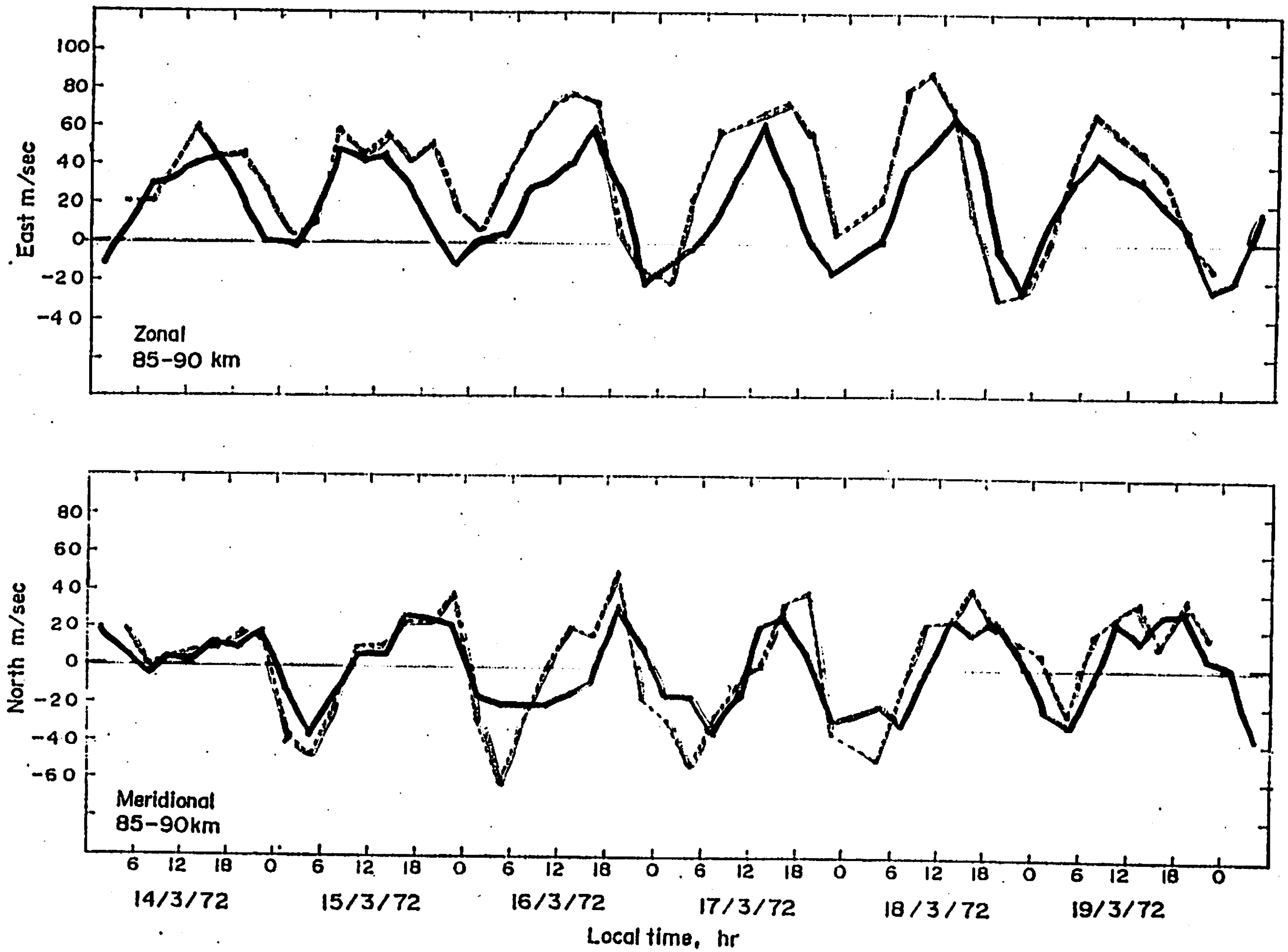

Fig. 2. A 6-day comparison of ionospheric drifts (full lines) and meteor radar wind estimates (broken lines) with each discrete point representing a 3-hourly average.

Stubbs (1973)

MF Techniques are now generally restricted to *partial reflections* in the 60 to 100 km height region. Here:

- The reflection height is known accurately
- Operation over twenty 2 km height gates in the 60 to 100 km height region is possible
- Gravity wave effects, if any, would be the same as those experienced by all atmospheric radars operating up into the Very High Frequency (VHF) band

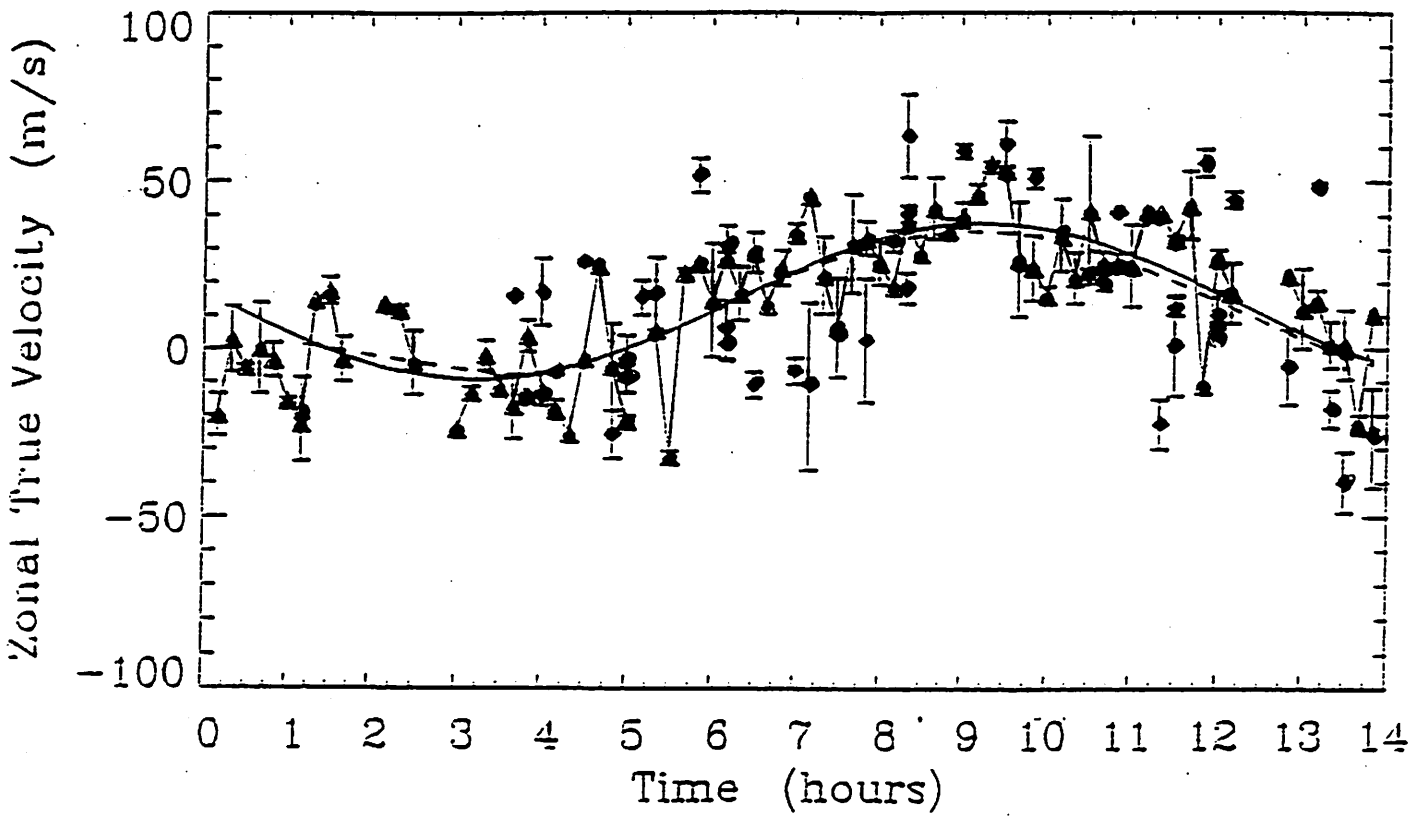

88km Cervera and Reid (1995)

extra

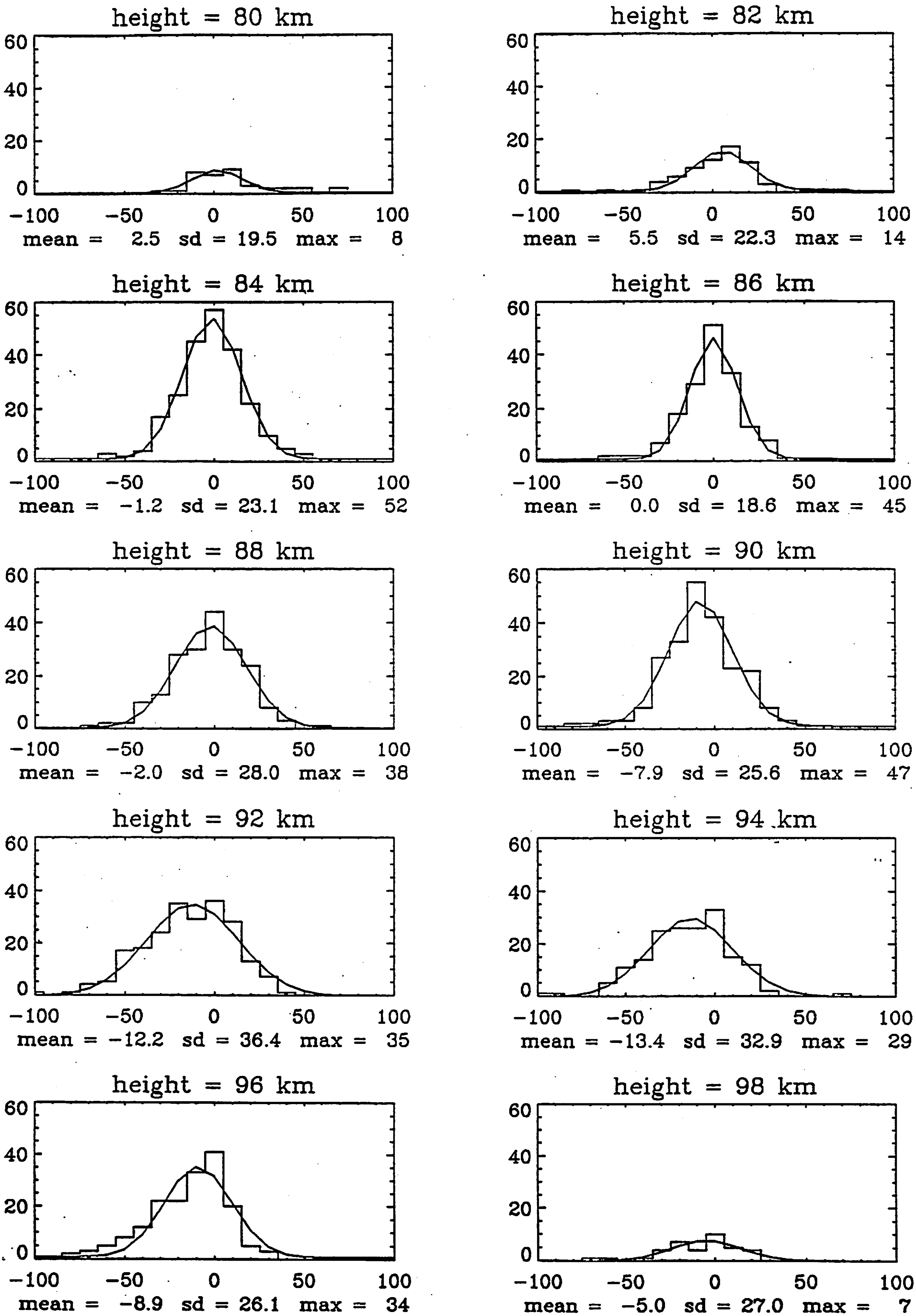

Cervera and Reid (1995)

extra

MF partial reflection from the 60 - 100 km height region

- Still not fully understood
- Different in character above and below about 80 km
  - Above
    - scatter from a range of angles up to about 10 to 15 degrees centered on the zenith
    - mixture of quasi-isotropic and specular scatter
  - Below
    - scatter from a rather more restricted range of angles. Typically less than 5 degrees.
    - rather more specular in character

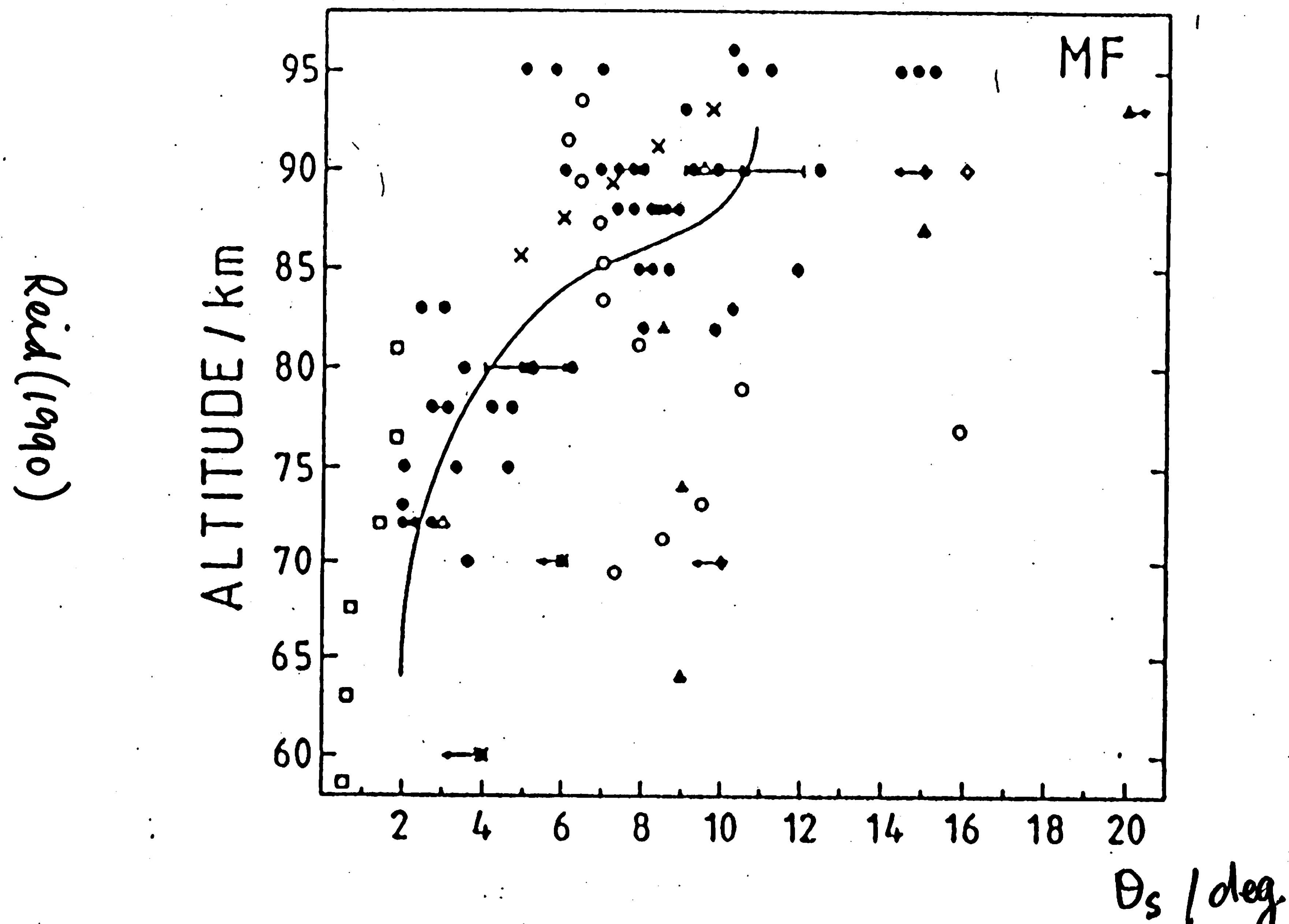
MF
ALTITUDE / km
95
90
85
80
75
70
65
60
2
4
6
8
10
12
14
16
18
20
θs / deg.
Reid (1990)

MF Radars 1

- Mode: Spaced Antenna Technique
- Strengths
  - Moderate to good range and time resolution
    - range ~ 2 - 4 km
    - time ~ 2 - 5 min
  - Good height coverage
    - 60 - 100 km (day)
    - 80 - 100 km (night)
  - Low power, inexpensive to set up and run
  - Reliable continous operation

extra

Plan of M.F. Radar
Pontianak

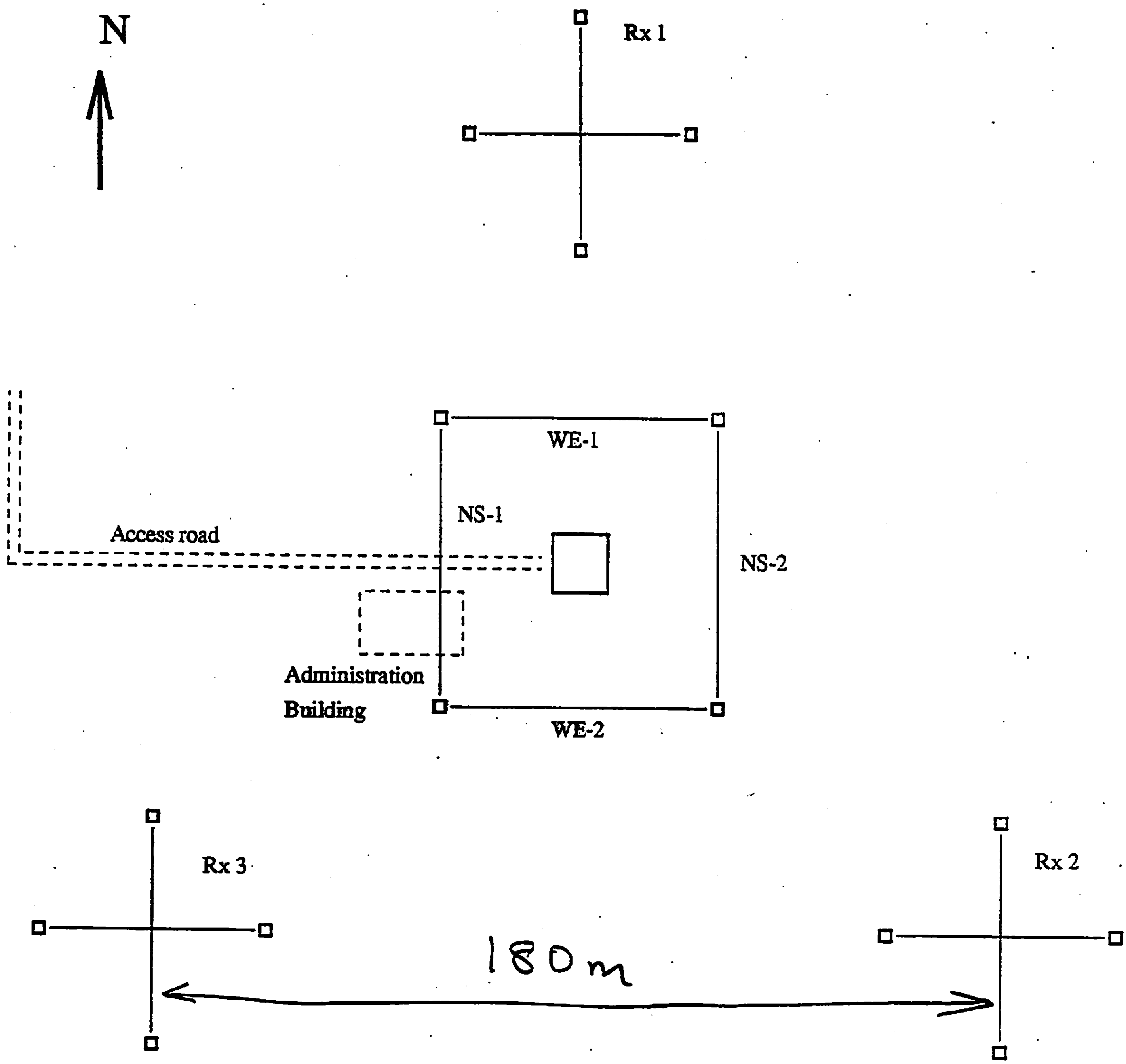

extra

MF Radars 2

- Limitations
  - Small antennas, wide beams. This means that height resolution can degrade if angular scatter is wide (> 10 deg)
  - Group retardation near midday causes incorrect heights to be measured above about 95 km
  - Total reflection occurs near 100 km at MF. This represents an upper limit to the technique during daytime

MF Radars: Practical Considerations 1

- Best triangle shape is equilateral. This reduces the chances of bias
- Optimum antenna spacing depends on
  - Antennas
  - Scattering irregularities
- So a spacing is chosen so that the mean correlation between antennas is about 0.5

extra

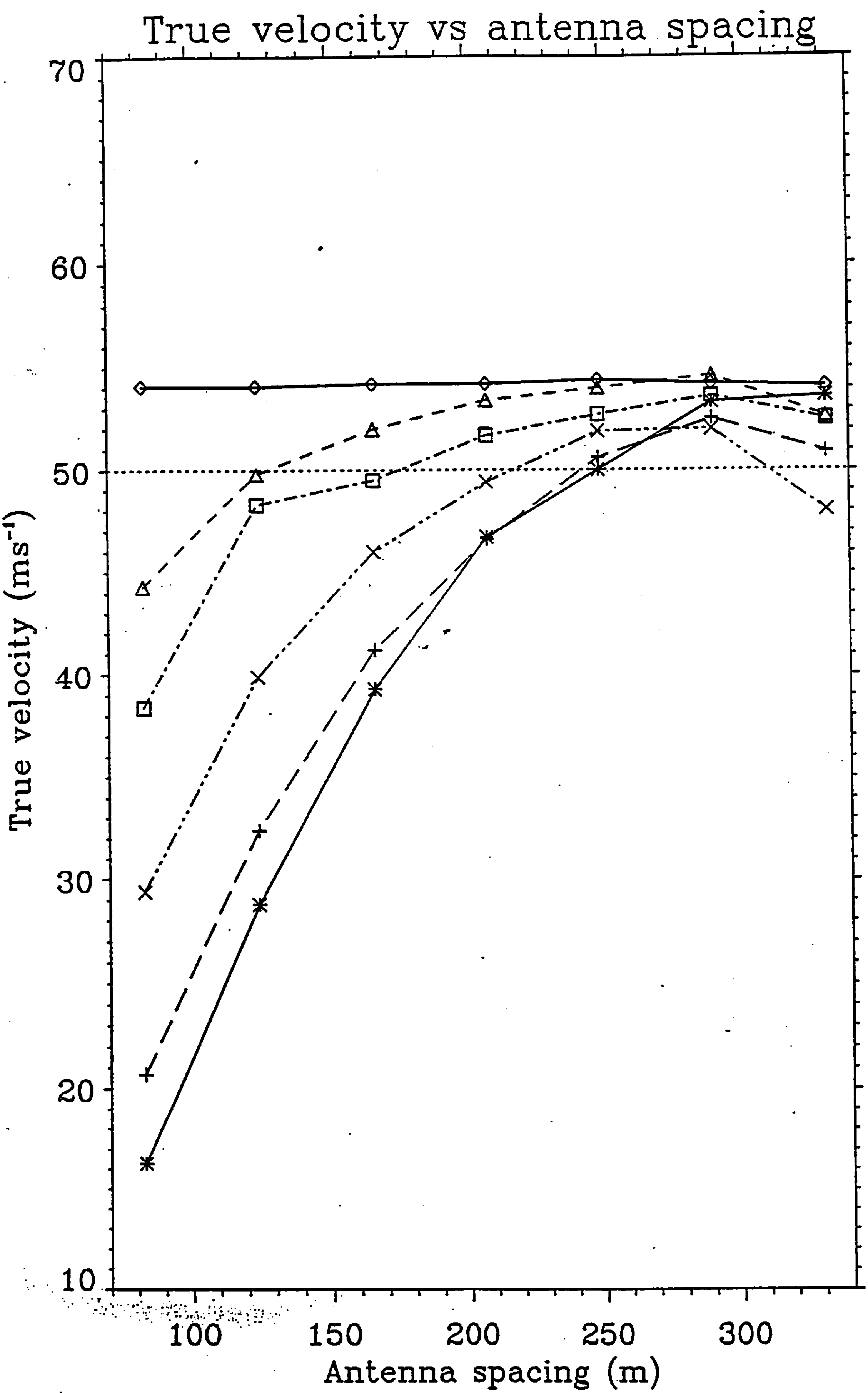

Holdsworth and Reid (1995)

extra

MF Radars: Practical Considerations 2

- Receiver gains, or the gain control scheme, must have sufficient dynamic range to accommodate the huge variation in received power in the 60 - 100 km height range
  - If the receiver channels do saturate, the net result is an underestimation on wind speed. Saturation is likely to occur above 90 km
  - If the receiver channels reach their quantization limits, the net result is again an underestimate in wind speed. This is likely to occur during times of very weak returns

extra

EFFECT OF Rx SATURATION

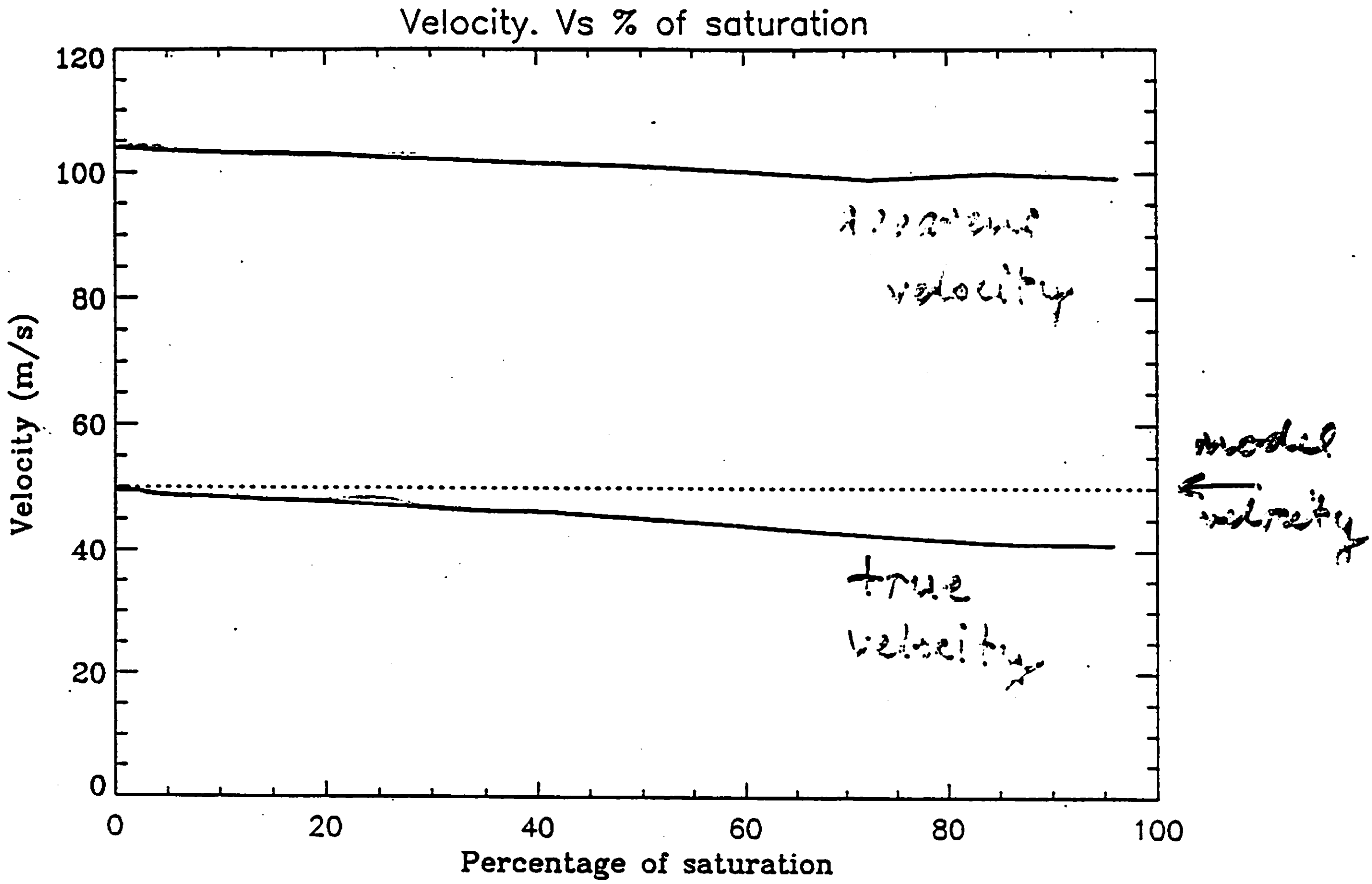

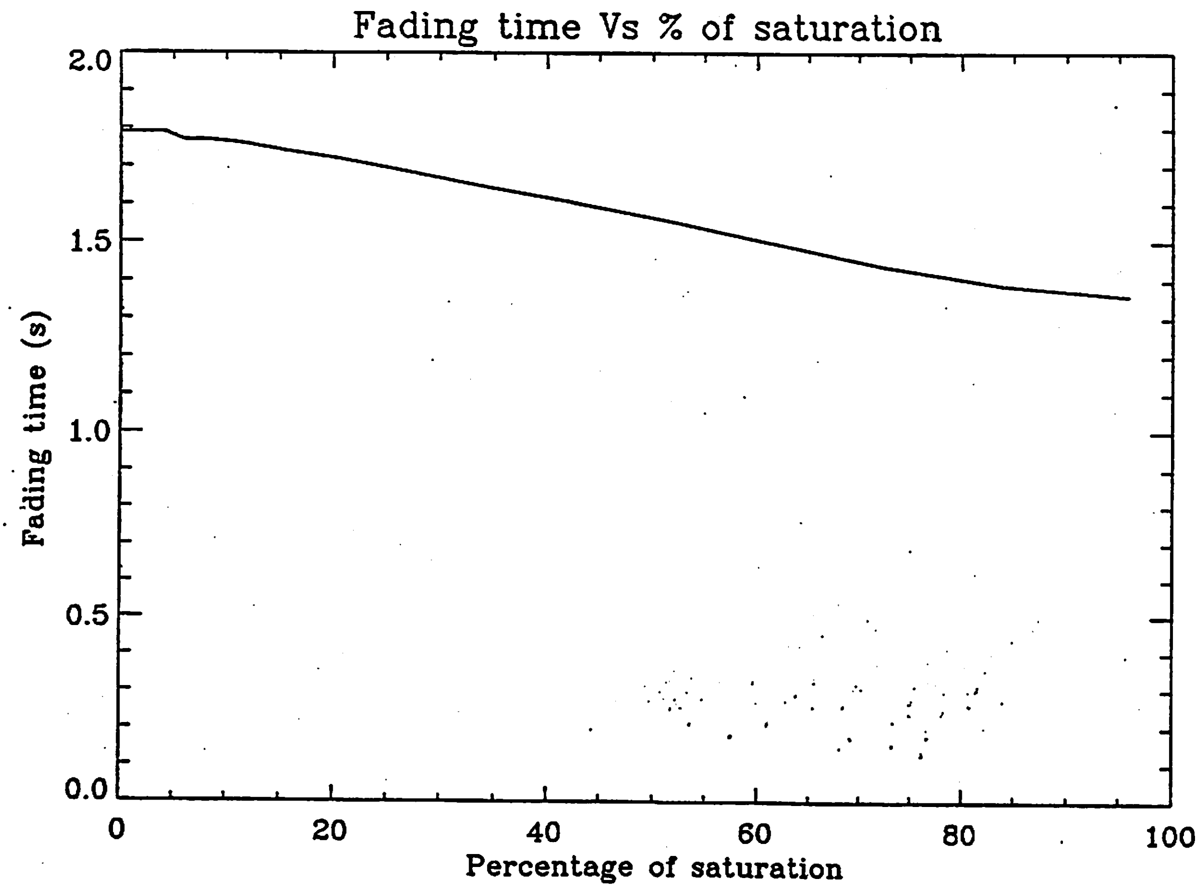

Holdsworth (1995)

extra

MF Radars: Practical Considerations 3

- The sampling rate must be sufficient to adequately sample the pattern as it moves across the antennas. If the sampling is too slow, there will be an upper limit to the wind speeds that can be measured. (This is similar to aliasing with a Doppler radar.) In practice this will depend on wind speed, antenna spacing, and fading times (a measure of turbulent intensity).

extra

MF Radars: Practical Considerations 4

- There is a tendency for the derived velocity to be too small if antennas are too closely spaced (cf. Doppler velocities if pointing angle is too small)
- Best operating frequency
  - Scattered power goes as $1/f^2$
    - This favours a lower frequency
  - Reflection height goes as f
    - This favours a higher frequency
  - Noise
    - Mainly man-made
  - Need to avoid Martitime Safety Frequencies

extra

MF Radars: Recent Developments

- **Modeling and observational comparisons of various SA analysis techniques.**
  - **- Full Correlation Analysis (FCA).**
  - **- Full Spectral Analysis (FSA).**
  - **- Interferometry.**
  - **→ FCA most robust technique.**

- **Underestimation of Velocity**

  Noise.

  Signal saturation.

  Digitizer quantization.

  Undersampling.

  → All lead to depression of correlation functions.

  → Cross-correlation affected more than Autocorrelation function.

  "Triangle-size effect".

- **Four-receiver Spatial Correlation technique.**

MF Radars operating as interferometers

- Mode: Interferometric (Many varieties)
- It has been shown
  - Theoretically (Vandepeer & Reid, 1995a; Briggs, 1995)
  - Experimentally (Brown, 1995; Franke et al., 1990; Meek & Manson, 1987; Vandepeer & Reid, 1995b), and by
  - Using modelling (Holdsworth & Reid, 1995a,b)
- that most interferometric techniques do not measure the background wind velocity
- This is a result that is independent of radar operating frequency

- but interferometry does work for total reflection at MF on occasion

Holdsworth and Reid (1995)

Radar backscatter model

• Selected number of scatterers randomly distributed throughout scattering volume. These scatterers represent regions of refractive index irregularities, rather than physical objects.

• At each sampling time the complex returns from scatterers within the radar-pulse volume are added. The amplitude of the complex return for the ith scatterer is given by

$$a_i = p_i R_i \sqrt{P(\theta_i)}, \tag{1}$$

where R_i is a range gate function varying from unity in the middle of the range gate to zero at the outside, and p is a random reflectivity ratio, and

$$P(\theta) = exp\left(-\left(\frac{sin\theta}{sin\theta_s}\right)^2 - \left(\frac{sin\theta - sin\theta_a}{sin\theta_b}\right)^2\right), \tag{2}$$

where θ_b is the effective beam-width, θ_a is the beam pointing angle, and θ_s is the aspect sensitivity.

• For a large number of scattering positions, the model is not a "point scatterer model". It corresponds to a random array of diffracting irregularities, each of which has a polar diagram corresponding to θ_s, and thus corresponds to a "volume scatter model". For a small number of scatterers, the model corresponds to a discrete scatter model.

extra

Analysis Techniques

Radar Interferometry

• There exist~~s~~ a number of subtlely different interferometric techniques, using different criteria to determine whether the spectral information for each Doppler frequency is consistent with the returns from a single scattering location.

• IDI uses two orthogonal rows of equally spaced antennae. Only Doppler frequencies where a linear phase variation is seen along both rows of antennae are used for the analysis. The receiver phase difference obtained from the line fitted to this phase variation is used in place of ϕ_{ijk} in equation 7.

• MSIRI uses only Doppler frequencies where a local maxima is seen in the spectral magnitude.

• NSIRI uses no single scatterer criteria.

• Experimental results indicate IDI, MSIRI and NSIRI using smoothed spectra give the FCA apparent velocity, while NSIRI using unsmoothed spectra gives the FCA true velocity.

extra

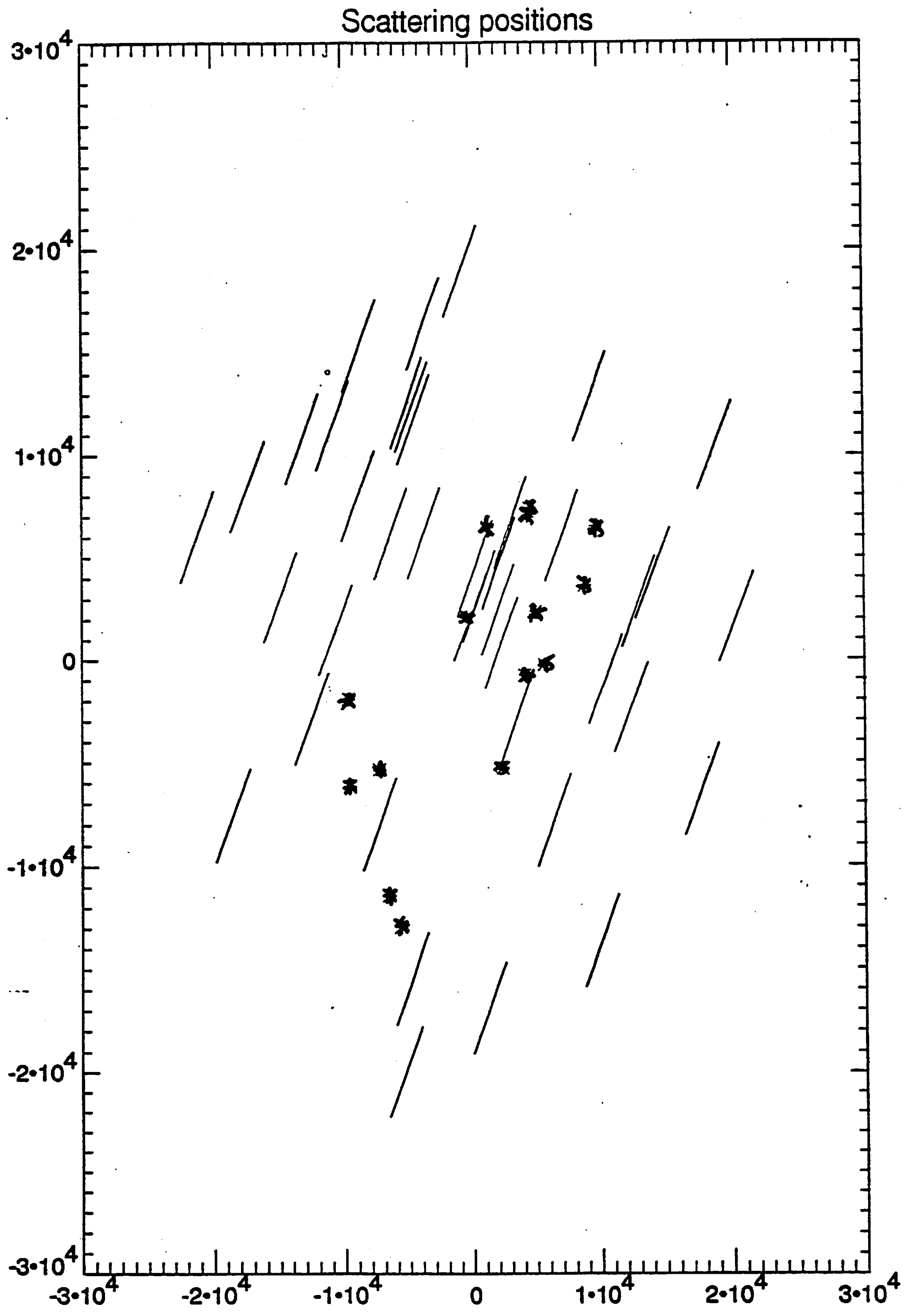

Holdsworth (1995)

extra

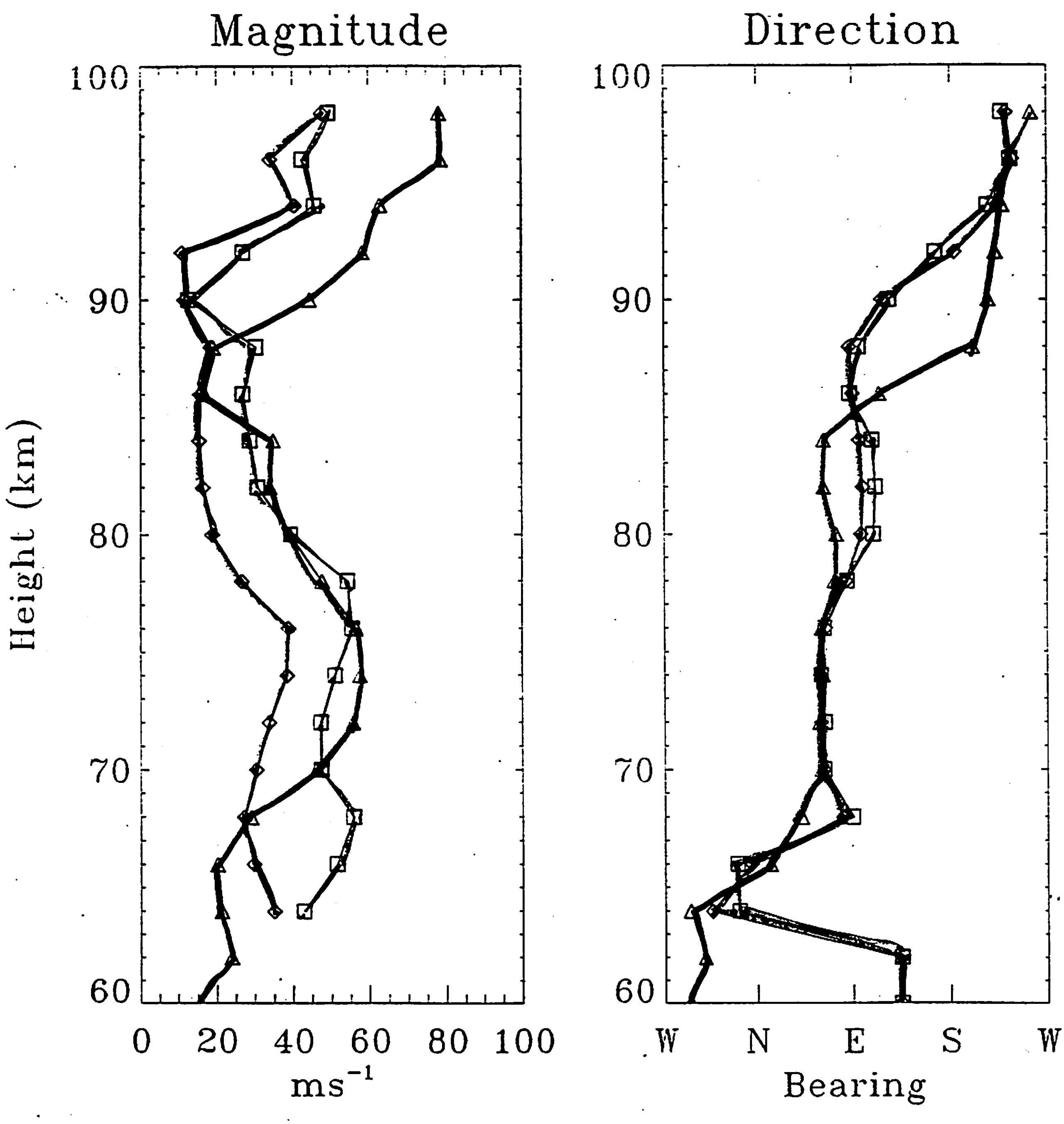

◆ = spaced antenna true velocity
■ = spaced antenna apparent velocity
▲ = IDI velocity

Vandepeer and Reid (1995)

extra

FRANKE ET AL GRL, 17, 2193-2196, 1990

extra

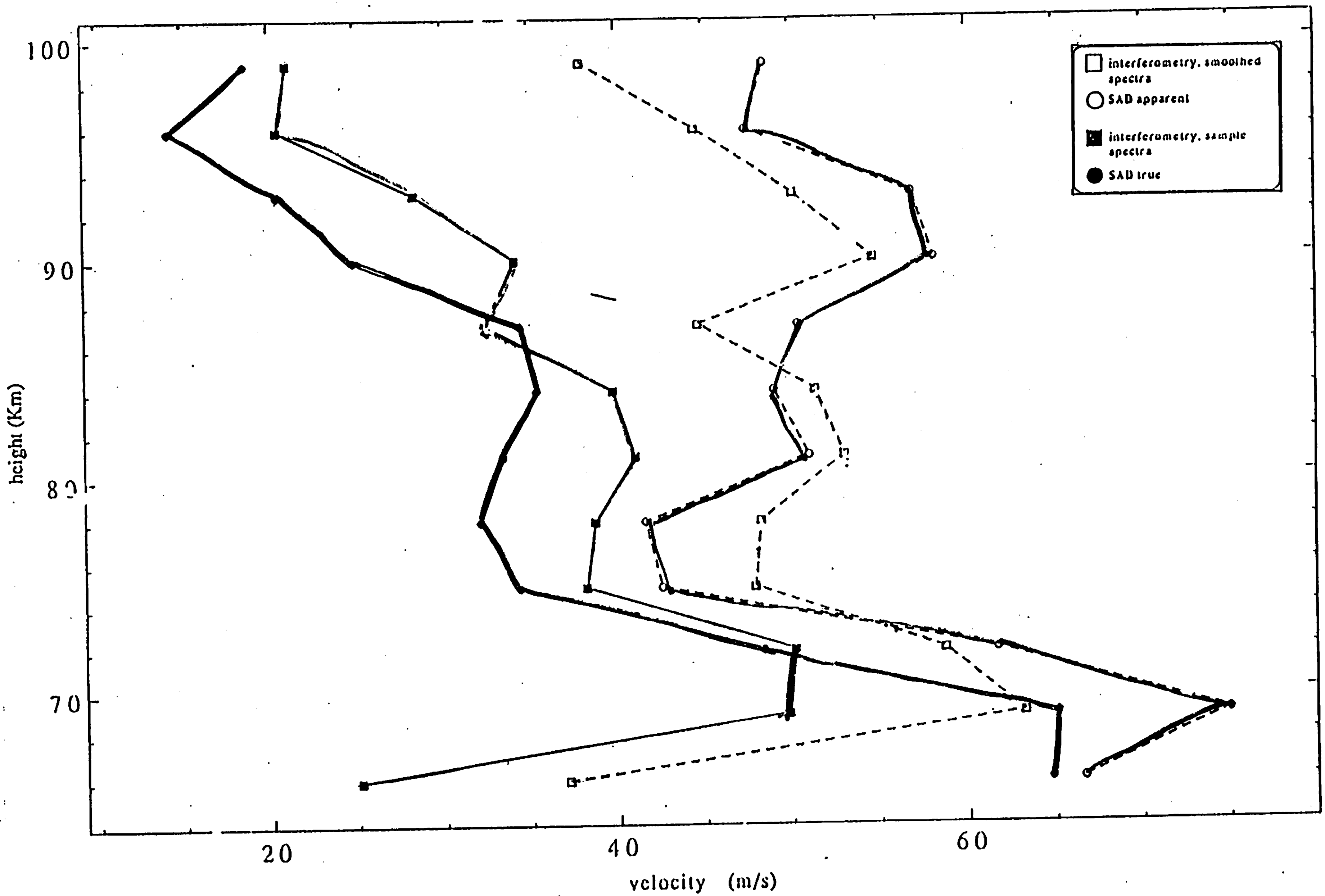

Figure 2: Velocity profiles of estimates averaged over the entire nine hours, representing the SA true and apparent velocities, and interferometric velocities obtained using sample cross-spectra and smoothed cross-spectra.

Why?

- They fail to take account of the changes of the ground diffraction pattern with time. This means they measure something between the correct wind speed and the "apparent wind speed"

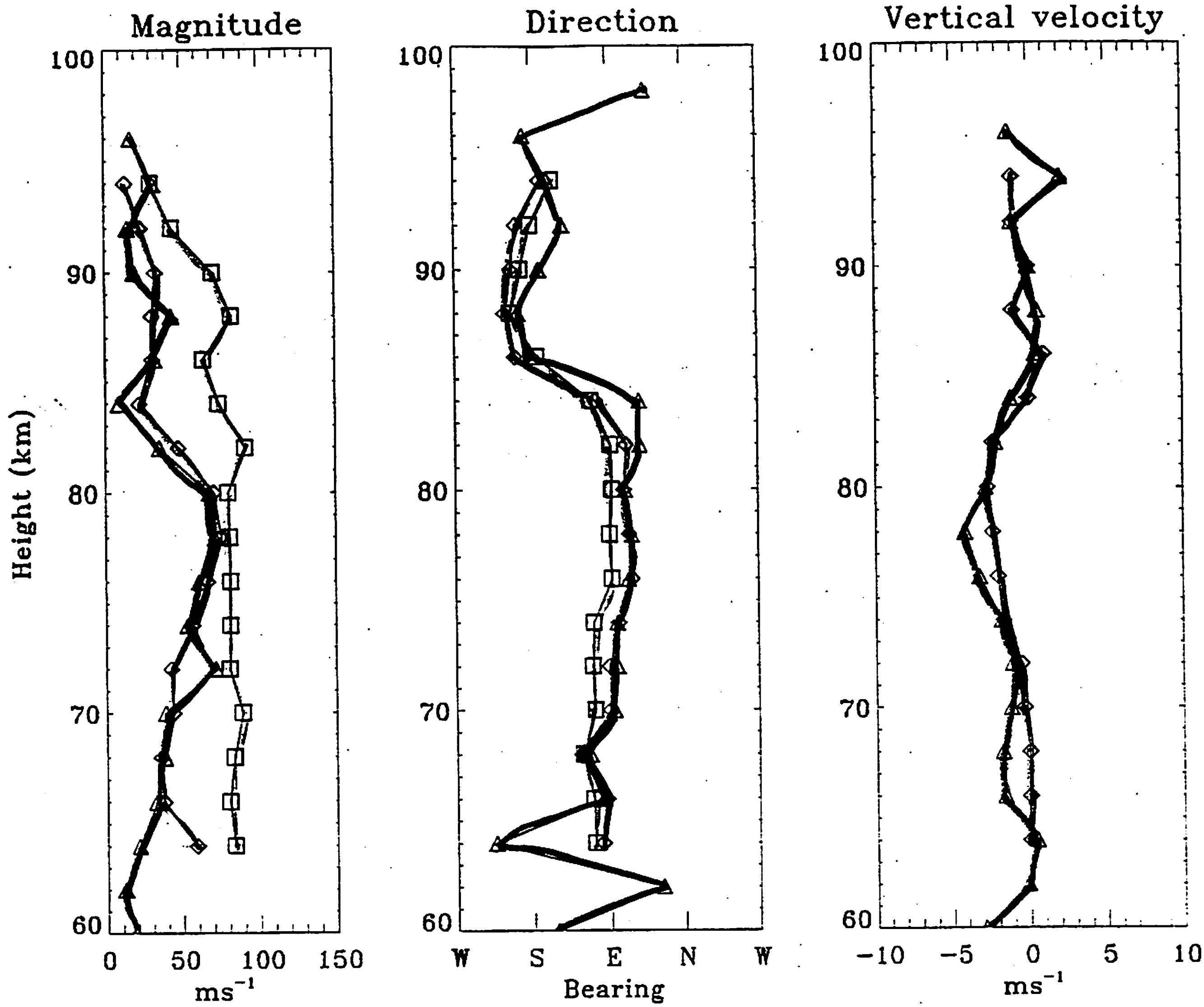

◆ = spaced antenna true velocity

■ = spaced antenna apparent velocity

▲ = TDI velocity

Vandepeer and Reid (1995)

extra

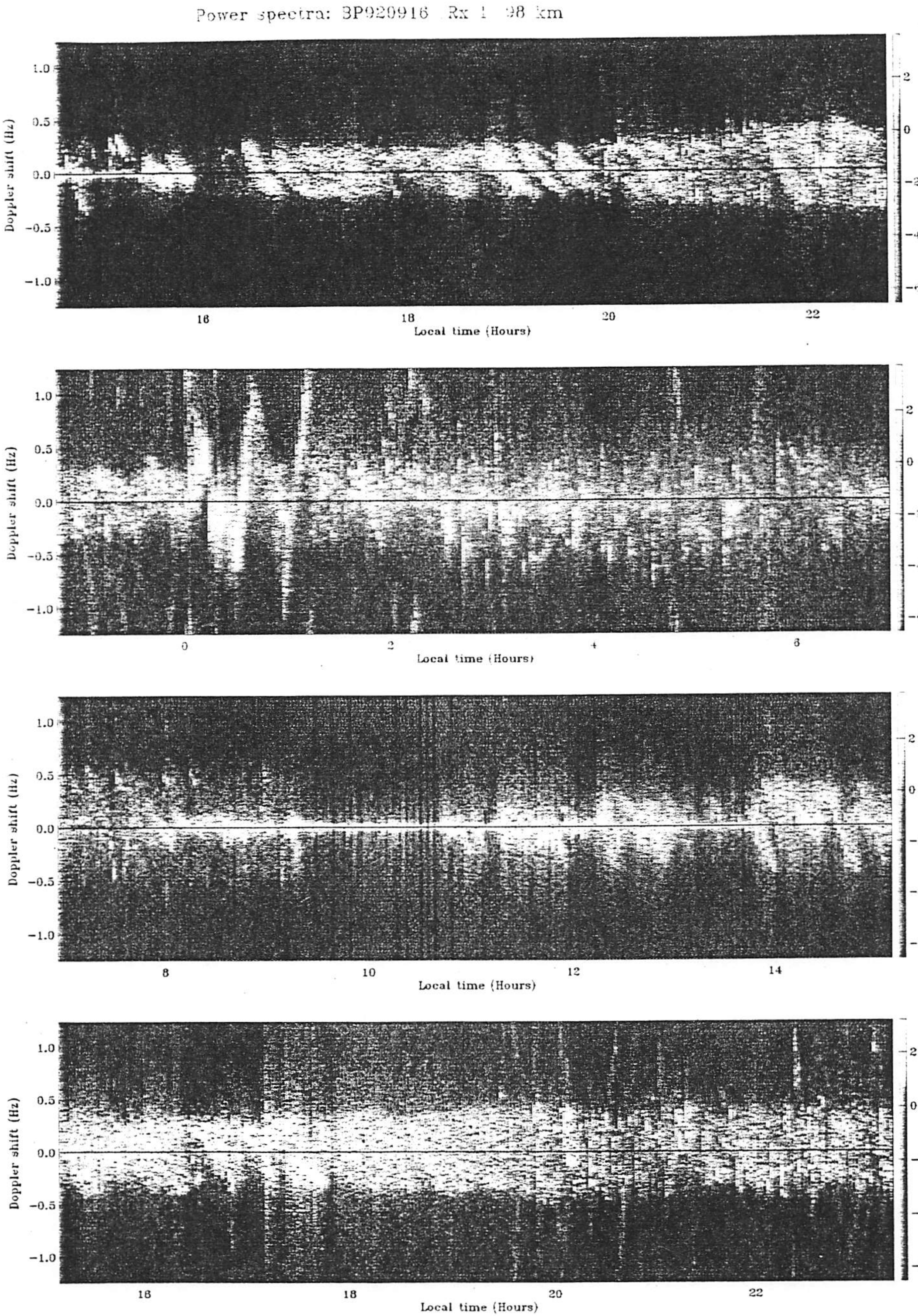
Power spectra: 3P920916 Rx 1 98 km
Doppler shift (Hz)
Local time (Hours)
1.0
0.5
0.0
-0.5
-1.0
16
18
20
22
0
2
4
6
8
10
12
14
2
0
-2
-4
-6

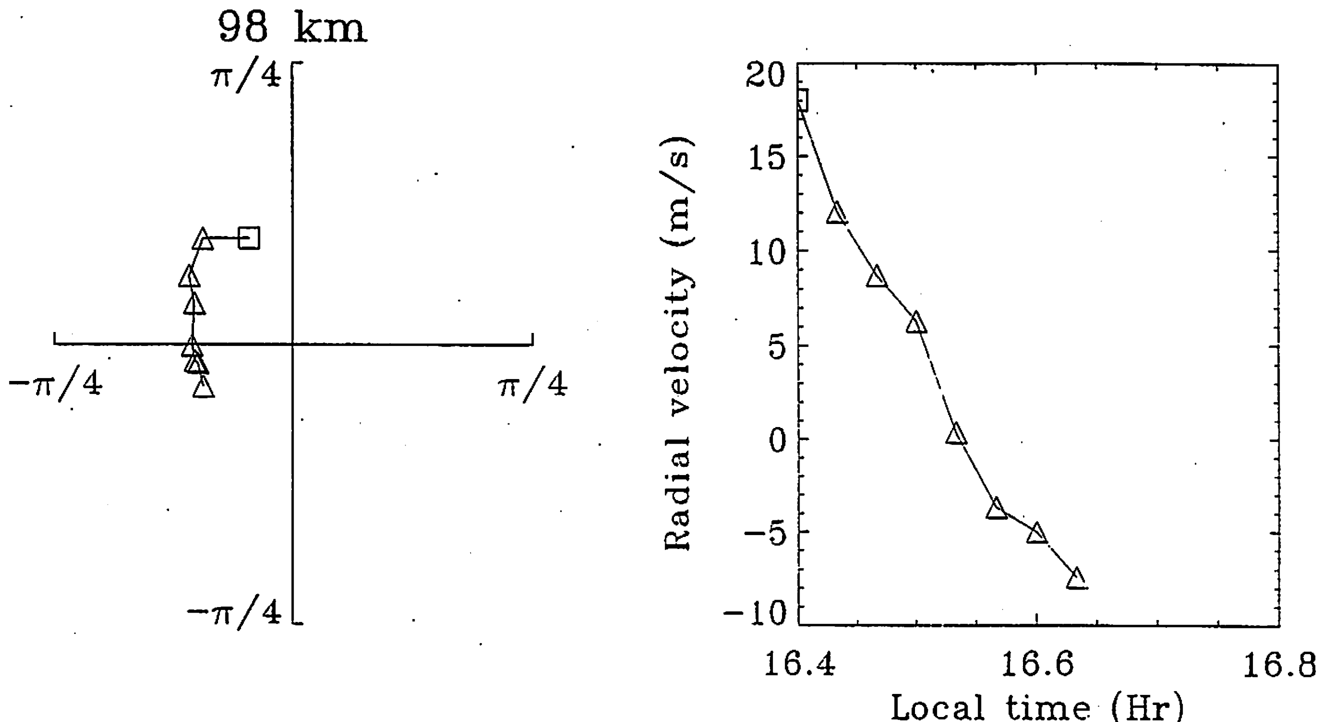

98 km
π/4
−π/4
−π/4
π/4
20
15
10
5
0
−5
−10
Radial velocity (m/s)
16.4
16.6
16.8
Local time (Hr)

(a) (b)

extra

METEOR RADARS

Operating Frequencies - ~ 30 MHz

Mode - cw and/or pulsed

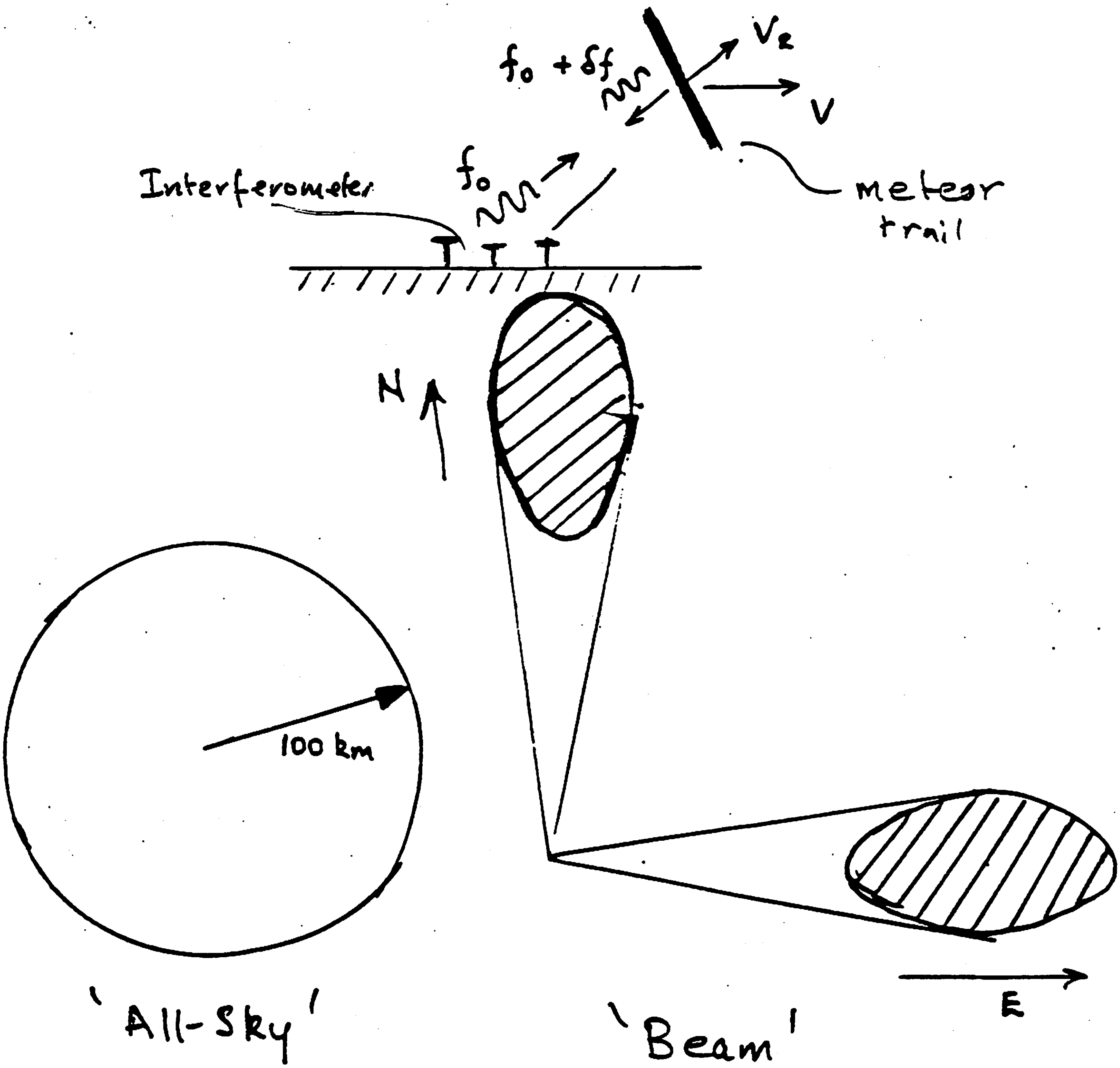

Meteor Radars 1

- Mode: All Sky
- Typical frequency around 30 MHz using either pulsed or CW transmission
- Meteors detected using interferometric techniques

extra

Meteor Radars 2

- Mode: narrow beam
- Typically piggy-backed on an ST or MST radar
- Operational frequencies generally around 50 MHz
- Radial velocity of the drift of the meteor ionization trial within beam is measured using standard Doppler technique.

extra

Meteor Radars 3

- Strengths
  - Reliable
  - 24-h observations
  - Continuous long-term observations ~~fro lomg~~ for long period winds and tides
  - May be possible to infer T'/T from diffusion of trails
- Limitations
  - Large diurnal variation of echoes
  - Large spatial average
  - Height coverage 80 - 105 km
  - Low echo rates (~500 - 1000 day)

extra.

Meteor Radars 4

- Limitations (cont.)
  - With narrow beam technique:
    - not always possible to discriminate echoes detected in side-lobes
    - response function may allow considerable variation in the actual azimuth and zenith of the echo
  - Results may still be dependent on the analysis scheme used (see eg., Valentic et *al*., 1996)

extra

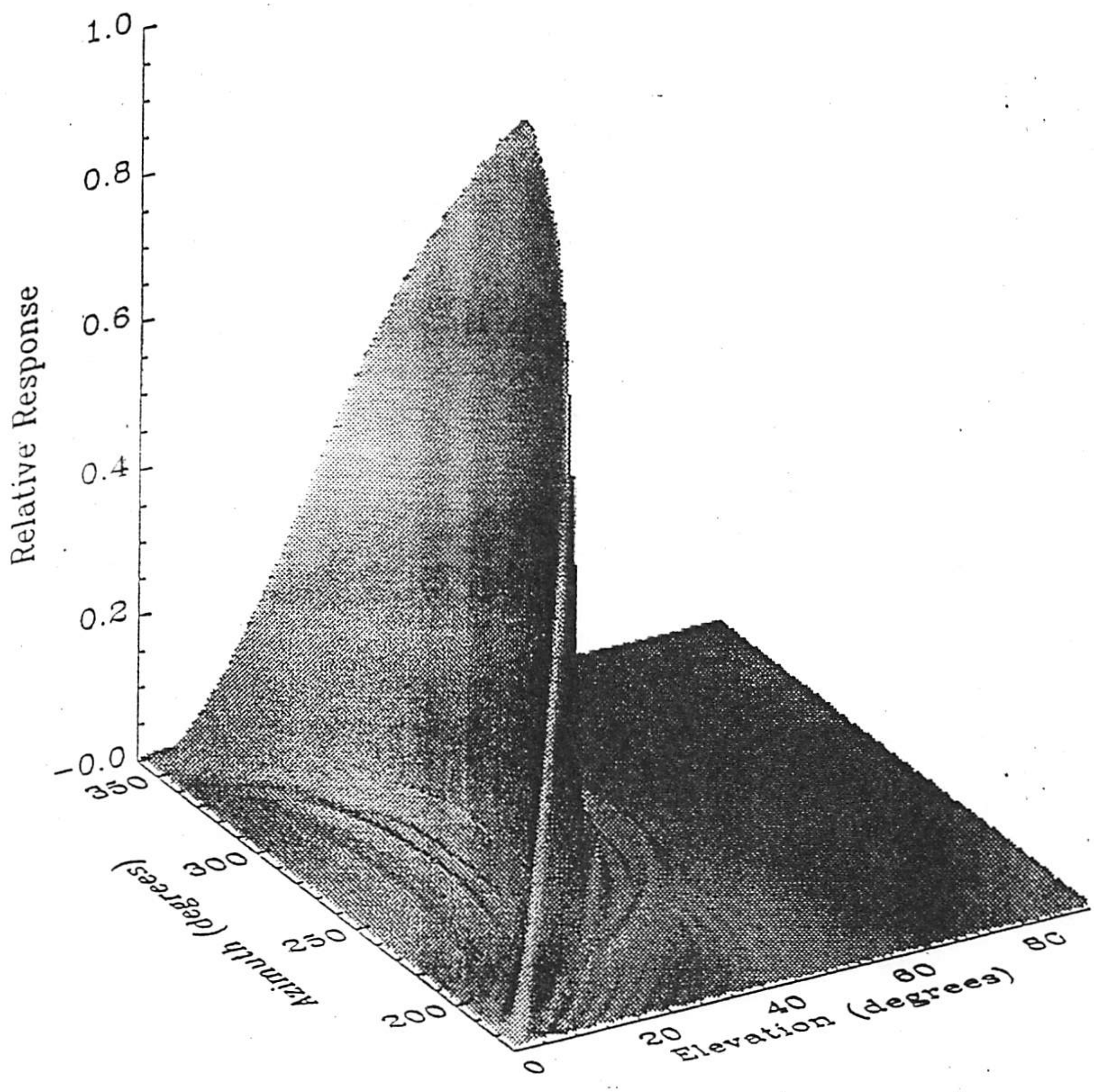

Figure 4.4: The response function (normalized to the peak response) of the Buckland Park VHF radar for an Eastward pointing (azimuth : 84°) beam. The initial geocentric velocity of the meteoroid is 30 $km\ s^{-1}$.

Cervera (1995)

Meteor Response Function vs Zenith angle

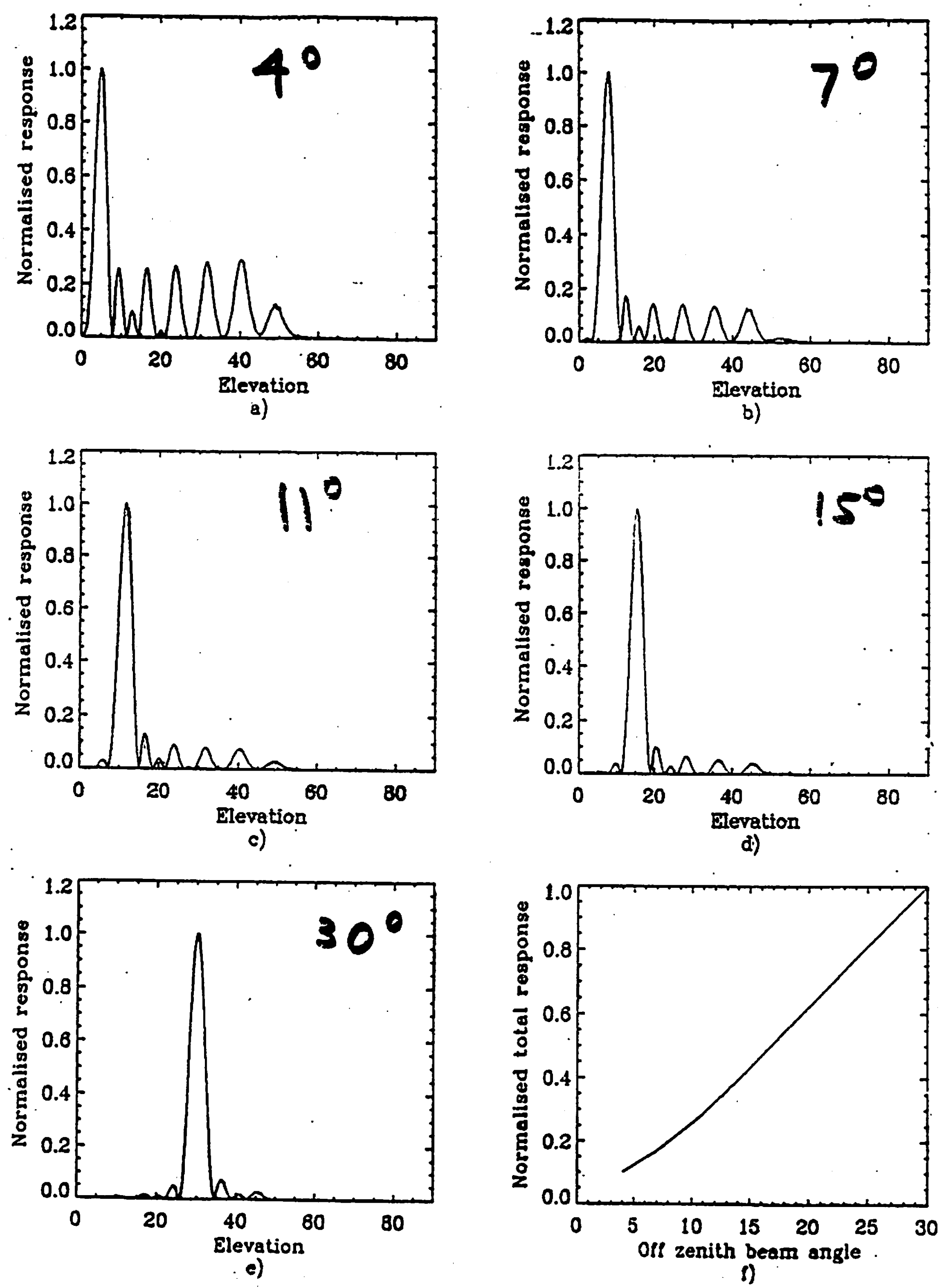

Cervera (1996)

Total Response Function
Adelaide VHF Radar
$\theta = 30°$

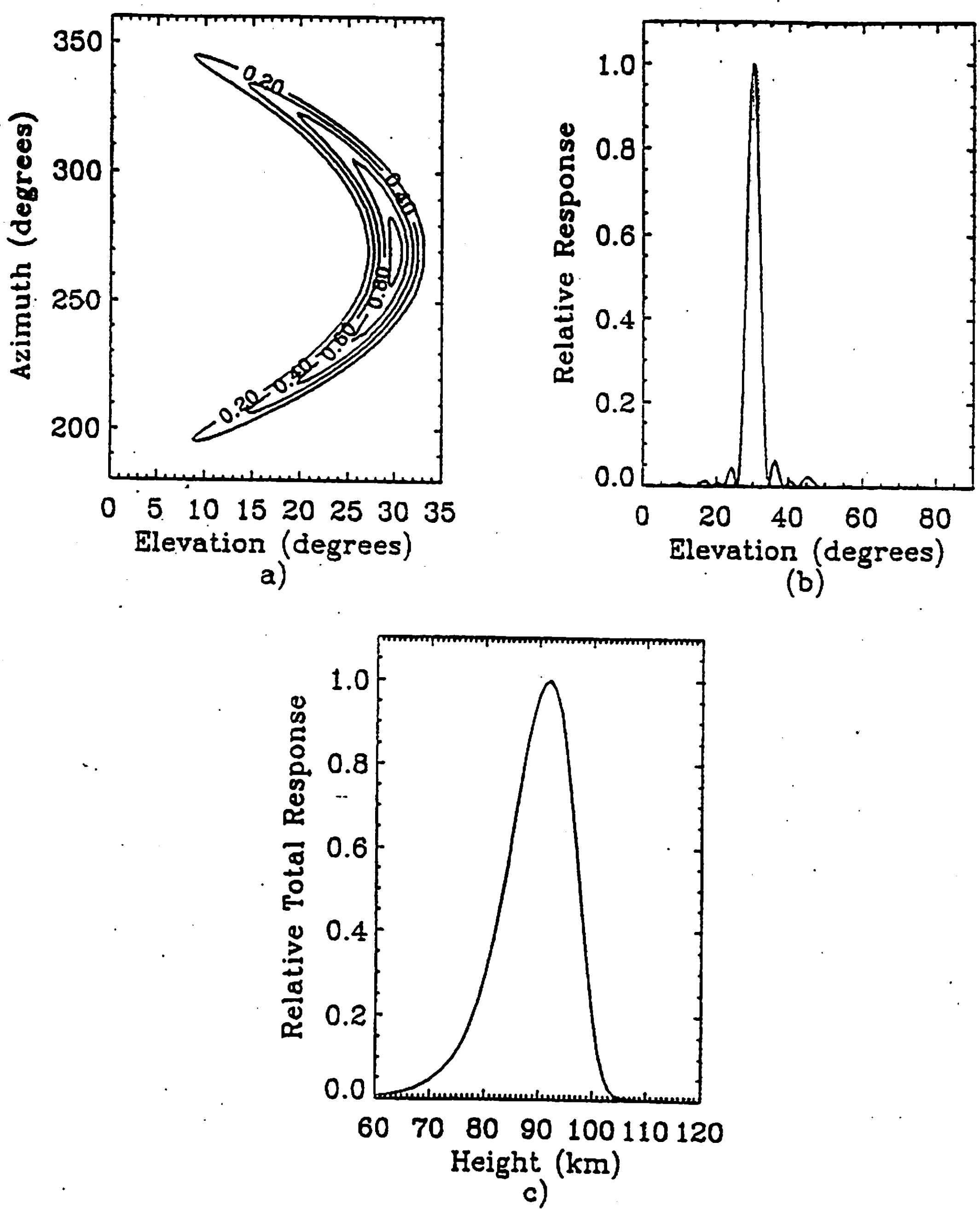

a) (b) c)

~ 8-10% sidelobe contribution $\Rightarrow$ need for interferometry

Cervera (1996)

HRDI / WINDII

- HRDI
  - several hundred km averages in the meridional direction. Sharp gradients in tides, winds may colour results

extra

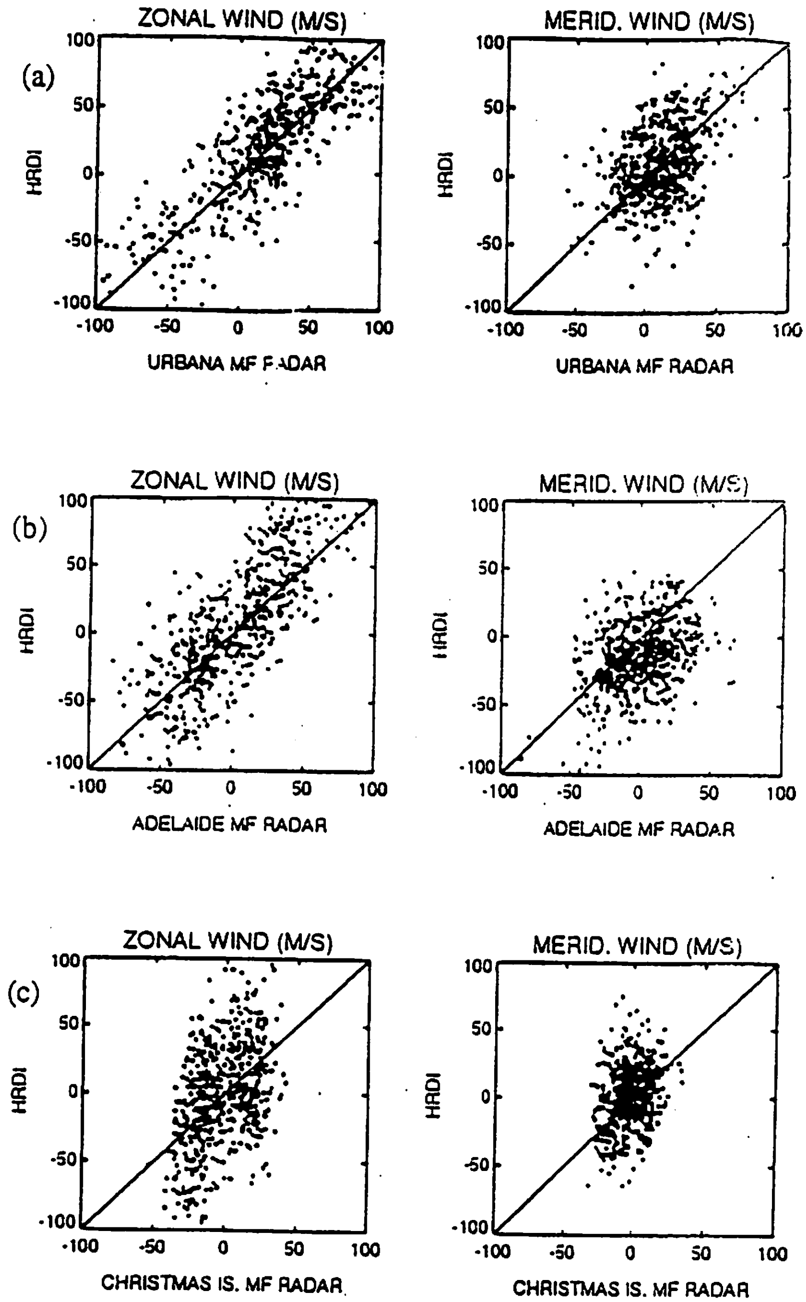

Figure 11. Scatterplots of HRDI winds in the altitude range 65-85 km for the zonal and the meridional components using (a) 106 coincidences with the Urbana MF radar between December 1991 and December 1993, (b) 118 coincidences with the Adelaide MF radar between December 1991 and January 1994, and (c) 137 coincidences with the Christmas Island MF radar between December 1991 and January 1994.

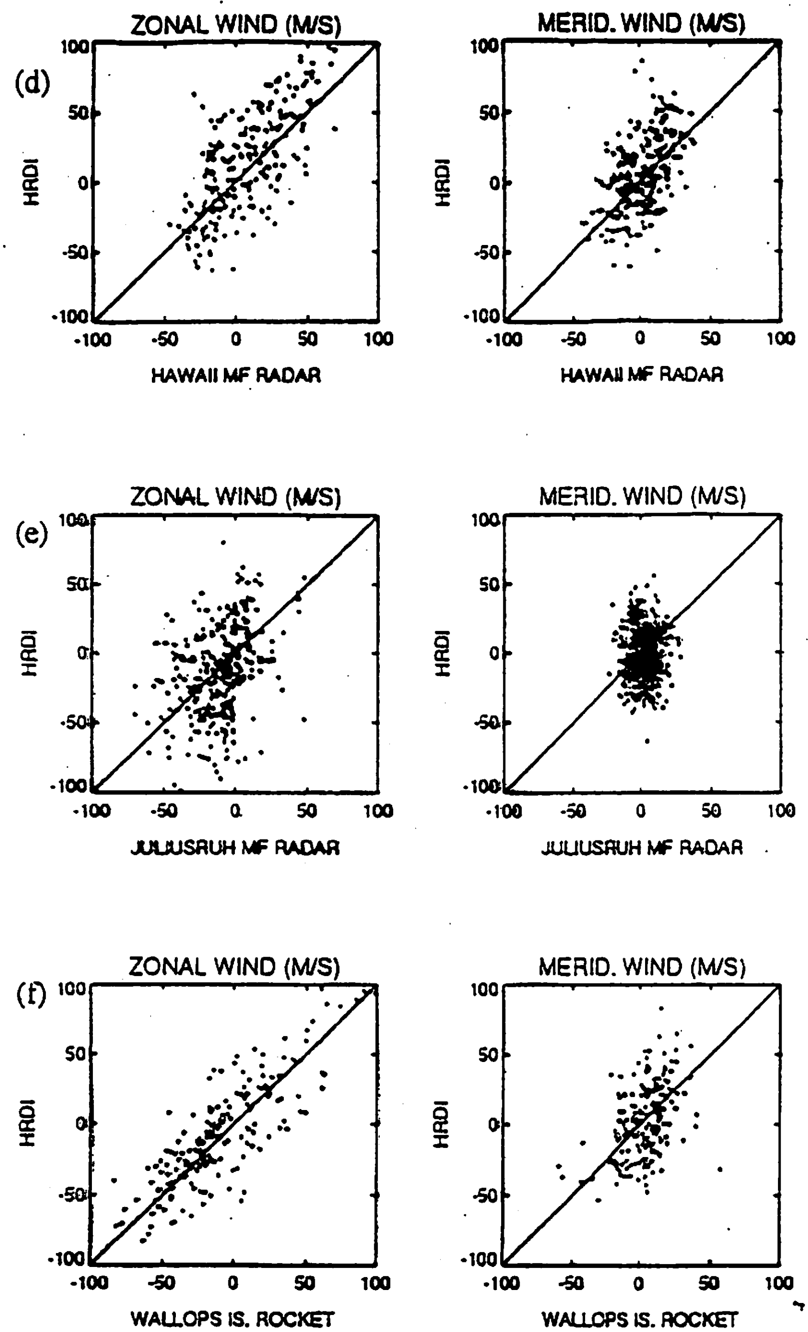

Figure 11. (d) Same as Figure 11a, but for 59 coincidences with the Hawaii MF radar between December 1991 and December 1992. (e) Same as Figure 11a, but for 26 coincidences with the Saskatoon MF radar between December 1991 and December 1992. (f) Same as Figure 11a, but for 23 rockets launched from Wallops Island du ing the period from December 1991 to December 1993.

extra

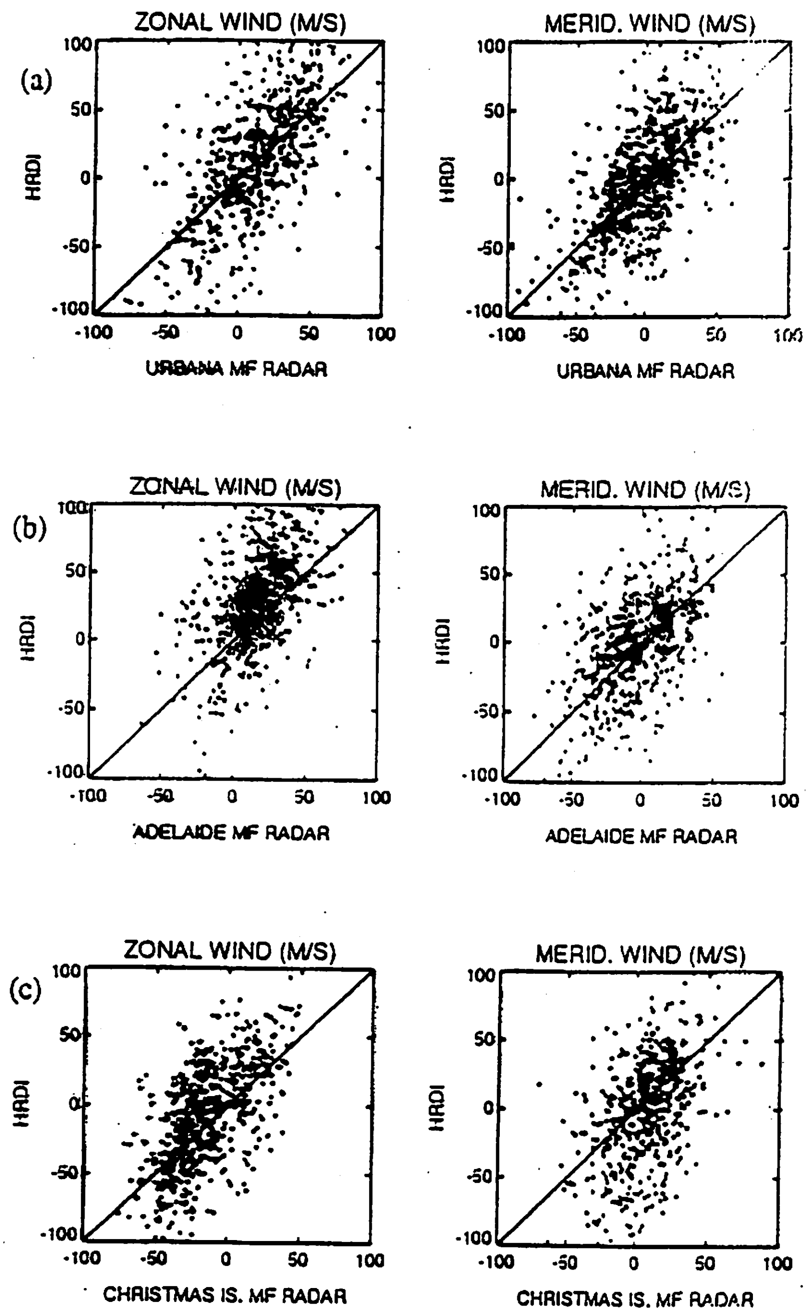

Figure 12. (a) Same as Figure 11a, but for the altitude range 85-105 km. (b) Same as Figure 11b, but for the altitude range 85-105 km. (c) Same as Figure 11c, but for the altitude range 85-105 km.

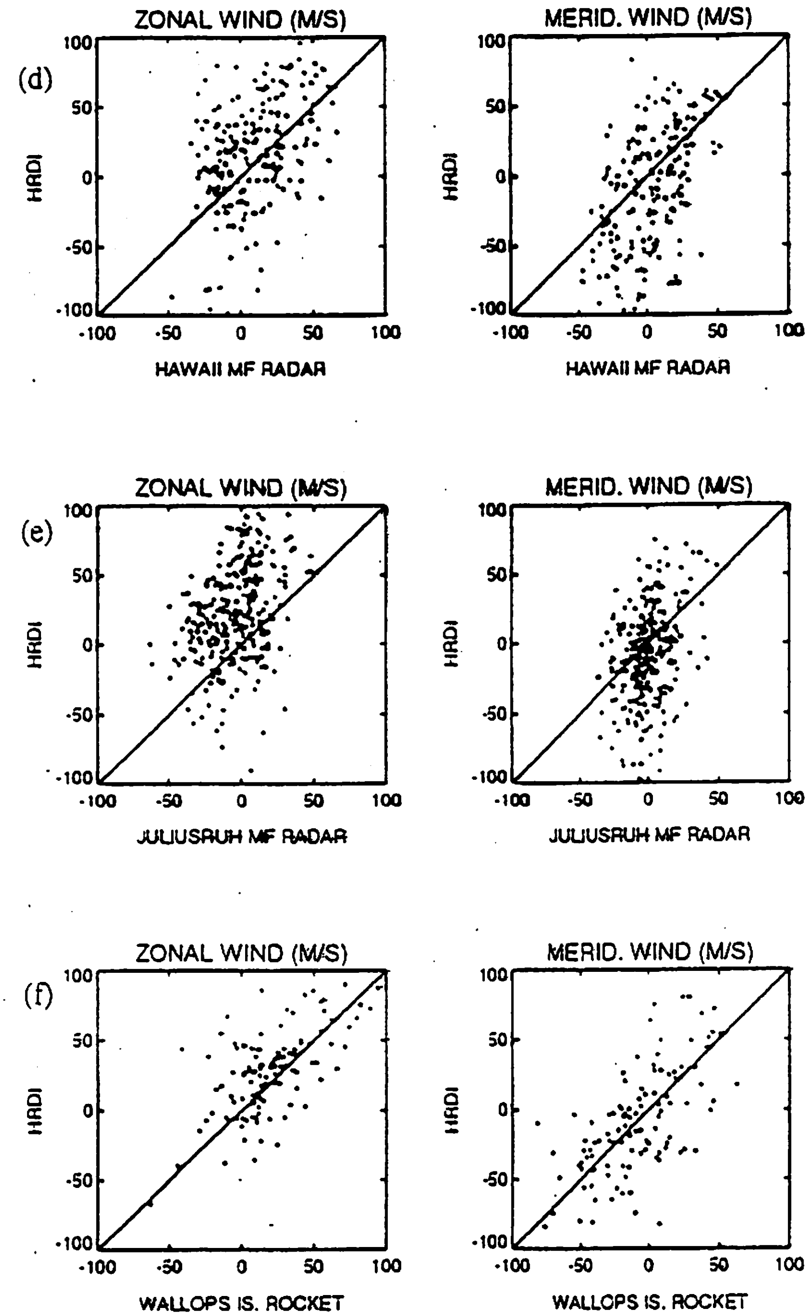

Figure 12. (d) Same as Figure 11d, but for the altitude range 85-105 km. (e) Same as Figure 11e, but for the altitude range 85-105 km. (f) Same as Figure 11f, but for altitude range 85-105 km.

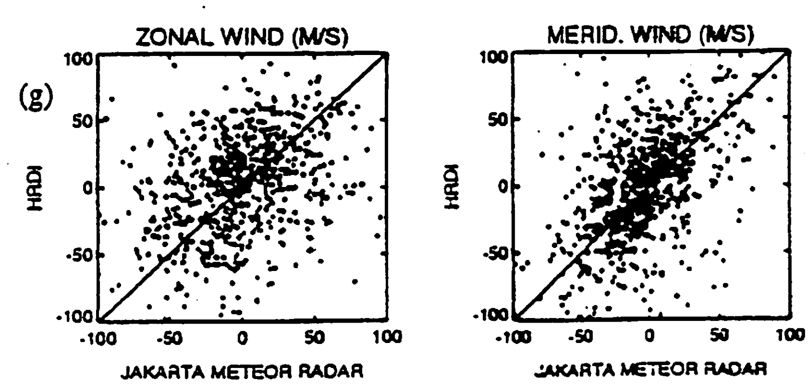

Figure 12g. Scatterplots of HRDI and Jakarta meteor radar winds in the altitude range 80-110 km for the zonal and the meridional components using 125 coincidences between November 1992 and September 1994.

extra

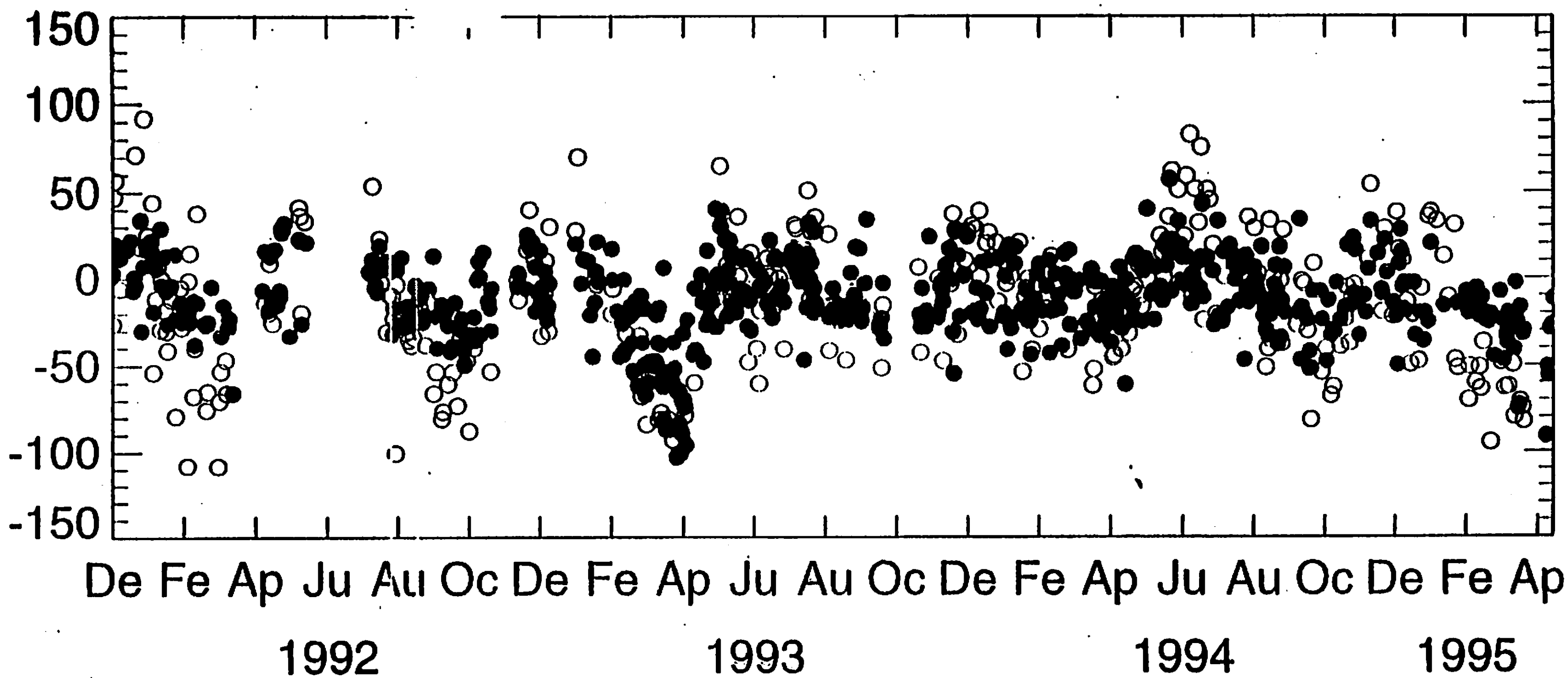

150
100
50
0
-50
-100
-150
De Fe Ap Ju Au Oc De Fe Ap Ju Au Oc De Fe Ap Ju Au Oc De Fe Ap
1992
1993
1994
1995

extra

Christmas Island ~~Meridional~~ Zonal : 82.5–87.5 km

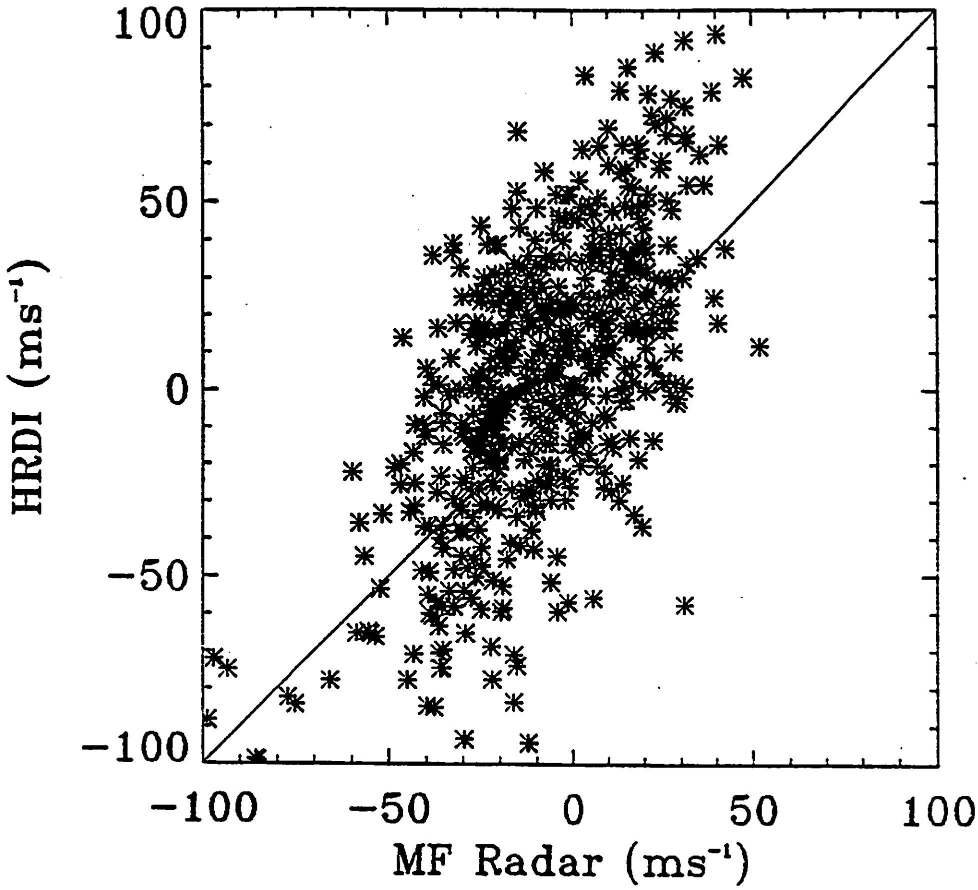

1.73

Christmas Island Meridional : 82.5–87.5 km

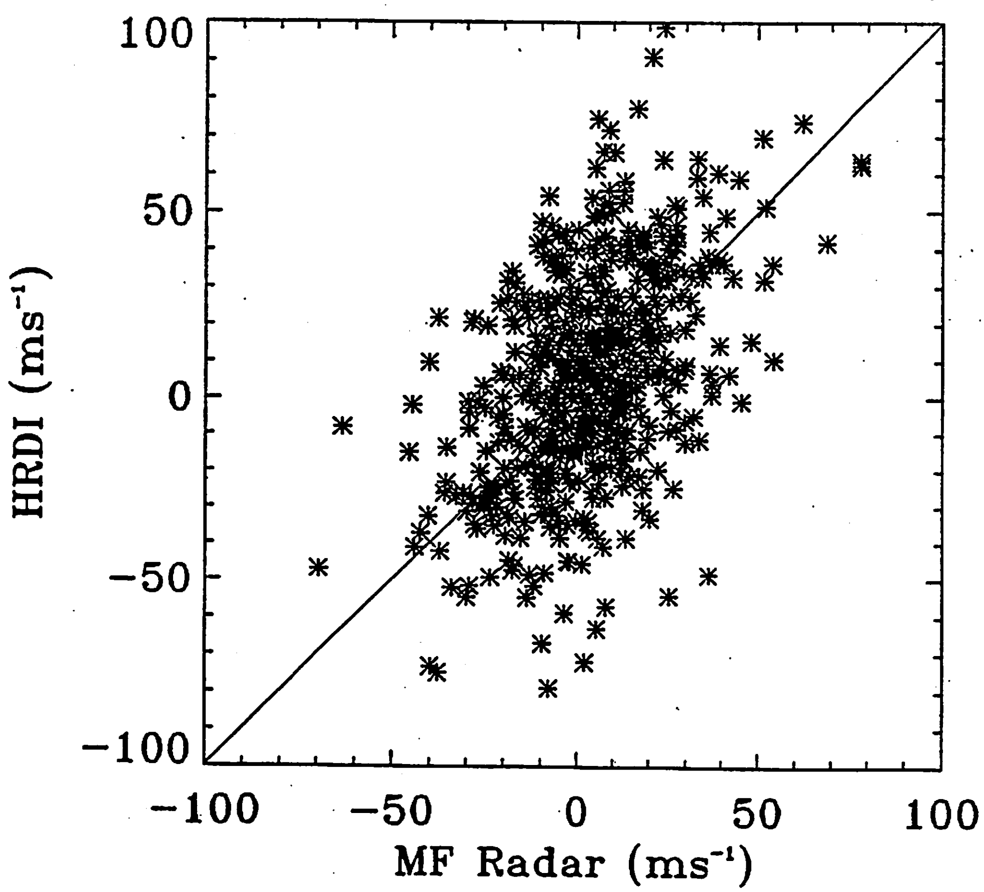

2.13

extra

Back to the spotlight

- AIDA 89
  - comparison with an MF interferometer
- Radar Interferometric techniques
  - generally do not work
- Lidar Wavelength-Period relations
  - selection effect
- HRDI / WINDI / MF
  - Consistent with an underestimation of wind speeds above 90 km for radars that have not been optimised

Back to the spotlight (cont.)

- Meteor / MF wind comparisons
  - as for point above. Have demonstrated some limitations of the meteor technique

Consequences for MF radars

- Scrutiny has very much enhanced our understanding of the technique
- Very much better understood in terms of limitations
- It has become clear that the MF radar technique can be extended considerably

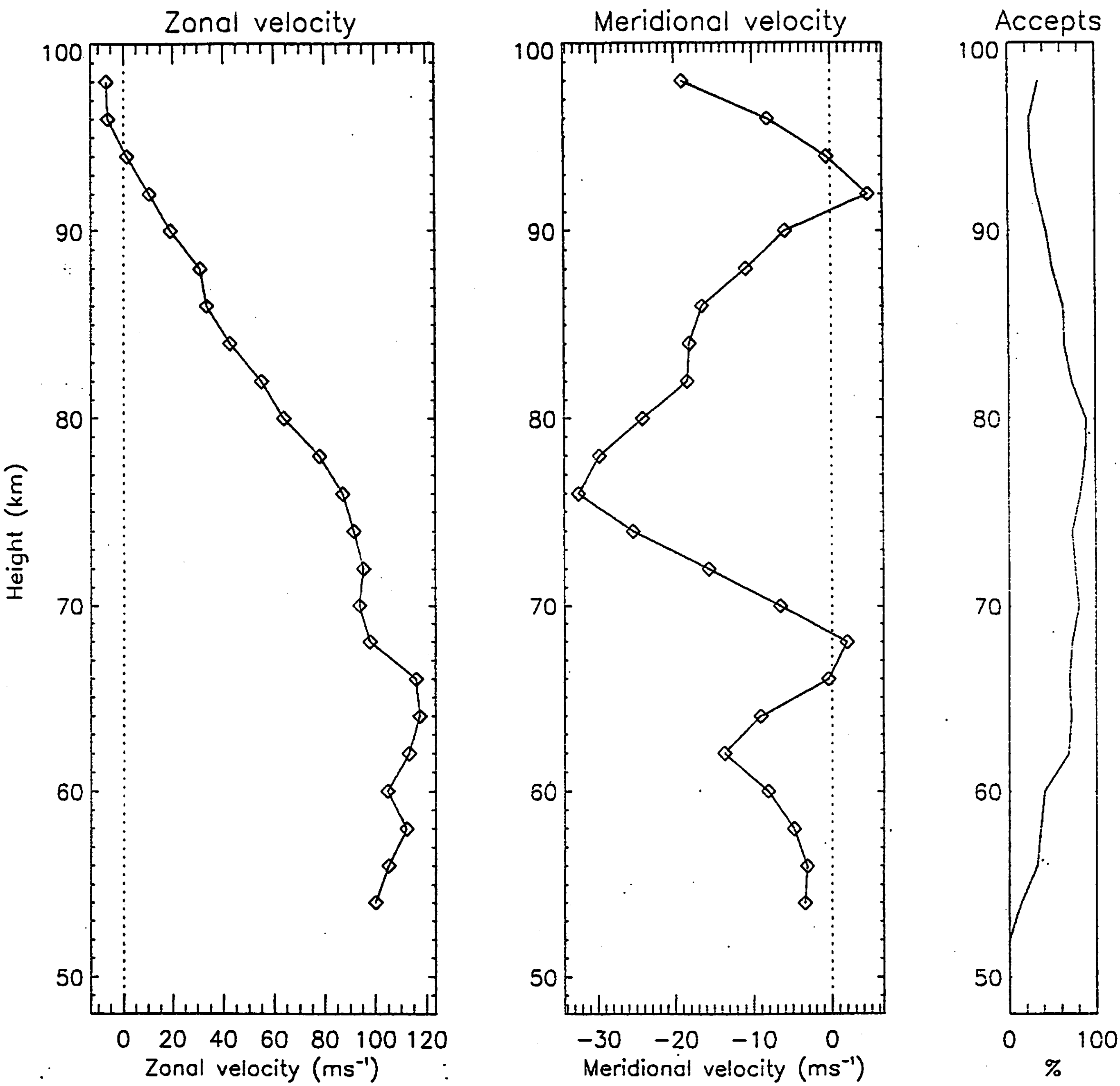

04/06/1996 07:59:20 to 04/06/1996 15:00:10

$\frac{1}{12}$th Power Apeture Product of New Buckland Park MF Radar

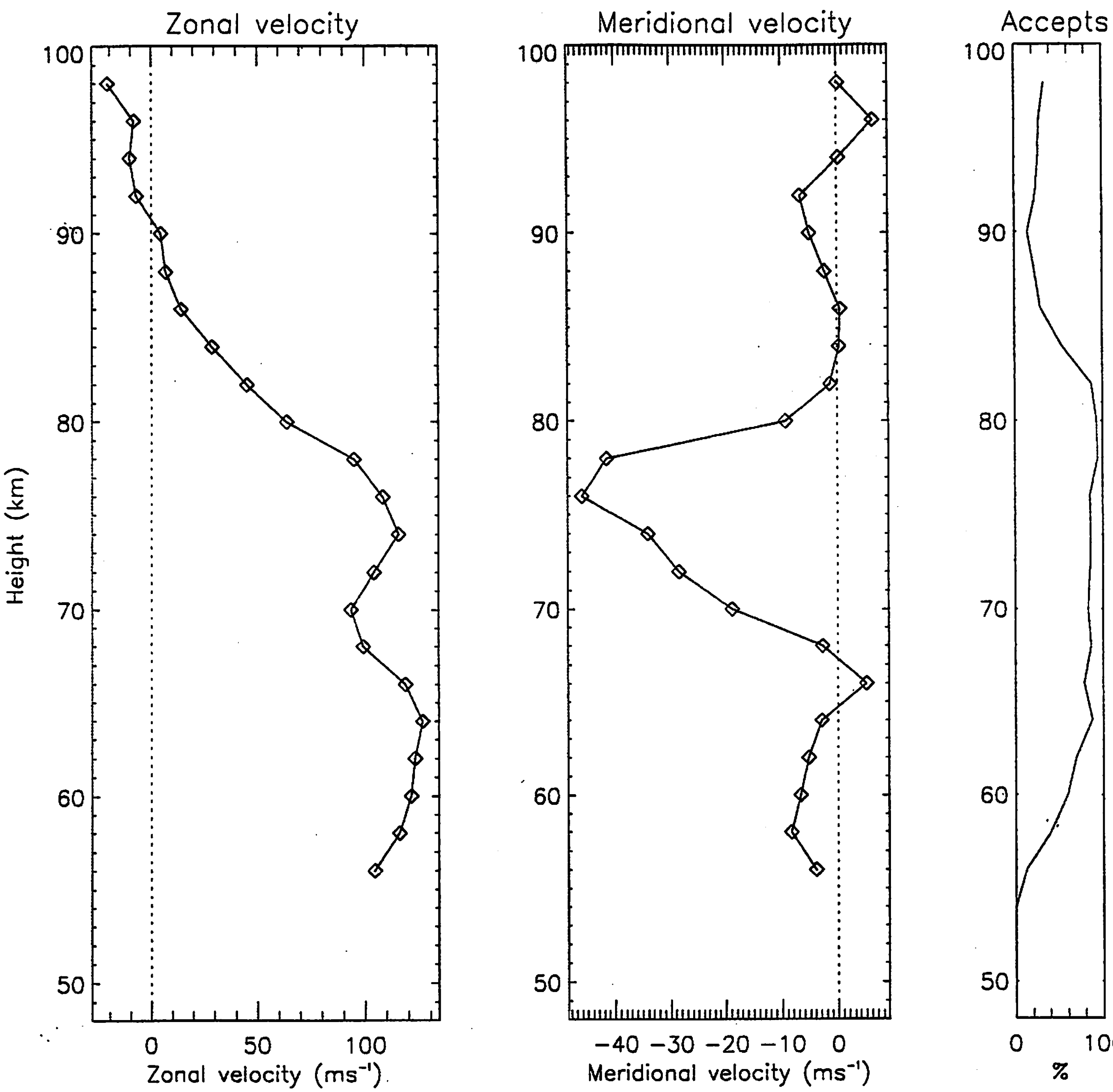

05/06/1996 12:23:30 to 05/06/1996 15:24:00

extra

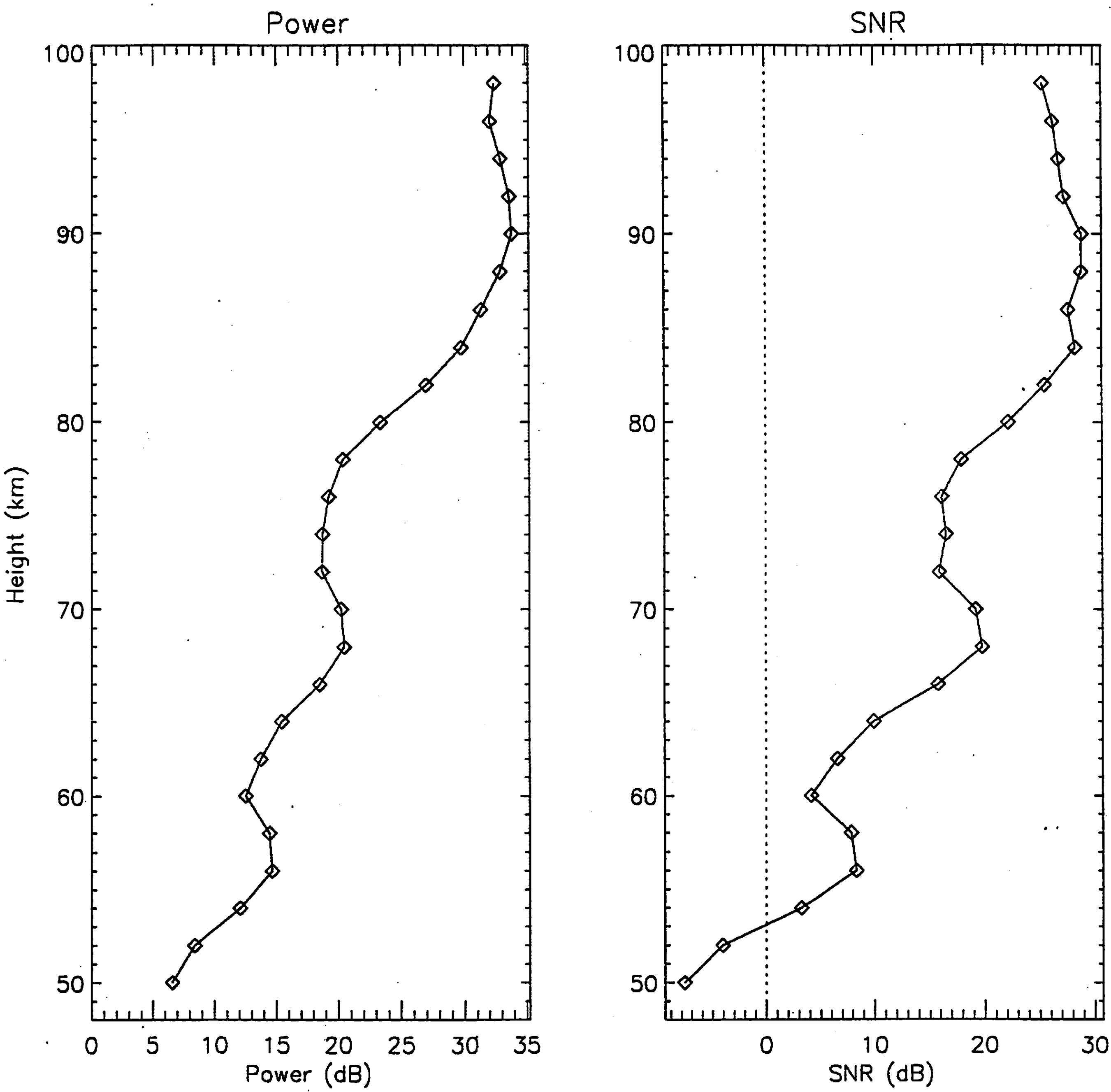

04/06/1996 12:00:50 to 04/06/1996 17:00:10

extra

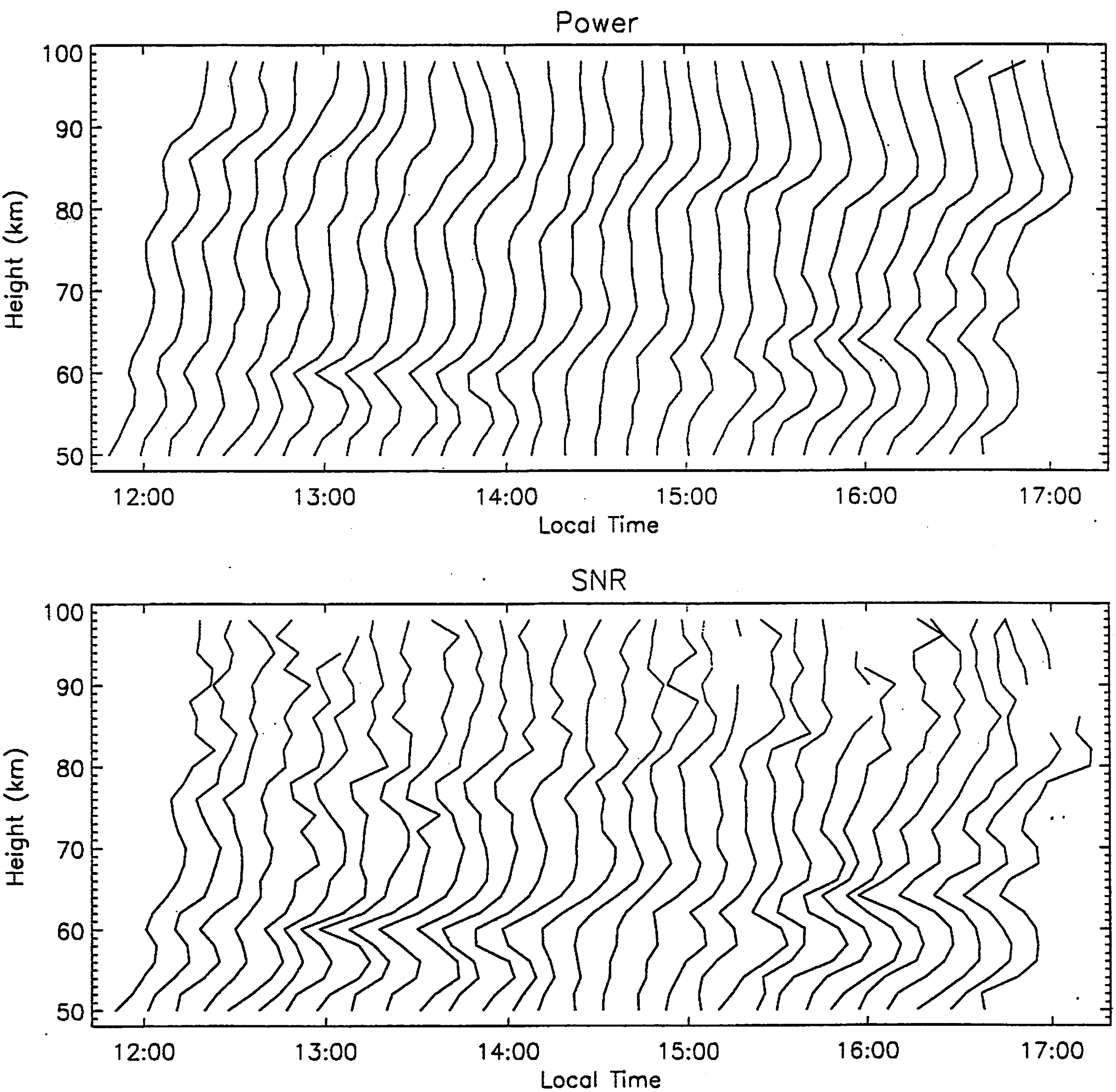

04/06/1996 12:00:50 to 04/06/1996 17:00:10

extra

Next Steps

- Further intercomparison of MF Doppler / Meteor Winds
- Intercomparison of airglow / MF winds
- Detailed investigation of the nature of the irregularities in the 60 - 100 km height region

extra

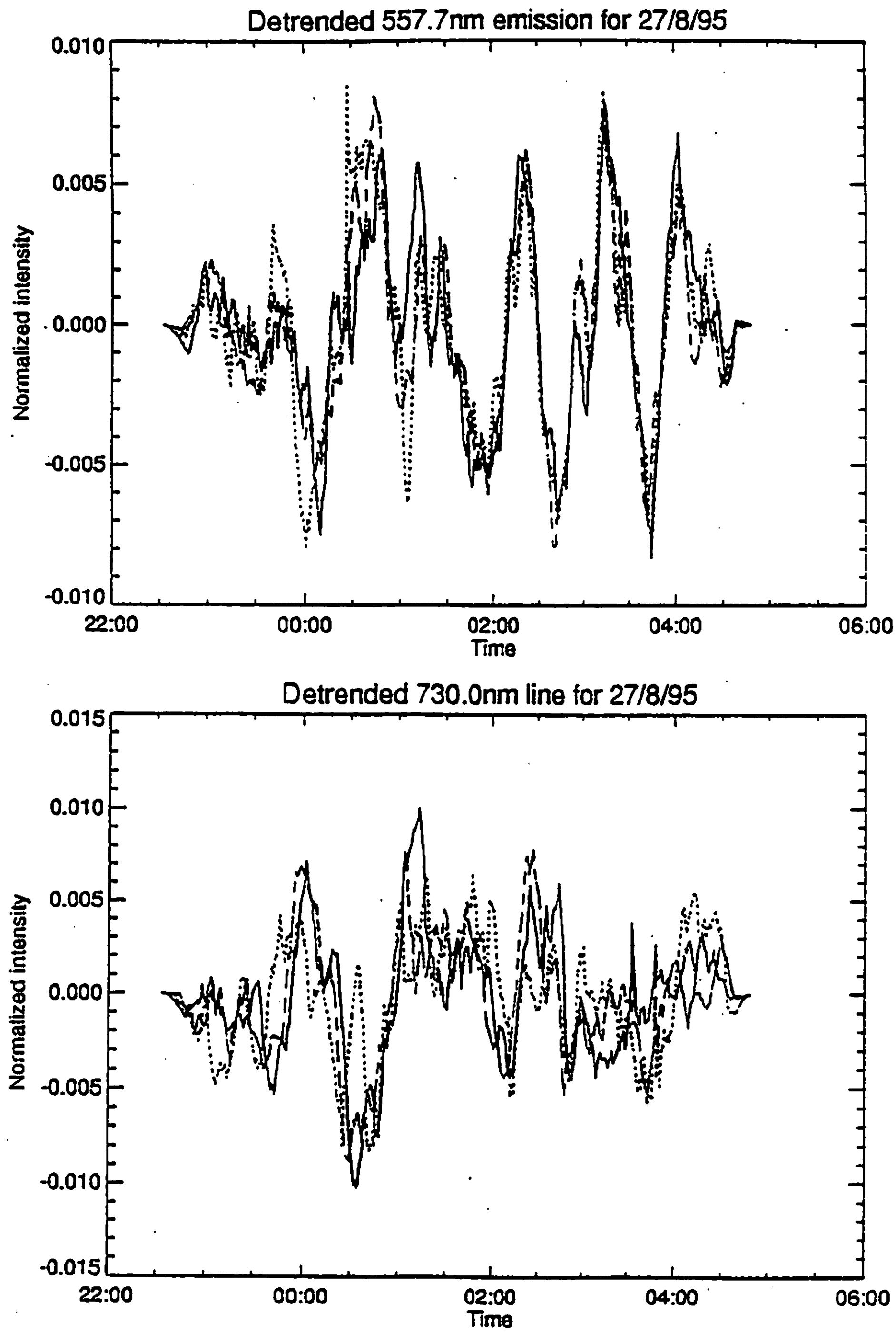

Figure 4.13: Detrended photometer intensities for 27/08/95. A wave component with period approximately 30 minutes is clearly visible in the 557.7nm plot.

extra

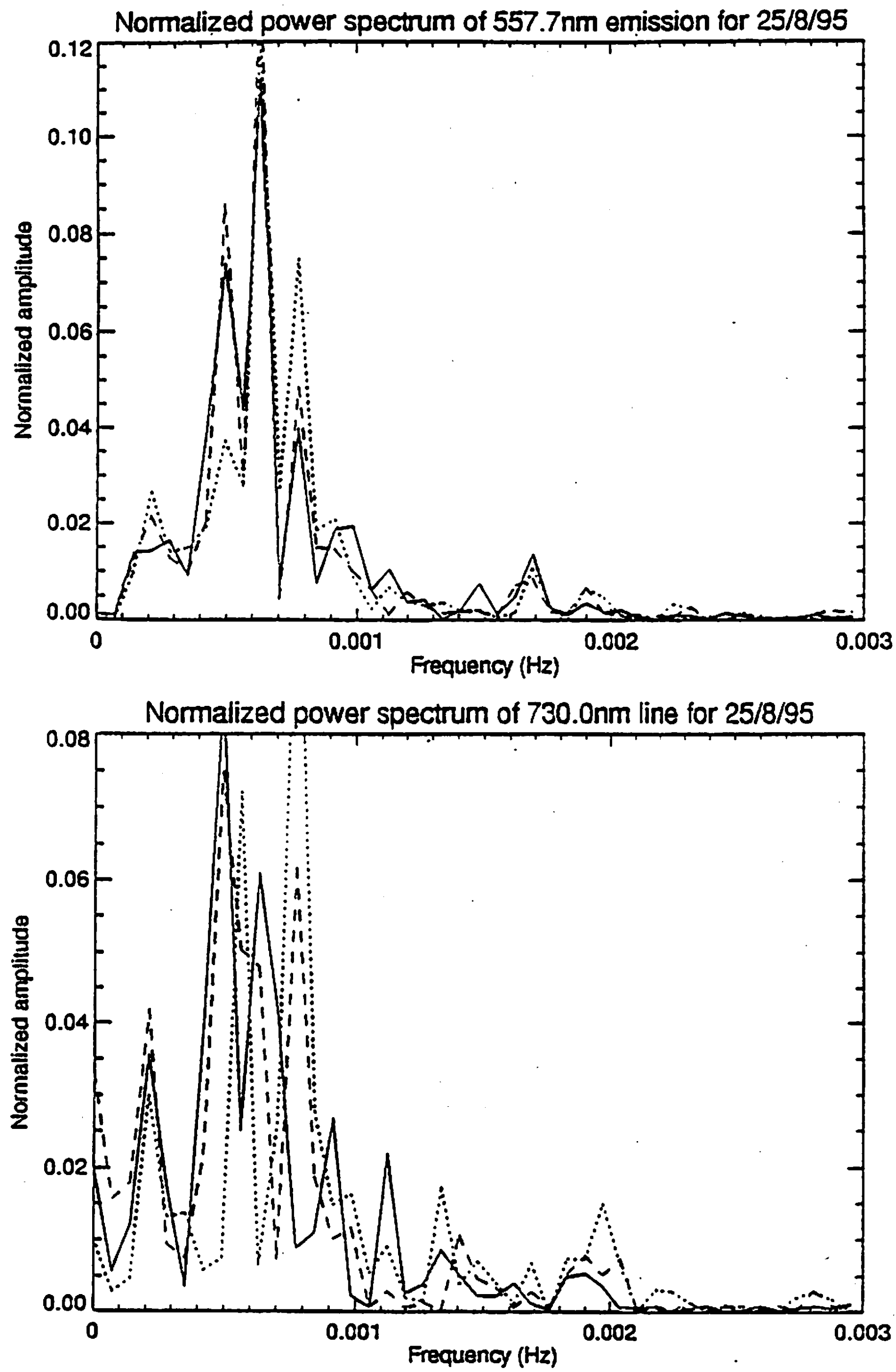

Figure 4.10: Power spectrum obtained from photometer observations on 25/08/95. The three dominant frequencies in the 557.7nm line are also the dominant ones in the 730.0nm spectrum.

extra

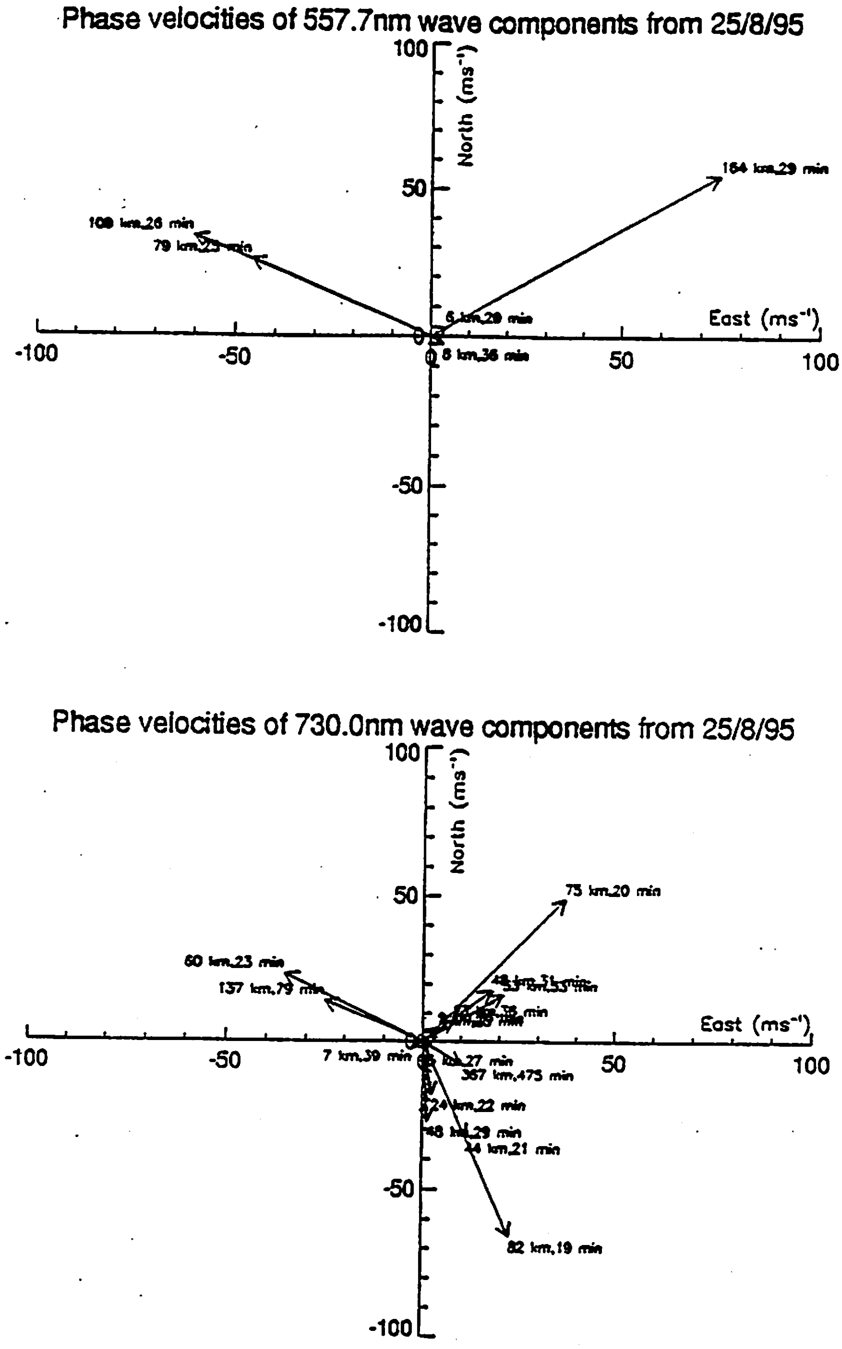

Figure 4.11: Horizontal phase velocities from the photometer on 25/08/95. The south-east components were present predominantly before midnight.

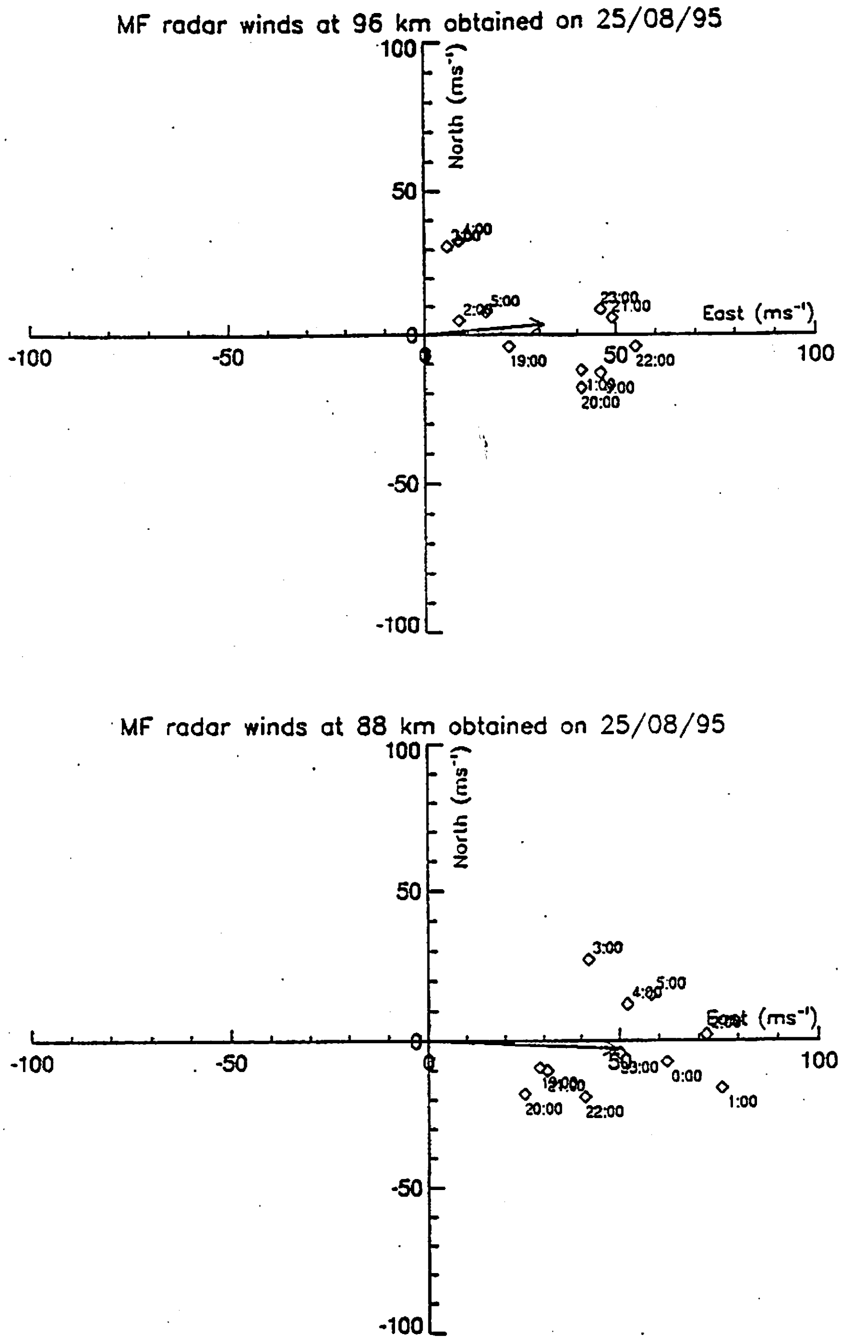

Figure 4.12: Wind velocities determined by the MF radar on 25/08/95 showing time variation.. The arrow heads indicate the nightly average wind velocities at both heights. These are discussed in section 4.2.3 on page 48.

extra

Additional Information

- Planned and Operational MF Radars
- Typical MF radar operating parameters

extra

Planned and Current MF Radars

Facility	Lat./Long	Mode	Freq. (MHz)	Peak Power (kW)	Typ Ave Power (W)
Adelaide, Australia	35S, 138E	SA, DBS	1.98	100	240
Andoya, Norway	69N,16E	SA	1.98	50	120
Bribie Island, Aus	28S,153E	SA, DBS	1.98	25	60
Christchurch, NZ	44S,172E	SA	2.40	100	10
Christmas Island	2N,157W	SA	1.98	25	60
Davis Base, Ant	69S,78E	SA	1.98	25	60
Hawaii, USA	22N,156W	SA	1.98	25	60
Kolhapur, India	17N,78E	SA	1.94	25	60
Juliusruh, Germany	55N,13E	SA (FMCW)	3.18	1	1
London, Canada	43N,81W	SA	2.22	25	60
McMurdo, Antarctica	78S,166E	SA	1.98	50	120
Palmer Pen, Ant	Planned	SA	1.98	25	60
Pontianak, Indonesia	0S,109E	SA	1.98	25	60
Robsart, Canada	49N,109W	SA	2.22	25	60
Saskatoon, Canada	52N,107W	SA	2.22	50	120
Scott Base, Ant	78S,167E	SA	2.90	60	8
Sylvan Lake, Canada	52N,114W	SA	2.22	25	60
Syowa Base, Ant	Planned	SA	TBD	50	120
Trivandrum, India	8N,77E	SA	1.94	25	60
Urbana, USA	40N,88W	SA	2.66	25	60
Wakkanai, Japan	Planned	SA	TBD	50	120
Wuhan, China	Planned	SA	TBD	25	60
Yamagawa, Japan	31N,131E	SA	1.95	50	120
Tromso, Norway	70N,19E	SA	2.78	50	120

extra

Typical MF Radar Operating Parameters

- In Spaced Antenna mode a typical daytime configuration might be:

■ Start Height (Day)	60 km
■ Start Height (Night)	80 km
■ Sampling Height Interval	2 km
■ No. Heights per Sample	20
■ Pulse Repetition Frequency	80 Hz
■ Integrations per Sample Point	32
■ No. of Points per Data Set	256

- Time for data set: 256 points / 80 Hz * 32 integrations = 102.4 seconds, providing a wind profile every 2 minutes and covering the height range 60 to 98 km (day).

extra

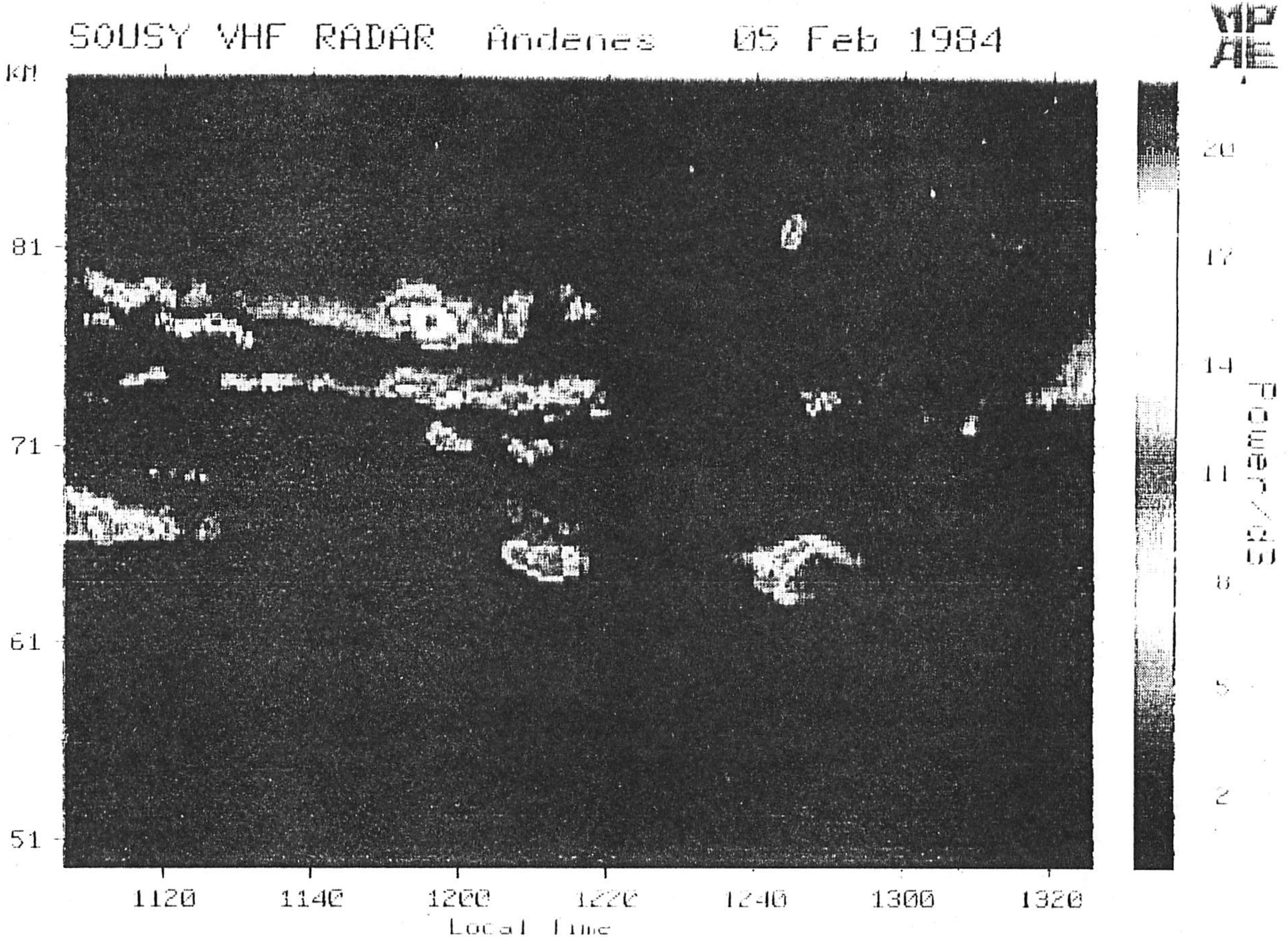

SOUSY VHF RADAR Andenes 05 Feb 1984
KM
81
71
61
51
1120
1140
1200
1220
1240
1300
1320
Local Time
20
17
14
11
8
5
2
SNR / dB

extra

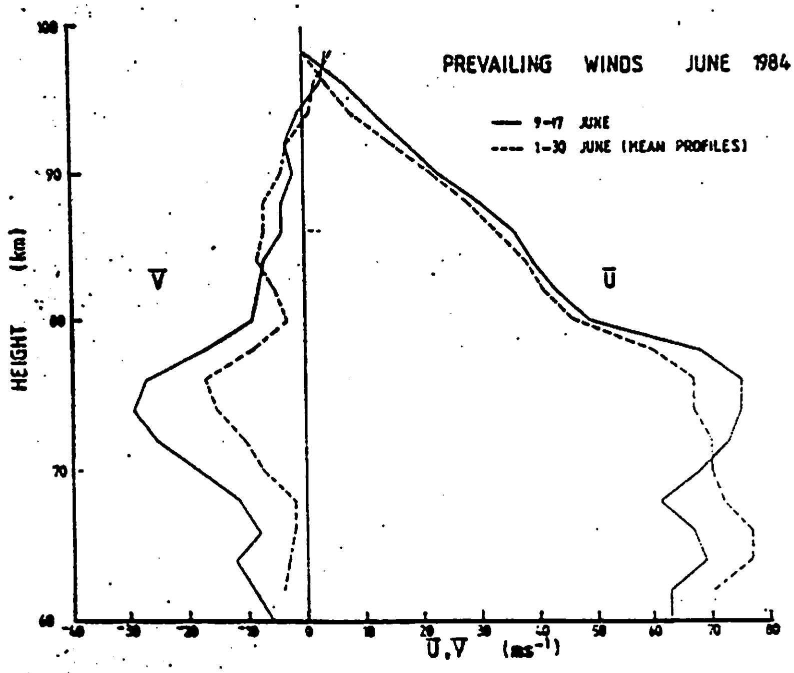

ZONAL MOMENTUM FLUXES JUNE 9-17

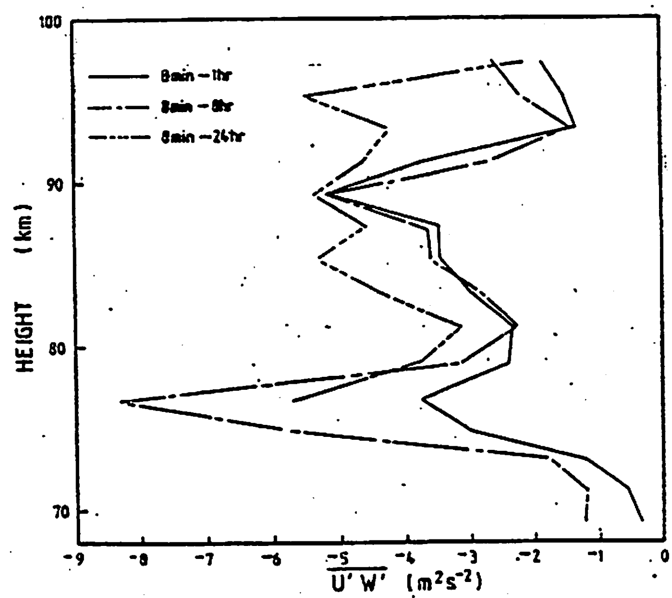

extra